The University Of Sheffield.

Array Signal Processing Based on Traditional and Sparse Arrays

Syed Ahsan Raza

Supervisors:

Dr. Wei Liu

and

Dr. Mohammed Benaissa

Thesis submitted in candidature for graduating with degree of doctor of philosophy

February 2019

Array Signal Processing Based on Traditional and Sparse Arrays

Syed Ahsan Raza

PhD Thesis

Communications Group

Department of Electrical and Electronic Engineering

The University of Sheffield

February 2019

Abstract

Array signal processing is based on using an array of sensors to receive the impinging signals. The received data is either spatially filtered to focus the signals from a desired direction or it may be used for estimating a parameter of source signal like direction of arrival (DOA), polarization and source power. Spatial filtering also known as beamforming and DOA estimation are integral parts of array signal processing and this thesis is aimed at solving some key probems related to these two areas. Wideband beamforming holds numerous applications in the bandwidth hungry data traffic of present day world. Several techniques exist to design fixed wideband beamformers based on traditional arrays like uniform linear array (ULA). Among these techniques, least squares based eigenfilter method is a key technique which has been used extensively in filter and wideband beamformer design. The first contribution of this thesis comes in the form of critically analyzing the standard eigenfilter method where a serious flaw in the design formulation is highlighted which generates inconsistent design performance, and an additional constraint is added to stabilize the achieved design. Simulation results show the validity and significance of the proposed method.

Traditional arrays based on ULAs have limited applications in array signal processing due to the large number of sensors required and this problem has been addressed by the application of sparse arrays. Sparse arrays have been exploited from the perspective of their difference co-array structures which provide significantly higher number of degrees of freedoms (DOFs) compared to ULAs for the same number of sensors. These DOFs (consecutive and unique lags) are utilized in the application of DOA estimation with the help of difference co-array based DOA estimators. Several types of sparse arrays include minimum redundancy array (MRA), minimum hole array (MHA), nested array, prototype coprime array, conventional coprime array, coprime array with compressed interelement spacing (CACIS), coprime array with displaced subarrays (CADiS) and super nested array. As a second contribution of this thesis, a new sparse array termed thinned coprime array (TCA) is proposed which holds all the properties of a conventional coprime array but with $\lceil \frac{M}{2} \rceil$ fewer sensors where M is the number of sensors of a subarray in the

conventional structure. TCA possesses improved level of sparsity and is robust against mutual coupling compared to other sparse arrays. In addition, TCA holds higher number of DOFs utilizable for DOA estimation using variety of methods. TCA also shows lower estimation error compared to super nested arrays and MRA with increasing array size.

Although TCA holds numerous desirable features, the number of unique lags offered by TCA are close to the sparsest CADiS and nested array and significantly lower than MRA which limits the estimation error performance offered by TCA through (compressive sensing) CS-based methods. In this direction, the structure of TCA is studied to explore the possibility of an array which can provide significantly higher number of unique lags with improved sparsity for a given number of sensors. The result of this investigation is the third contribution of this thesis in the form of a new sparse array, displaced thinned coprime array with additional sensor (DiTCAAS), which is based on a displaced version of TCA. The displacement of the subarrays generates an increase in the unique lags but the minimum spacing between the sensors becomes an integer multiple of half wavelength. To avoid spatial aliasing, an additional sensor is added at half wavelength from one of the sensors of the displaced subarray. The proposed placement of the additional sensor generates significantly higher number of unique lags for DiTCAAS, even more than the DOFs provided by MRA. Due to its improved sparsity and higher number of unique lags, DiTCAAS generates the lowest estimation error and robustness against heavy mutual coupling compared to super nested arrays, MRA, TCA and sparse CADiS with CS-based DOA estimation.

Contents

List of Publications

Journal papers

1. A. Raza, W. Liu, and Q. Shen. "Thinned Coprime Array for Second-Order Difference Co-Array Generation with Reduced Mutual Coupling", IEEE Transactions on Signal Processing, accepted, 2019.

2. A. Raza, and W. Liu. "Revisit of the eigenfilter method for the design of FIR filters and wideband beamformers", Systems Science & Control Engineering 6(1), 482 – 491, October, 2018.

Conference papers

1. A. Raza, W. Liu, and Q. Shen. "Displaced Thinned Coprime Arrays with an Additional Sensor for DOA Estimation", in Proc. 18th IEEE International Symposium on Signal Processing and Information Technology (ISSPIT), Louisville, Kentucky, USA, December, 2018, pp. 95 – 100.

2. A. Raza, W. Liu, and Q. Shen. "Thinned Coprime Arrays for DOA Estimation", in Proc. of the European Signal Processing Conference (EUSIPCO), Kos, Greece, September, 2017, pp. 395 – 399.

3. A. Raza and W. Liu. "Critical Analysis of the Eigenfilter Method for the Design of FIR Filters and Wideband Beamformers", in Proc. 22nd International Conference on Automation and Computing (ICAC), 2016, Colchester, UK, September, 2016, pp. 504 – 509.

List of Figures

List of Tables

Acknowledgements

First of all, I would like to take this opportunity to express my deepest gratitude to my supervisor Dr. Wei Liu for his persistent encouragement, guidance and support. He has always been there to support me and his hard working attitude inspired me to work hard. He played a fundamental role in imparting the necessary skills of research to me. His critical feedback on every occasion helped me improve my work.

I would like to thank my second supervisor Dr. Mohammed Benaissa for his valuable advice and help with the doctoral development program.

I would also like to offer my deepest gratitude to Commonwealth Scholarship Commission who provided me with this great opportunity to pursue my doctoral studies in UK which would otherwise have been impossible. I am thankful to all the colleagues at the Commission who helped me with my queries.

I would like to thank The Edith Evelyn Wali Muhammad Memorial Fund who provided me with the financial grant at a critical stage of my PhD. I would also appreciate the support I got from Pakistan High Commission, London.

I would like to thank my fellow Commonwealth Scholars for the amazing time we spent in Sheffield, my colleagues from Communication Group especially Zhang Bo for his support and inspiring attitude towards academics. Dr Zaffar Zaidi, my friend, my brother, and a person who is always there to guide me, from settling down in Sheffield to the writing phase of my PhD thesis.

My PhD would not have reached the final stages without the continuous emotional support from my wife, Mazeya Zaidi and my daughter, Aaleen who mean the world to me.

Finally, all this hard work during my PhD journey will not mean anything without mentioning the support of my parents and my brother who have always encouraged me and helped me keep my focus.

List of Abbreviations

CACIS	Coprime Array with Compressed Interelement Spacing
CADiS	Coprime Array with Displaced Subarrays
CS	Compressive Sensing
DOA	Direction of Arrival
DOF	Degree of Freedom
DiTCAAS	Displaced Thinned Coprime Array with Additional Sensor
ESPRIT	Estimation of Signal Parameters via Rotational Invariance Techniques
FIR	Finite Impulse Response
IIR	Infinite Impulse Response
MRA	Minimum Redundancy Array
MHA	Minimum Hole Array
MUSIC	MUltiple SIgnal Classification
SNR	Signal-to-Noise Ratio

SINR	Signal-to-Interference plus Noise Ratio
SS	Spatial Smoothing
SNA	Super Nested Array
TDL	Tapped Delay Line
TCA	Thinned Coprime Array
ULA	Uniform Linear Array

Chapter 1

Introduction

1.1 Introduction

Humans perceive the outside world with the aid of sensors. The natural sensor organs in the shape of eyes, nose, ears, tongue and skin bring to life the classic five senses of sight, smell, hearing, taste and touch respectively. As ancient as this natural mechanism of perception, humans have carried the same principles to solve complex problems of modern times. Different types of sensors have been developed to sense different signals. Applications of these sensors include the likes of medical diagnosis, communication, RADAR, SONAR, seismology and radio astronomy [1–8].

Placing a group of sensors together in a particular configuration paves the way for an array of sensors. These arrays of sensors offer certain desirable characteristics compared to the application of a single sensor. First of all, an element of redundancy is available in the scenario of a sensor failure. Secondly, the received data from the array can be combined together to improve the signal to noise ratio (SNR) of the received signal by averaging out the noise. Another attractive property of arrays is their ability to work as a spatial filter. This implies that the overall reponse of the array is directional and focuses on an intended drection while rejecting the signals/interferences from unwanted directions [1]. This has the same effect as boosting the SNR of the received signal and is termed as beamforming.

The concept of beamforming is shown with the help of a simple beamformer in Fig.

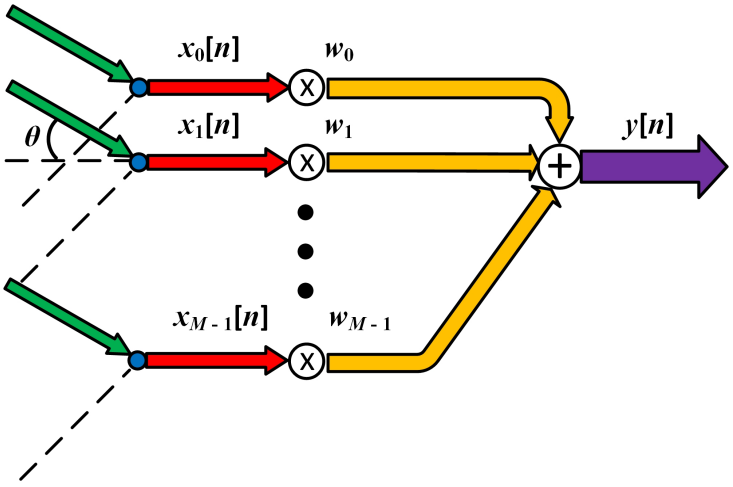

Figure 1.1: A simple beamformer with the output as linear combination of weighted received array signals.

1.1 where the beamformer output $y[n]$ is a linear combination of the received array signals $x_0[n]$, $x_1[n]$, ..., $x_{M-1}[n]$ weighted with the coefficients w_0, w_1, ..., w_{M-1}, where n is the discrete time index, M is the number of sensors in the array and θ is the angle of arrival (AOA) of the impinging signal. The values of these coefficients depend on the required directional response and objective based on maximizing the signal to interference plus noise ratio (SINR). Depending on the channel conditions, the values of these weights can be fixed or altered leading to fixed and adaptive beamformers where adaptive beamformers perform significantly better than fixed beamformers in adverse channel conditions at the cost of extra computations [1]. Depending on the bandwidth of the impinging signal, beamforming is divided into narrowband and wideband beamforming. As wideband signals are commonplace in the bandwidth hungry applications of today, the importance of wideband beamforming can never be under estimated.

To design fixed wideband beamformers, several techniques exist in the literature like convex optimization [9] and standard least squares [10]. Another technique based on least squares is the eigenfilter technique, which is desirable for fixed wideband beamformer design in comparison to convex optimization and least squares due to its low computational requirements and numerical stability [11]. However, the design formulation has a serious flaw resulting in the design method being error-prone and providing inconsistent results.

As the first contribution of this thesis, we propose a correction to the design formulation and show the improved wideband beamformer design with the help of simulation results.

Arrays can also be used to extract certain useful parameters embedded in the signals like direction of arrival (DOA). A particular signal originating from a specific direction may fall at different sensors of the array at different times creating inter-sensor delays. Then by analyzing the received array output with the help of different DOA estimators, the DOA of the impinging source can be estimated [2, 6, 7]. In addition to wideband beamformer design, the DOA estimation aspect is also a key subject of this thesis.

A lot of literature is dedicated to developing DOA estimators which determine the DOA of signals with high resolution utilizing a finite number of snapshots from array outputs. These snapshots refer to the number of samples of received signals taken at each sensor to measure the array output [2, 6, 7]. Some key DOA estimators like Bartlett beamformer [12], the Capon beamformer [13], the pisarenko harmonic decomposition [14], the minimum-norm method [15], multiple signal classification (MUSIC) [16, 17], estimation of signal parameters via rotational invariance techniques (ESPRIT) [18], maximum likelihood estimator [19, 20], methods of DOA estimation (MODE) [21] and sparse iterative covariance based estimation (SPICE) [22], have been developed for this purpose.

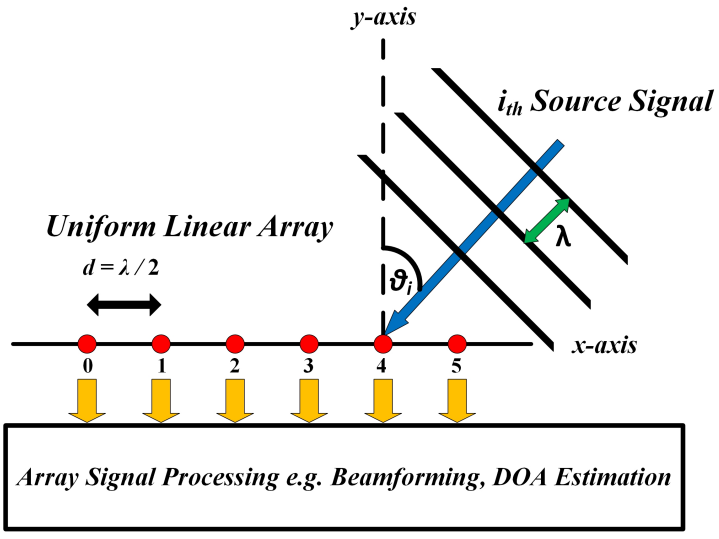

Figure 1.2: Array signal processing based on traditional arrays.

Conventional array processing involves the use of traditional arrays for beamforming,

DOA estimation and other array signal processing tasks. These traditional arrays have the nature of a uniform linear array (ULA) with inter-sensor spacing d where $d = \frac{\lambda}{2}$, and λ corresponds to the wavelength of the impinging signal. In this thesis, the impinging signals are always represented by plane waves, i.e. the array is assumed to be located in the far field of the sources generating the waves and the received signals have a planar wavefront [1]. Such an array is presented in Figure 1.2, which shows a source signal impinging on a ULA with an angle θ_i with the dashed line perpendicular to the plane of the array or broadside of the array as y-axis. The output of this sensor array is processed by different signal processing algorithms depending on the objective to be acheived. These different objectives range from extracting the source information like the distance between source and the array, DOA of the source, source power to determining the polarization of the impinging wave. In this figure, x-axis represents the plane of the array where the sensors are placed, while y-axis represents the broadside of the array. It can be noticed that the ULA has the inter-sensor spacing of $d = \frac{\lambda}{2}$ as increasing d beyond $\frac{\lambda}{2}$ generates spatial ambiguity. The spatial ambiguity in this case is analogous to aliasing in time domain according to the sampling theorem [2, 7]. Spatial ambiguity manifests itself as multiple source signals having different DOA's corresponding to the same array output which will result in erroneous DOA estimation.

The search to optimize the resources for best possible performance has been a long standing human endeavour. In the context of modern technology, there has been a constant struggle from the array signal processing perspective to explore new horizons and target diversified set of applications with resources that are usually limited e.g. power, bandwidth and number of sensors. With the ever decreasing cost of computing power, this challenge has been addressed in the domain of sparse sensing. The concept of sparse sensing revolves around exploiting prior konowledge about signals, through which a small chunk of high-dimensional big data is delivered to the signal processing algorithms to extract the low-dimensional information of interest. This technique makes it possible to deliver sophisticated novel set of applications with limited resources.

The domain of sparse sensing has two key elements in the shape of sparse sampling and information extraction. By considering the prior knowledge about signals and the

information of interest, sparse sampling gathers low-dimensional sparse samples from the big data while the information extraction element efficiently brings out the information of interest from the sparse samples. For applications dependent on the sparse representation of data, a relatively recent phenomenon termed compressed sensing has shown the ability to recover the original signal of interest from sparse samples under certain conditions [23, 24].

Compressed sensing or CS is a novel sensing/sampling paradigm that goes against the common wisdom in data acquisition which states that the sampling rate must be atleast twice the maximum frequency present in the signal (the so-called Nyquist rate). CS theory asserts that certain signals and images can be recovered from far fewer samples or measurements than traditional methods use. To make this possible, CS relies on two conditions/principles : sparsity, which pertains to the signal of interest, and incoherence, which pertains to the sensing modality.

Sparsity expresses the idea that the "information rate" of a continuous time signal may be much smaller than suggested by its bandwidth. More precisely, CS exploits the fact that many natural signals are sparse or compressible in the sense that they have concise representations when expressed in the proper basis Ψ.

Incoherence extends the duality between time and frequency and expresses the idea that objects having a sparse representation in Ψ must be spread out in the domain in which they are acquired, just as a Dirac or a spike in the time domain is spread out in the frequency domain. Incoherence means that unlike the signal of interest, the sampling/sensing waveforms have an extremely dense representation in Ψ.

For a signal $f(t)$ which is sparse in a certain basis Ψ where $f \in \mathbb{R}^n$, the representation of this signal in a sparse basis is given as

$$f(t) = \sum_{i=1}^{n} x_i \psi_i(t)\,, \tag{1.1}$$

where x is the coefficient sequence of f. It is convenient to express f as Ψx (where Ψ is the $n \times n$ matrix with $\psi_1, \ldots, \psi_n$ as columns). When the signal has sparse expansion, small coefficients corresponding to less information can be discarded without much perceptual loss. The coefficient vector x_s then will have all but the S largest coefficents set to zero.

This vector will be sparse in a strict sense and termed $S-$sparse with at most S non-zero entries.

Then sparse sensing involves linear functionals measuring the signal using a suitable sensing basis Φ

$$y_k = f\varphi_k, \qquad k = 1, \ldots, m\,, \tag{1.2}$$

where the object to be acquired is correlated with the waveforms $\varphi_k(t)$. This is an undersampled situation where the number m of available measurements is significantly smaller than the dimension n of the signal f. For signals of interest satisfying sparsity and sensing matrices/basis Φ incoherent with the representation basis Ψ, the $S-$sparse vector of coefficients can be easily recovered by posing the recovery problem as a l_1-norm minimization problem and solving using methods like convex optimization.

For CS to be powerful, it needs to deal with both nearly sparse signals and with noise. First, general objects of interest are not exactly sparse but approximately sparse. The main challenge is to obtain accurate reconstructions of such objects from highly undersampled measurements. Secondly, in any real application measured data will invariably be corrupted by at least a small amont of noise as sensing devices do not have infinite precision. It is therefore imperative that CS be robust with such nonidealities. At the very least, small perturbations in the data should cause small perturbations in the reconstruction. To make understanding simpler, the problem of recovering a vector $x \in \mathbb{R}^n$ from data is posed as follows.

$$y = Ax + z\,, \tag{1.3}$$

where A is an $m \times n$ "sensing matrix" giving information about x, and z is a stochastic or deterministic unknown error term. As $f = \Psi x$ and $y = \Phi f$ (Φ is the $m \times n$ matrix extracting the m samples), y can be written as $y = Ax$, where $A = \Phi\Psi$ and x is the coefficient sequence of the object in a proper basis.

For a robust CS, a very useful property exists called as the restricted isometry property (RIP). For each integer $S = 1, 2, \ldots$, for a $S-$sparse x, isometry constant δ_s of a matrix A is defined as the smallest number such that

$$(1 - \delta_S)\,\|x\|_{l_2}^2 \leq \|Ax\|_{l_2}^2 \leq (1 + \delta_S)\,\|x\|_{l_2}^2 \tag{1.4}$$

holds for all $S-$sparse vectors x. A matrix A is loosely said to obey the RIP of order S if δ_S is not too close to one. When this property holds, matrix A approximately preserves the Euclidean length of $S-$sparse signals.

It has been shown in the literature [25] that x is exactly recovered provided 1) x is sufficiently sparse and 2) the sensing basis Φ obeys RIP. In this context, the reconstruction of x is given as the solution to the following convex optimization problem

$$\min_{\tilde{x}\in\mathbb{R}^n} \|\tilde{x}\|_{l_1} \qquad \text{subject to} \qquad \|y-\Phi\tilde{x}\|_{l_2} \leq \epsilon\,, \tag{1.5}$$

where $\|.\|_{l_2}$ is the Euclidean norm and ϵ is an upper bound on the size of the noisy distribution.

A number of state of the art sparse sensing schemes include nested sampling [26], coprime sampling [27], power spectrum sensing [28], and quadratic sampling [29], which provide applications in the areas of source localization, cognitive radio, and optical imaging, with significantly reduced data rate but comparable performance to the classical methods. Sparse arrays are a perfect example of sparse sensing with their characteristic sparse sampling of the incoming data. As opposed to a traditional array shown in Figure 1.2, which represents a 6-sensor ULA with an aperture of $5d$, sparse arrays tend to have significantly fewer number of sensors for the same aperture compared to a ULA.

In the last 50 years of radio astronomy, human curiosity has inspired the mankind to explore the universe and solve its underlying mysteries. To see our own solar system, distant stars, galaxies and black holes in an unprecedented detail and accuracy, large arrays of radio telescopes have been deployed like the Very Large Array (VLA) in USA [30], Atacama Large Millimeter/submillimeter Array (ALMA) in Chile [31], and the very recent Square Kilometer Array (SKA) in Australia and South Africa [32]. Due to the significance of arrays and their functionality, a key challenge in array signal processing deals with reducing the cost of these projects. As a practical signal processing scenario will always be aimed at lowering the costs, minimizing the number of sensors while maintaining the required performance is an appealing prospect. Sparse arrays which offer the possibility of arranging sensors in diverse configurations with different performance characteristics, while minimizing the required number of sensors, are the perfect candidate to overcome this challenge.

In array signal processing, the nature of electromagnetic waves results in mutual coupling between sensors and causes the individual sensor response to interfere with the other sensors [33], [34]. This interference adversely affects parametric estimation like DOA, signal power and polarization. Due to the practical application of sparse sensing, a significant part of this thesis is aimed at investigating the design of novel sparse array configurations from the perspective of DOA estimation with special focus on sparse arrays robust against mutual coupling. These kinds of sparse arrays have applications in the fields of communication, RADAR, SONAR, medical imaging, seismic engineering and radio astronomy [2, 34–37].

ULA holds the ability to resolve at most $N-1$ sources with N physical sensors, irrespective of the algorithm deployed [2]. However, recent progress in the state of the art has shown that, under specific conditions, it is possible to identify more sources than the number of sensors using sparse arrays. This result is possible because multiple time-domain snapshots are available.

A comparison of DOA estimation scenario for a 6-sensor ULA and sparse array is shown in Figure 1.3, where it can be seen that sparse arrays do not have uniform spacing $\frac{\lambda}{2}$. Under mild assumptions, the array output of the sparse arrays can be converted to the samples on the difference co-array. In particular, the difference co-array $\mathbb{D}$ for an array $\mathbb{S}$ irrespective of being a ULA or a sparse array, is defined as the set of differences between sensor locations:

$$\mathbb{D} = \{n_1 - n_2 : n_1, n_2 \in \mathbb{S}\}, \tag{1.6}$$

where the integer $\mathbb{S}$ represents the sensor locations of an array normalized by d. A number of co-array based DOA estimators utilizing the difference co-array structure of a particular array have been developed in the past few decades including the augmented covariance matrix [38, 39], Toeplitz completion [40, 41], co-array MUSIC or spatial smoothing MUSIC [42], [26], [43], co-array interpolation [44–46], and Khatri Rao methods [47–49]. Some of the algorithms mentioned above are also applicable to ULA as long as their specific requirements are met by the structure of the difference co-array.

Sparse arrays are superior to ULA due to their ability to resolve more uncorrelated sources than sensors [26, 27, 40, 41, 50]. In addition to that, with sufficient amount of

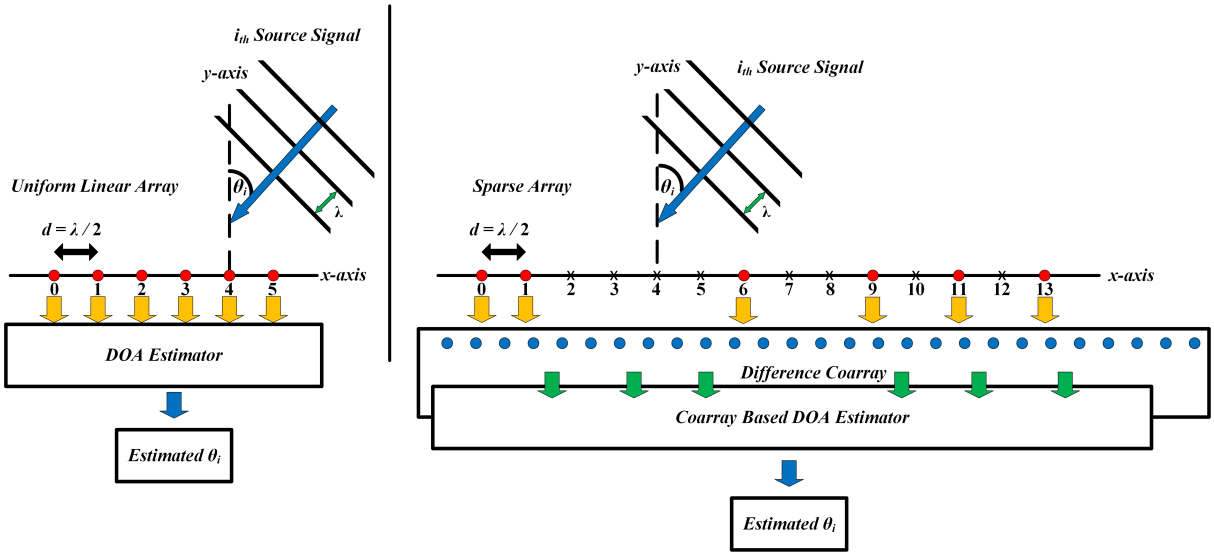

Figure 1.3: ULA and sparse array for DOA estimation.

data, sparse arrays typically provide better estimation performance and resolution than ULA [26, 27, 40, 41]. The key to these benefits of sparse arrays lies in the structure of their difference co-array. The differences contained in the difference co-array of a physical array correspond to the different lags at which the autocorrelation can be computed and are regarded as the degrees of freedom (DOF) provided by the array, which can be utilized by co-array based DOA estimators. The set of these lags in the difference co-array which are consecutive are of special interest to spatial smoothing based MUSIC. As will be shown later in Chapter 5, the array output from different sensors is used to build the covariance marix which is used for different parametric estimations.

Utilizing the difference co-array requires an extra step which involves vectorization of the covariance matrix [43] to achieve a virtual array. Then, the consecutive portion of the lags is extracted and the spatial smoothing technique [51–53] is applied for decorrelation to build a new covariance matrix, on which MUSIC based algorithms can be applied for DOA estimation. The more the set of consecutive lags resulting from the difference co-array, the more the number of sources estimated from spatial smoothing MUSIC. Although the use of a virtual array increases the DOFs and thereby the source detection capacity of an array, the application of spatial smoothing halves the utilizable DOFs [54]. An alternate approach is through sparse signal reconstruction by taking advantage of the fact that

the spatial spectra of signals is usually sparse. The application of recently developed compressive sensing (CS) techniques enables such sparse signal reconstruction [55], [56].

A number of sparse arrays have been proposed in the literature like minimum redundancy array (MRA) [50, 57], minimum hole array (MHA) [58], nested array [26] and its variant super nested array [59, 60], which have hole-free difference co-arrays implying difference co-arrays without any missing lags. As a co-array based DOA estimator like spatial smoothing MUSIC depends on the consecutive lags generated from the difference co-array, the above mentioned sparse arrays enjoy great application for this method. Another class of sparse arrays are proposed on the coprime nature of numbers termed coprime arrays [27]. The basic coprime array called prototype coprime array, its variant conventional coprime array [43] and generalized coprime array configurations [54] resulting in coprime array with compressed inter-element spacing (CACIS) and coprime array with displaced subarrays (CADiS), all share difference co-arrays with holes resulting in a combination of consecutive lags and total lags (consecutive and non consecutive) represented as unique lags. The unique lags of all kinds of arrays can be fully utilized with the application of CS based techniques. The sparse arrays mentioned above will all be covered in detail in Chapter 4. In the light of all this discussion on beamforming, DOA estimation, traditional arrays and sparse arrays, the original contributions of this thesis are presented in the next section.

1.2 Original Contributions

1. The classic eigenfilter method for fixed wideband beamformer design based on traditional arrays has been critically analyzed. It has been shown that the performance of the designed wideband beamformer is inconsistent with different scenarios. This inconsistency is then tracked down to a fault in the design formulation of the passband/look direction part of the cost function. The passband part of the cost function provides a mechanism for the desired flat passband response by minimizing the relative variation of the response between the reference frequency and other frequencies in the passband. However, it fails to control the absolute value of the passband/look

direction response of the beamformer, which is desired to be equal to unity gain. As a result, the designed wideband beamformer often takes a zero response at the passband/look direction which satisfies the original formulation, resulting in an overall design failure. A solution is proposed by adding a linear constraint which reinforces the designed passband/look direction response at the reference frequency point to achieve the desired response. As a result, the designed response consistently matches the desired response. To show a wider perspective, results are provided for different design scenarios based on FIR filter design and wideband beamformer design to demonstrate the crucial issue of the original formulation and the satisfactory performance by the proposed one [61].

2. Coprime arrays are a class of sparse arrays which have been used effectively for beamforming and DOA estimation under the difference co-array model. The flexibility to construct coprime arrays for arbitrary number of sensors, the inherent sparsity to tackle mutual coupling and provision of DOFs make these sparse arrays very exciting especially for parametric estimation. Different versions of coprime arrays exist with varying characteristics suitable for a specific design scenario. In this direction, a new sparse array termed thinned coprime array (TCA) is proposed, which retains all the properties of the conventional coprime array like aperture, consecutive lags and unique lags, but with $\lceil \frac{M}{2} \rceil$ fewer sensors where M and N are coprime numbers and the conventional coprime array has a total of $2M + N-1$ sensors [62]. For the same number of sensors, they possess greater number of unique lags than the hole-free structure of the nested array and nested CADiS, and comparable number of unique lags to the sparsest CADiS. The number of consecutive lags of the TCAs are around 75 percent to those of nested arrays which showcases their application in both spatial smoothing (SS) MUSIC and CS-based DOA estimation methods. Moreover, they can be easily constructed for an arbitrary number of sensors. TCAs have a significantly sparser array structure with robustness against severe mutual coupling especially when using CS-based DOA estimation. With the increasing array size, TCAs also offer better error performance in parameter estimates compared to super nested arrays and MRA for both CS and SS-MUSIC based methods in the

presence of mutual coupling.

3. The more the DOFs generated by a sparse array through its difference co-array, the lesser the parametric estimation error. In this direction, the structure of proposed TCA is investigated from the perspective of increasing unique lags which can be utilized by CS-based DOA estimation methods. The result is a new sparse array termed displaced thinned coprime array with additional sensor (DiTCAAS). The construction of DiTCAAS from TCA takes place in a two-step process where the second and third subarrays of TCA are displaced from their original position in the first step. This displacement of the subarrays generates an increase in the unique lags but the minimum spacing between the sensors becomes an integer multiple of half wavelength. To avoid spatial aliasing, an additional sensor is added at half wavelength from one of the sensors of the displaced third subarray in the second step. Two strategic locations are proposed for the placement of this additional sensor which generates significantly higher number of unique lags for DiTCAAS, even more than the DOFs provided by MRA. Due to its improved sparsity and higher number of unique lags, DiTCAAS shows the lowest estimation error and robustness to heavy mutual coupling compared to super nested arrays, MRA, proposed TCA and sparse CADiS. If a signal processing scenario allows for a relatively larger aperture, then DiTCAAS is the ideal sparse array for CS-based DOA estimation.

1.3 Scope and Outline of the Thesis

This thesis is divided into two major parts based on the contributions related to traditional arrays and sparse arrays. The first part includes Chapters 2 and 3, where Chapter 2 covers the underlying theory of traditional arrays, beamforming and different methods for fixed wideband beamformer design, and Chapter 3 presents the first contribution of this thesis on eigenfilters. The second part of the thesis revolves around sparse arrays and includes Chapters 4, 5 and 6. Chapter 4 reviews the different types of sparse arrays while Chapters 5 and 6 present the other two contributions of this thesis in the shape of two proposed sparse arrays, TCA and DiTCAAS, respectively. In the next section, the scope of each

Chapter will be introduced.

In Chapter 2, different techniques for fixed wideband beamformer design are reviewed. The chapter starts with some basics of wideband beamforming followed by a discussion on fixed and adaptive wideband beamformers. Fixed wideband beamformer design techniques like traditional methods, convex optimization and standard least squares are presented with a touch of least squares based eigenfilter design technique at the end.

In Chapter 3, the least squares based eigenfilter method is revisited for the design of FIR filter and wideband beamformer, where a critical analysis of the method is presented highlighting the problem with the formulation of the cost function in the passband/look direction followed by a proposed solution. Design examples are provided to show the problem with the original formulation and the consistent design performance achieved with the proposed solution for both FIR filters and wideband beamformers.

In Chapter 4, the discussion moves from the perspective of traditional arrays to sparse arrays. A brief introduction to sparse arrays is followed by definitions related to the concept of difference co-array model and underlying DOFs for consecutive and unique lags. Some perspective on mutual coupling and the concept of sparsity is presented followed by a detailed review of state of the art on sparse arrays like MRA, MHA, nested arrays, prototype coprime array, conventional coprime array, CACIS, CADiS, nested versions of CACIS and CADiS, and super nested arrays along with a discussion on each of their characteristics with examples.

In Chapter 5, TCA is proposed by analyzing the difference co-array model of conventional coprime array and proving the presence of a series of $\lceil \frac{M}{2} \rceil$ redundant sensors. It has been shown that TCA enjoys the same properties (aperture and difference co-array) as that of a conventional coprime array with significantly fewer sensors. A systematic procedure to construct a TCA for an arbitrary number of sensors is also presented. A detailed comparison of the DOFs (both consecutive and unique lags) provided by TCA in relation to other sparse arrays is presented to show the increased consecutive and unique lags for a given number of sensors, making TCA feasible for both SS-MUSIC and CS-based DOA estimation. The sparsity of TCA is investigated and it has been proved that TCA has very few sensor pairs with small separations ($\frac{\lambda}{2}$, λ, $\frac{3\lambda}{2}$), which shows the desir-

able trait of TCA to counter mutual coupling. The DOA performance of TCA in high levels of mutual coupling is investigated along with the error performance for a variety of scenarios in comparison to sparse arrays like super nested array, MRA and CADiS to show the superior performance of TCA.

In Chapter 6, the difference co-array structure of TCA proposed in Chapter 5 is further investigated to construct an array which can provide more DOFs for the same number of sensors. A detailed analysis paves the way for a new sparse array termed DiTCAAS based on the displacement of subarrays of TCA. An appropriate displacement of the two subarrays from their original position maximizes the possible unique lags for a given number of sensors. However, the minimum inter-element spacing becomes an integer multiple of half wavelength and makes the new structure vulnerable to spatial aliasing. By carefully adding another sensor at half wavelength from one of the sensors in the displaced subarray at any one of the two proposed locations, it has been shown that the number of unique lags can be significantly increased. DiTCAAS generates the highest number of unique lags for a given number of sensors compared to other sparse arrays as shown in the DOF comparison. Through the help of proven properties and simulation results, it is shown that DiTCAAS is much sparser than TCA and also achieves the lowest DOA estimation error among other sparse arrays in the presence of mutual coupling when CS-based DOA estimation is employed.

Finally, conclusions are drawn in Chapter 7 with recommended directions for future work.

Chapter 2

Review of Fixed Wideband Beamforming

2.1 Introduction

In this chapter, a general overview of wideband beamforming is presented followed by reviewing the existing design techniques for fixed wideband beamformers which include iterative optimization based methods and least squares based approaches. This chapter is organized as follows. Wideband beamforming is covered in Section 2.2 followed by the review of fixed wideband beamformer design methods in Section 2.3.

2.2 Wideband Beamforming

Wideband beamforming refers to the beamforming architecture deployed for processing wideband signals. Wideband signals are significant in our day to day communications. As the need for increased data capacity and high speeds arises with more and more consumers using bandwidth hungry applications based on video processing, wideband signals stand to answer this challenge. The increased bandwidth of wideband signals directly offers their application in high data rate provision to consumers. The task of performing beamforming on such signals requires the application of frequency dependent weights. The frequency dependent weights can be achieved with different types of architectures like

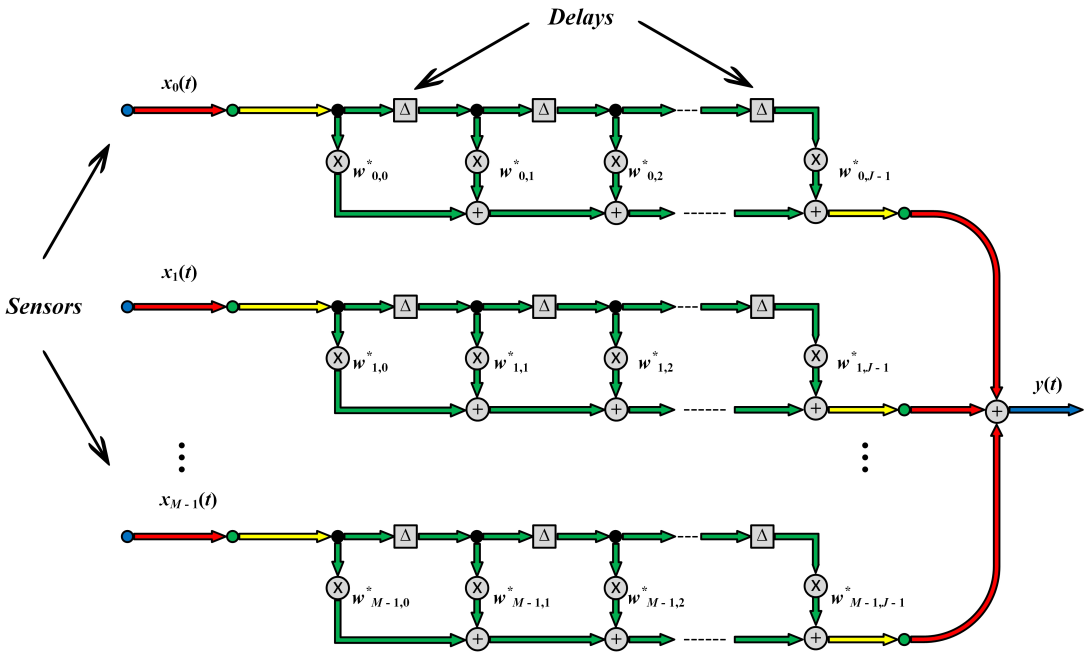

Figure 2.1: A general structure for wideband beamforming.

sensor delay-lines (SDL) [63]. Traditionally, an easy way to form such a set of frequency dependent weights is to use a series of tapped delay-lines(TDLs) or FIR/IIR filters in its discrete form [1]. Both TDLs and FIR/IIR filters perform a temporal filtering process to form a frequency dependent response for each of the received wideband sensor signals to compensate for the phase difference for different frequency components.

A wideband beamformer based on a TDL architecture is shown in Figure 2.1. This beamformer samples the propagating wave field in both space and time. The output of such a wideband beamformer can be expressed as

$$y(t) = \sum_{m=0}^{M-1} \sum_{i=0}^{J-1} x_m(t - iT_s) \times w^*_{m,i}\,, \tag{2.1}$$

where $J-1$ is the number of delay elements associated with each of the M sensor channels in Figure 2.1 and T_s is the delay between adjacent taps of the TDLs. In vector form (2.1) can be written as

$$y(t) = \mathbf{w}^H \mathbf{x}(t) \tag{2.2}$$

The weight vector $\mathbf{w}$ holds all MJ sensor coefficients with:

$$\mathbf{w} = [\mathbf{w}_0\, \mathbf{w}_1 \ldots \mathbf{w}_{J-1}]^H\,, \tag{2.3}$$

where each vector $\mathbf{w}_i$, $i = 0,\ 1,\ \ldots\ ,\ J-1$, contains the M *complex conjugate coefficients* found at the ith tap position of the M TDLs and is expressed as:

$$\mathbf{w}_i = [w_{0,i}\, w_{1,i} \ldots w_{M-1,i}]^T \tag{2.4}$$

Similarly, the input data are also accumulated in a vector form $\mathbf{x}$ as follows:

$$\mathbf{x} = [\mathbf{x}_0(t)\, \mathbf{x}_1(t - T_s) \ldots \mathbf{x}_{J-1}(t - (J-1)T_s)]^T\,, \tag{2.5}$$

where $\mathbf{x}_i(t - iT_s)$, $i = 0,\ 1,\ \ldots\ ,\ J-1$, holds the ith data slice corresponding to the ith coefficient vector $\mathbf{w}_i$:

$$\mathbf{x}(t - iT_s) = [x_0(t - iT_s)\, x_1(t - iT_s) \ldots x_{M-1}(t - iT_s)]^T \tag{2.6}$$

For an impinging complex plane wave signal $e^{j\omega t}$, assume $x_0(t) = e^{j\omega t}$. Then we have:

$$x_m(t - iT_s) = e^{j\omega(t-(\tau_m + iT_s))} \tag{2.7}$$

with $m = 0,\ 1,\ \ldots\ ,\ J-1$. The array output is given by

$$y(t) = e^{j\omega t} \sum_{m=0}^{M-1} \sum_{i=0}^{J-1} e^{-j\omega(\tau_m + iT_s)}.w_{m,i}^*\,, \tag{2.8}$$

$$= e^{j\omega t} \times P(\theta, \omega)\,, \tag{2.9}$$

where $P(\theta, \omega)$ is the beamformer's angle and frequency dependent response. It can be expressed in vector form as:

$$P(\theta, \omega) = \mathbf{w}^H \mathbf{d}(\theta, \omega)\,, \tag{2.10}$$

where $\mathbf{d}(\theta, \omega)$ is the steering vector for the wideband beamformer and its elements correspond to the complex exponentials $e^{-j\omega(\tau_m + iT_s)}$:

$$\mathbf{d}(\theta,\omega) = [e^{-j\omega\tau_0} \dots e^{-j\omega\tau_{M-1}}\, e^{-j\omega(\tau_0+T_s)} \dots e^{-j\omega(\tau_{M-1}+T_s)} \dots e^{-j\omega(\tau_0+(J-1)T_s)} \dots e^{-j\omega(\tau_{M-1}+(J-1)T_s)}]^T \tag{2.11}$$

For an equally spaced linear array with an inter-element spacing d, $\tau_m = m\tau_1$ and $\omega\tau_m = m(2\pi d sin\theta)/\lambda$ for $m = 0,\ 1,\ \dots,\ M-1$. To avoid aliasing, $d < \lambda_{min}/2$, where λ_{min} is the wavelength of the signal component with the highest frequency ω_{max}. Assume the operating frequency of the array is $\omega \in [\omega_{min}\, \omega_{max}]$ and $d = \alpha\lambda_{min}/2$ with $\alpha \leq 1$. In its discrete form, T_s is the temporal sampling period of the system and should be no more than half the period T_{min} of the signal component with the highest frequency according to the Nyquist sampling theorem, i.e. $T_s \leq T_{min}/2$.

With the normalized frequency $\Omega = \omega T_s$, $\omega\ (m\tau_1 + iT_s)$ changes to $m\mu\Omega \sin\theta + i\Omega$ with $\mu = d/(cT_s)$, and then the steering vector $\mathbf{d}(\theta,\omega)$ changes to:

$$\mathbf{d}(\theta,\omega) = [1 \dots e^{-j(M-1)\mu\Omega sin\theta}\, e^{-j\Omega} \dots e^{-j\Omega(\mu sin\theta(M-1)+1)} \dots e^{-j(J-1)\Omega} \dots e^{-j\Omega(\mu \sin\theta(M-1)+J-1)}]^T \tag{2.12}$$

Finally, the wideband beamformer's response as a function of angle and frequency is given as:

$$P(\theta,\omega) = \sum_{m=0}^{M-1} \sum_{i=0}^{J-1} e^{-j\Omega(m\mu \sin\theta+i)} \times w^*_{m,i} \tag{2.13}$$

Wideband beamformers depending upon the channel conditions can be classifed into fixed wideband beamformers and adaptive wideband beamformers. Fixed wideband beamformers have fixed values of weight coefficients irrespective of the channel conditions and the resultant beamformer will always maintain a fixed response independent of the signal/interference scenarios. Although such a beamformer may not be able to achieve a high output signal to interference plus noise ratio (SINR) as in the adaptive case, it has a lower computational complexity and can be implemented easily in real time. Additionally, for some very complicated situations, such as multipath, the adaptive beamformer may not work well [1] and a fixed beamformer may be the only viable choice when the main direction of the desired source signal is known.

Adaptive wideband beamformers on the other hand are statistically optimum beamformers where the weight coefficients are updated based on the statistics of the array data. When the data statistics are unknown or time varying, adaptive optimization is required where according to different signal environments and application requirements, different beamforming techniques may be employed [1].

This thesis will be focus on fixed wideband beamformers and will explore the methods used to design fixed wideband beamformers in the next section.

2.3 Fixed Wideband Beamformer Design Techniques

The fixed beamformer design problem is also called an array pattern synthesis problem and there are mainly two classes of design approaches for a fixed wideband beamformer. The first one is the iterative optimization approach, where many iterative optimization methods can be applied directly; the second one is the analytical approach, which includes the classical least squares formulation and the eigenfilter based solutions. The iterative optimization based design methods covered in this Chapter include traditional methods and convex optimization which will be discussed in the following section.

2.3.1 Traditional Methods

Given the desired beam pattern $P_d(\Omega, \theta)$, the design of a wideband beamformer meeting the desired response can be considered as a general optimization problem and solved by all kinds of iterative optimization methods. For example, the design can be formulated as a weighted Chebyshev approximation problem or a minmax problem [1]:

$$\min_{\mathbf{w}} \{ \max_{\Omega,\theta} v(\Omega, \theta) \mid \mathbf{w}^H \mathbf{d}(\Omega, \theta) - P_d(\Omega, \theta) \mid \}, \tag{2.14}$$

where $v(\Omega, \theta)$ is the weighting function with real positive values applied to the difference between the desired response $P_d(\Omega, \theta)$ and the designed response $P(\Omega, \theta) = \mathbf{w}^H \mathbf{d}(\Omega, \theta)$.

The cost function is evaluated on all values of Ω and θ within the frequency range of interest and the direction range of the impinging signals. Although it may not be necessary for some algorithms [1], in practice, Ω and θ can be discretized and the cost

function can be evaluated on a finite number of grid points as an approximation and the design problem is then changed to

$$\min_{\mathbf{w}}\{\max_{\forall i,j} v(\Omega_i,\theta_j) \mid \mathbf{w}^H\mathbf{d}(\Omega_i,\theta_j) - P_d(\Omega_i,\theta_j) \mid\}\,, \tag{2.15}$$

where the frequency range of interest is discretized into I_Ω points, Ω_i, $i = 0,\ 1,\ \ldots\ ,\ I_\Omega - 1$ and the direction range into J_θ points, $j = 0,\ 1,\ \ldots\ ,\ J_\theta - 1$.

The weight coefficients $\mathbf{w}$ can be obtained by a sequential quadratic programming method [1].

2.3.2 Convex Optimization

Recently, with the development of convex optimization techniques, especially the interior-point methods [9], convex optimization has become a popular and efficient tool for solving the wideband array pattern synthesis problem [64], [65]. An optimization problem is considered to be convex when both its objective function and its constraint functions are convex, expressed in the following general form:

$$\begin{aligned}
&\min_{\mathbf{w}} f_0(\mathbf{w}) \\
&\text{Subject to} f_i(\mathbf{w}) \le b_i \\
&i = 1,\ldots,m\,,
\end{aligned}$$

where the vector $\mathbf{w}$ represents a set of real-valued variables, $f_i(\mathbf{w})$, $i = 0,\ 1,\ \ldots\ ,\ m$, are convex functions and b_i is the upper bound for the corresponding constraint function. A function is said to be convex if it satisfies:

$$f_i(\alpha\mathbf{w}_1 + (1-\alpha)\mathbf{w}_2) \le \alpha f_i(\mathbf{w}_i) + (1-\alpha) f_i(\mathbf{w}_2) \tag{2.16}$$

for all real-valued α and real-valued vectors $\mathbf{w}_1$ and $\mathbf{w}_2$, which lie in the same space as $\mathbf{w}$, i.e. $\mathbf{w}_1$ and $\mathbf{w}_2$ are all of the possible values of $\mathbf{w}$. Examples of convex functions include the norms $|\mathbf{w}|$, $|\mathbf{w}|^2$ of the vector $\mathbf{w}$, and the quadratic vector function $\mathbf{w}^T\mathbf{R}\mathbf{w}$, where $\mathbf{R}$ is a symmetric positive semi-definite matrix.

It has been mentioned in [1] that most of the wideband array pattern synthesis problem can be reformulated into the convex form shown above and therefore can be solved efficiently employing the interior-point methods or other appropriate convex optimization algorithms.

For a design scenario, consider the design of a wideband linear array. Suppose the frequency range of interest is represented by $\Omega_{pb} = [\Omega_{min}\, \Omega_{max}]$ and the sidelobe area of the beamformer is denoted by Θ_{sl}. The look direction of the beamformer is θ_0 and the sidelobe area Θ_{sl} is discretized into into $J_\theta - 1$ points $(\theta_j, j = 1, \ldots, J_\theta - 1)$ and the frequency range Ω_{pb} into I_Ω points $(\Omega_i, i = 0,\ 1, \ldots, I_\Omega - 1)$. The aim is to minimize the maximum value of the beamformer response at the sidelobe area Θ_{sl} within the frequency range Ω_{pb} subject to the constraints that it has a distortion-less response at the look direction θ_0 over the whole frequency range Ω_{pb} i.e. a pure delay of T_0 which can be written as

$$\mathbf{C}(\Omega, \theta_0)^T \mathbf{w} = \mathbf{f}(\Omega), \tag{2.17}$$

where $\mathbf{C}(\Omega, \theta_0)^T$ is the steering matrix for the look direction and $\mathbf{f}(\Omega)$ is the desired distortion-less response vector with a pure delay T_0. Moreover, with a known direction θ_k of the possible interfering signals, the response of the beamformer can also be constrained at the direction θ_k to be smaller than a very small constant δ_k. Then this design problem can be formulated as

$$\begin{aligned}
&\min_{\mathbf{w}}\{\max\ |\mathbf{C}(\Omega_i, \theta_j)^T \mathbf{w}|\} \\
&i = 0, \ldots, I_\Omega - 1 \\
&j = 1, \ldots, J_\theta - 1 \\
&\text{Subject to } \mathbf{C}(\Omega_i, \theta_0)^T \mathbf{w} = \mathbf{f}(\Omega_i), i = 0, \ldots, I_\Omega - 1 \\
&|\mathbf{C}(\Omega_i, \theta_k)^T \mathbf{w}| < \delta_k, i = 0, \ldots, I_\Omega - 1
\end{aligned}$$

It can be solved conveniently using existing convex optimization toolboxes. It is also possible to design a wideband beamformer employing adaptive array techniques. The

basic idea is to simulate an environment with many interfering signals from different directions and then the optimum array coefficients with the desired pattern can be obtained after array adaptation to form a beam in the desired direction and low sidelobes at the interfering directions. Relevant work done in this regard can be found in [66] and [67].

2.3.3 Least Squares Approach

Although the fixed beamformer design problem can be solved using the iterative optimization approaches, they become less efficient for the case with a very large number of coefficients and cannot provide a closed form solution to the problem. There are two classes of analytical approaches which can provide such a closed-form solution: the least squares approach and the eigenfilter approach.

The least squares problem is a traditional subject and has been well-studied in the past [10] and [68]. Given the desired beam pattern $P_d(\Omega, \theta)$, the design mechanism tends to minimize the sum of the squares of the error between $P_d(\Omega, \theta)$ and the designed response $P(\Omega, \theta)$ over the frequency range Ω_{pb} and the range of signal arrival angle Θ:

$$\underset{\boldsymbol{w}}{\text{Min}} \quad \int_{\Omega_{pb}} \int_{\Theta} |P(\Omega,\theta) - P_d(\Omega,\theta)|^2 d\Omega d\theta \tag{2.18}$$

Weighting function can be added to $v(\Omega,\theta)$ to form a weighted least squares problem

$$\underset{\boldsymbol{w}}{\text{Min}} \quad \int_{\Omega_{pb}} \int_{\Theta} v(\Omega,\theta)|P(\Omega,\theta) - P_d(\Omega,\theta)|^2 d\Omega d\theta \tag{2.19}$$

This cost function can be expanded into the following form

$$J_{ls}(\boldsymbol{w}) = \int_{\Omega_{pb}} \int_{\Theta} v(\Omega,\theta)|P(\Omega,\theta) - P_d(\Omega,\theta)|^2 d\Omega d\theta \tag{2.20}$$

$$= \int_{\Omega_{pb}} \int_{\Theta} v(\Omega,\theta)(P(\Omega,\theta) - P_d(\Omega,\theta))(P(\Omega,\theta) - P_d(\Omega,\theta))^H d\Omega d\theta \tag{2.21}$$

$$= \int_{\Omega_{pb}} \int_{\Theta} v(\Omega,\theta)(|(P(\Omega,\theta)|^2 + |P_d(\Omega,\theta)|^2 - 2Re[P(\Omega,\theta)P_d^*(\Omega,\theta)])d\Omega d\theta \tag{2.22}$$

$$= \boldsymbol{w}^H \boldsymbol{G}_{ls} \boldsymbol{w} - \boldsymbol{w}^H \boldsymbol{g}_{ls}^- - \boldsymbol{g}_{ls}^{-H} \boldsymbol{w} + g_{ls} \tag{2.23}$$

For real valued $\boldsymbol{w}$,

$$= \boldsymbol{w}^H \boldsymbol{G}_{ls} \boldsymbol{w} - 2\boldsymbol{w}^H \boldsymbol{g}_{ls} + g_{ls} \tag{2.24}$$

where

$$\boldsymbol{G}_{ls} = \int_{\Omega_{pb}} \int_{\Theta} v(\Omega, \theta)(\boldsymbol{d}(\Omega, \theta)\boldsymbol{d}^H(\Omega, \theta)) d\Omega d\theta \tag{2.25}$$

$$= \int_{\Omega_{pb}} \int_{\Theta} v(\Omega, \theta)\boldsymbol{D}(\Omega, \theta) d\Omega d\theta \tag{2.26}$$

$$\boldsymbol{g}_{ls}^- = \int_{\Omega_{pb}} \int_{\Theta} v(\Omega, \theta)(\boldsymbol{d}(\Omega, \theta)P_d^*(\Omega, \theta)) d\Omega d\theta \tag{2.27}$$

$$\boldsymbol{g}_{ls} = \int_{\Omega_{pb}} \int_{\Theta} v(\Omega, \theta)(\boldsymbol{d}_R(\Omega, \theta)P_{d,R}(\Omega, \theta) + \boldsymbol{d}_I(\Omega, \theta)P_{d,I}(\Omega, \theta)) d\Omega d\theta \tag{2.28}$$

$$g_{ls} = \int_{\Omega_{pb}} \int_{\Theta} v(\Omega, \theta)|P_d(\Omega, \theta)|^2 d\Omega d\theta \tag{2.29}$$

where $\boldsymbol{d}_R(\Omega, \theta)$ and $P_{d,R}(\Omega, \theta)$ are real parts of $\boldsymbol{d}(\Omega, \theta)$ and $P_d(\Omega,\ \theta)$, while $\boldsymbol{d}_I(\Omega, \theta)$ and $P_{d,I}(\Omega, \theta))$ denote imaginary parts of $\boldsymbol{d}(\Omega, \theta)$ and $P_d(\Omega,\ \theta)$.

For real-valued $\boldsymbol{w}$, $\boldsymbol{G}_{ls}$ changes to

$$\boldsymbol{G}_{ls} = \int_{\Omega_{pb}} \int_{\Theta} v(\Omega, \theta)\boldsymbol{D}_R(\Omega, \theta) d\Omega d\theta \tag{2.30}$$

The solution to minimize the cost function J_{ls} with respect to the weight vectors $\boldsymbol{w}$ is given by standard least squares solution

$$\boldsymbol{w}_{opt} = \boldsymbol{G}_{ls}^{-1} \boldsymbol{g}_{ls} \tag{2.31}$$

For the frequency range of interest, Ω_{pb}, if the desired response $P_d(\Omega, \theta)$ is $e^{-j(T_0/T_s)\Omega}$ for the mainlobe area Θ_{ml}, zero for the sidelobe area Θ_{sl}, and the weighting function is α for the mainlobe and $(1\ -\alpha)$ for the sidelobe, then the cost function changes to:

$$\mathbf{G}_{ls} = \alpha \int_{\Omega_{pb}} \int_{\Theta_{ml}} \mathbf{D}_R(\Omega, \theta) d\Omega d\theta + (1 - \alpha) \int_{\Omega_{pb}} \int_{\Theta_{sl}} \mathbf{D}_R(\Omega, \theta) d\Omega d\theta \tag{2.32}$$

$$\mathbf{g}_{ls} = \alpha \int_{\Omega_{pb}} \int_{\Theta_{ml}} \left(\mathbf{d}_R(\Omega, \theta) \cos\left(\frac{T_0}{T_s}\Omega\right) - \mathbf{d}_I(\Omega, \theta) \sin\left(\frac{T_0}{T_s}\right) \right) d\Omega d\theta \tag{2.33}$$

$$g_{ls} = \alpha \int_{\Omega_{pb}} \int_{\Theta_{ml}} 1 d\Omega d\theta \tag{2.34}$$

It is also possible to add linear constraints to constrain the response of the beamformer at some specific directions or frequencies. These constraints can be either of equality or inequality. For linear equality constraints applied to the standard least squares method, a derivation for the closed-form expression of the solution is provided in [1].

2.3.4 Eigenfilter Approach

The solution to the standard least squares cost function involves matrix inversion to obtain the required weight vector. Since matrix inversion poses numerical instability with long filters [11] and is computationally intensive, another method was proposed which was termed as eigenfilter method. The term eigenfilter is referred to as a filter with its coefficients being the elements of an eigenvector [1]. The method is also based on the least squares approach and works by performing eigenvector decomposition of the cost function to extract the required weight vector in the form of an eigenvector.

This method has been explored for designing different types of filters and beamformers [69–74]. Moreover, this method has been specifically used for the design of linear-phase FIR Hilbert transformers and arbitrary order digital differentiators by Pei and Shyu [75, 76], who also investigated the design of arbitrary complex coefficient nonlinear-phase filters [77, 78]. Two-dimensional (2-D) extension to the eigenfilter method was proposed by Nashashibi and Charalambous [79], and later considered by Pei [80, 81]. Eigenfilters have also been used to design infinite impulse response (IIR) and all-pass filters [82, 83].

2.4 Summary

The general idea of wideband beamforming was reviewed in this chapter. First the general structure of wideband beamforming based on TDL was presented followed by detailed derivation of the wideband beamformer's response which will be used later in Chapter 3. Then fixed wideband beamformer design methods are reviewed based on iterative optimization and least squares. It has been shown that iterative optimization based methods like convex optimization become computationally intensive with increasing number of weight coefficients. This long computation time required by convex optimization also makes it non-practical for real time signal processing scenarios. These methods are also unable to provide closed form solutions/analytical solutions for the design problem. A solution to these limitations comes in the form of least squares based design, where the designed weight vector is achievable through an analytical solution. As the solution to the standard least squares based design involves matrix inversion to obtain the weight vector, this inversion poses the issue of numerical instability with increasing number of weight coefficients. Eigenfilter method is a least squares based method which provides the benefit of an analytical solution along with inversion-free expressions. This method will be reviewed in detail in Chapter 3 where a critical analysis of the design method is provided along with a solution to the observed problem.

Chapter 3

Critical Analysis of Eigenfilter Method for the Design of FIR Filter and Wideband Beamformer

3.1 Introduction

FIR filters and wideband beamformers have numerous applications ranging from SONAR, RADAR, audio processing, ultrasound imaging, radio astronomy, earthquake prediction, medical diagnosis, to communications, etc [1, 2]. Many optimization methods have been employed in the past to design FIR filters and wideband beamformers with required specifications [84, 85]. Iterative optimization based methods like convex optimization and least squares based methods have also been used for this purpose with their respective drawbacks as shown in Chapter 2. In this chapter, the least squares based eigenfilter method for designing FIR filters and wideband beamformers is revisited and a serious performance issue is revealed in the passband of the designed FIR filters and the mainlobe of the designed wideband beamformers in the light of an inherent design formulation flaw. An overall critical analysis of the performance of this approach is presented with the suggested modification for tackling this issue [86]. In particular, an additional constraint is imposed at the passband/mainlobe of the system to control the resultant responses.

This chapter is organized as follows. The eigenfilter based design formulation for FIR

filters and wideband beamformers along with the critical analysis is presented in Section 3.2. The proposed solution to the highlighted problem is given in Section 3.3. Design examples for different types of FIR filters and wideband beamformers affected by the problem are provided in Section 3.4 followed by results using the proposed solution.

3.2 Least Squares Based Design and Critical Analysis

In this section, the eigenfilter based design of FIR filter and wideband beamformer is presented and critical analysis is performed to highlight the underlying problem in the design formulation.

3.2.1 FIR Filter Design

Consider an $N-$tap FIR filter. Its frequency response $W(e^{j\omega})$ is given by

$$W(e^{j\omega}) = \sum_{n=0}^{N-1} w_n e^{-jn\omega}\,, \tag{3.1}$$

where w_n is the $n-$th tap/coefficient of the filter. In vector form, it can be expressed as

$$W(e^{j\omega}) = \mathbf{w}^H \mathbf{c}(\omega)\,, \tag{3.2}$$

where $\mathbf{w}$ is the $N \times 1$ weight vector holding the coefficients w_n, $n = 0, 1, \ldots, N-1$, and

$$\mathbf{c}(\omega) = \left[1, e^{-j\omega}, \cdots, e^{-j(N-1)\omega}\right]^T. \tag{3.3}$$

Now consider designing a lowpass filter as an example. The desired response $D(\omega)$ is given by

$$D(\omega) = \begin{cases} e^{-j\omega\frac{N-1}{2}}, & 0 \le \omega \le \omega_p \\ 0, & \omega_s \le \omega \le \pi \end{cases} \tag{3.4}$$

where $e^{-j\omega\frac{N-1}{2}}$ represents the desired linear phase at the passband with a delay of $\frac{N-1}{2}$ samples along with the desired stopband response equal to zero.

The design process involves formulating the cost function in the standard eigenfilter form, based on the Rayleigh-Ritz principle which states that for any Hermitian matrix $\mathbf{R}$, its Rayleigh-Ritz ratio is given by

$$\frac{\mathbf{w}^H\mathbf{R}\mathbf{w}}{\mathbf{w}^H\mathbf{w}}\,. \tag{3.5}$$

This ratio reaches its maximum/minimum when $\mathbf{w}$ is the eigenvector corresponding to the maximum/minimum eigenvalue of $\mathbf{R}$. The maximum and minimum values of this ratio are respectively the maximum and minimum eigenvalues. For FIR filter design, a reference frequency point was introduced by Nguyen in the passband region of the cost function to help represent it into the quadratic form as desired by (3.5) [70]. The cost function with the reference frequency point incorporated is given as

$$E = \frac{1}{\pi}\int_{\omega} v(\omega)\left|\frac{D(\omega)}{D(\omega_r)}W(e^{j\omega_r}) - W(e^{j\omega})\right|^2 d\omega\,, \tag{3.6}$$

where $v(\omega)$ is the weighting function and $D(\omega_r)$ and $W(e^{j\omega_r})$ represent the desired and designed responses at reference frequency, respectively. This expression can also be written as

$$\begin{aligned} E = \frac{1}{\pi}\int_{\omega} v(\omega)\left(\frac{D(\omega)}{D(\omega_r)}W(e^{j\omega_r}) - W(e^{j\omega})\right) \\ \left(\frac{D(\omega)}{D(\omega_r)}W(e^{j\omega_r}) - W(e^{j\omega})\right)^H d\omega \end{aligned} \tag{3.7}$$

For stopband, the desired response $D(\omega) = 0$. Substituting this value into the expression above

$$E_s = \frac{1}{\pi}\int_{\omega_s}^{\pi} v(\omega)W(e^{j\omega})W(e^{j\omega})^H d\omega\,. \tag{3.8}$$

Substituting the expression in (3.2) into (3.8), the expression further simplifies to

$$E_s = \frac{1}{\pi}\int_{\omega_s}^{\pi} v(\omega)\mathbf{w}^H\mathbf{c}(\omega)\mathbf{c}(\omega)^H\mathbf{w}d\omega\,. \tag{3.9}$$

Then (3.9) can be expressed as

$$E_s = \mathbf{w}^H\mathbf{P}_s\mathbf{w}\,, \tag{3.10}$$

where $\mathbf{P}_s$ is a symmetric, positive definite matrix of order N x N given by

$$\mathbf{P}_s = \frac{1}{\pi}\int_{\omega_s}^{\pi} v(\omega)\mathbf{c}(\omega)\mathbf{c}(\omega)^H d\omega\,. \tag{3.11}$$

The passband cost function is derived by incorporating the desired passband response $D(\omega) = e^{-j\omega\frac{N-1}{2}}$ into (3.7)

$$E_p = \frac{1}{\pi}\int_0^{\omega_p} v(\omega)\left(\frac{e^{-j\omega\frac{N-1}{2}}}{e^{-j\omega_r\frac{N-1}{2}}}W(e^{j\omega_r}) - W(e^{j\omega})\right) \left(\frac{e^{-j\omega\frac{N-1}{2}}}{e^{-j\omega_r\frac{N-1}{2}}}W(e^{j\omega_r}) - W(e^{j\omega})\right)^H d\omega\,. \tag{3.12}$$

After simplification,

$$E_p = \frac{1}{\pi}\int_0^{\omega_p} v(\omega)\mathbf{w}^H\left(e^{-j\frac{N-1}{2}(\omega-\omega_r)}\mathbf{c}(\omega_r) - \mathbf{c}(\omega)\right) \left(e^{-j\frac{N-1}{2}(\omega-\omega_r)}\mathbf{c}(\omega_r) - \mathbf{c}(\omega)\right)^H \mathbf{w}d\omega\,. \tag{3.13}$$

This expression can also be written as

$$E_p = \mathbf{w}^H\mathbf{P}_p\mathbf{w}\,, \tag{3.14}$$

where $\mathbf{P}_p$ is a symmetric, positive definite matrix of order N x N given by

$$\mathbf{P}_p = \frac{1}{\pi}\int_0^{\omega_p} v(\omega)\left(e^{-j\frac{N-1}{2}(\omega-\omega_r)}\mathbf{c}(\omega_r) - \mathbf{c}(\omega)\right) \left(e^{-j\frac{N-1}{2}(\omega-\omega_r)}\mathbf{c}(\omega_r) - \mathbf{c}(\omega)\right)^H d\omega\,. \tag{3.15}$$

The total cost function is a combination of the passband and stopband cost functions with a trade-off factor α

$$E = \alpha E_p + (1-\alpha)E_s\,, \qquad 0 \le \alpha \le 1\,, \tag{3.16}$$

which can be transformed into

$$E = \mathbf{w}^H\mathbf{P}\mathbf{w}\,, \tag{3.17}$$

where

$$\mathbf{P} = \alpha\mathbf{P}_p + (1-\alpha)\mathbf{P}_s, 0 \le \alpha \le 1\,. \tag{3.18}$$

The weighting function $v(\omega)$ is a frequency dependent weighting function for passband and stopband part of the cost function of filter design. It is interchangable with the trade-off parameter α which varies in the range $0 \le \alpha \le 1$, where a value of α for passband will correspond to a value of $1-\alpha$ for the stopband. As a result, this parameter α provides a trade-off between the flatness in the passband of a filter and attenuation in the stopband.

Combining (3.11) and (3.15) in (3.18) and taking the real part

$$\begin{aligned}\mathbf{P} = \alpha \int_0^{\omega_p} \mathbf{Re}[&\Big(e^{-j\frac{N-1}{2}(\omega-\omega_r)}\mathbf{c}(\omega_r) - \mathbf{c}(\omega)\Big) \\ &\Big(e^{-j\frac{N-1}{2}(\omega-\omega_r)}\mathbf{c}(\omega_r) - \mathbf{c}(\omega)\Big)^H]d\omega \\ &+(1-\alpha)\int_{\omega_s}^{\pi} \mathbf{Re}[\mathbf{c}(\omega)\mathbf{c}(\omega)^H]d\omega\,.\end{aligned} \tag{3.19}$$

The solution rests in finding the eigenvector $\mathbf{w}$ corresponding to the minimum eigenvalue of $\mathbf{P}$ which minimizes E. The norm constraint $\mathbf{w}^H\mathbf{w} = 1$ is also incorporated to avoid trivial solution. The final expression of solution for the eigenfilter based FIR filter design problem is given by

$$\underset{\mathbf{w}}{\text{Min}} \quad \frac{\mathbf{w}^H\mathbf{P}\mathbf{w}}{\mathbf{w}^H\mathbf{w}} \tag{3.20}$$

After investigating the designed filter's performance, it is found that although the design performs well for most of the cases with varying specifications for short filters, it produces ever increasingly inconsistent results as the number of filter taps increases for the same set of specifications. With those longer filters, the passband performance starts varying and switches from one case with flatness around near unity gain to another case with flatness achieved at almost zero magnitude.

This unstable performance can be attributed to the formulation in (3.19) where the first part of the cost function measures the difference between the filter's response at the reference frequency ω_r and those at the other frequencies ω in the passband. The term $e^{-j\frac{N-1}{2}(\omega-\omega_r)}$ compensates for different phase shifts of the response at different frequencies. This expression minimizes the relative variation of the filter's response at different passband frequencies and ensures a flat passband response. However, there is no control over the absolute value of the filter's response in passband, allowing any type of flat passband response with arbitrary absolute magnitude leading to inconsistent design performance.

3.2.2 Wideband Beamformer Design

Consider a wideband beamformer with TDLs or FIR filters as previously shown in Figure 2.1, where J is the number of delay elements associated with each of the M sensors. Its response as a function of signal angular frequency ω and direction of arrival θ is given by

[1]

$$P(\omega,\theta)=\sum_{m=0}^{M-1}\sum_{k=0}^{J-1}w_{m,k}e^{-j\omega(\tau_m+kT_s)}\,, \tag{3.21}$$

where T_s is the delay between adjacent taps of the TDL and τ_m is the spatial propagation delay between the $m-th$ sensor and the reference sensor. (3.21) can be expressed as

$$P(\omega,\theta)=\mathbf{w}^T\mathbf{d}(\omega,\theta)\,, \tag{3.22}$$

where $\mathbf{w}$ is the coefficient vector

$$\mathbf{w}=\left[w_{0,0},\cdots w_{M-1,0},\cdots w_{0,J-1},\cdots,w_{M-1,J-1}\right]^T \tag{3.23}$$

and $\mathbf{d}(\omega,\theta)$ is the M x J steering vector

$$\mathbf{d}(\omega,\theta)=\mathbf{d}_{Ts}(\omega)\otimes\mathbf{d}_{\tau_m}(\omega,\theta)\,, \tag{3.24}$$

with $\otimes$ denoting the Kronecker product. The terms $\mathbf{d}_{Ts}(\omega)$ and $\mathbf{d}_{\tau_m}(\omega,\theta)$ are defined as

$$\mathbf{d}_{Ts}(\omega)=\left[1,e^{-j\omega T_s},\cdots,e^{-j(J-1)\omega T_s}\right]^T \tag{3.25}$$

$$\mathbf{d}_{\tau_m}(\omega,\theta)=\left[e^{-j\omega\tau_0},e^{-j\omega\tau_1},\cdots,e^{-j\omega\tau_{M-1}}\right]^T. \tag{3.26}$$

For a uniform linear array (ULA) with an inter-element spacing d, and angle θ measured from the broadside, the spatial propagation delay τ_m is given by $\tau_m=m\tau_1=\frac{md\sin\theta}{c}$. With normalized angular frequency, $\Omega=\omega T_s$, and $\mu=\frac{d}{cT_s}$, the steering vector is given by

$$\mathbf{d}(\Omega,\theta)=\mathbf{d}_{T_s}(\Omega)\otimes\mathbf{d}_{\tau_m}(\Omega,\theta) \tag{3.27}$$

$$\mathbf{d}_{T_s}(\Omega)=\left[1,e^{-j\Omega},\cdots,e^{-j(J-1)\Omega}\right]^T \tag{3.28}$$

$$\mathbf{d}_{\tau_m}(\Omega,\theta)=\left[1,e^{-j\mu\Omega sin\theta},\cdots,e^{-j(M-1)\mu\Omega sin\theta}\right]^T \tag{3.29}$$

Then (3.22) is represented as a function of Ω and θ, given by

$$P(\Omega,\theta)=\mathbf{w}^T\mathbf{d}(\Omega,\theta) \tag{3.30}$$

The desired response for the wideband beamformer is represented by $P_d(\Omega,\theta)$. Then, the eigenfilter based cost function can be expressed as

$$\begin{aligned}J_{ef}(\mathbf{w})=\int_{\Omega_{pb}}\int_{\Theta}v(\Omega,\theta)\\ \left|P(\Omega,\theta)-P(\Omega_r,\theta_r)\frac{P_d(\Omega,\theta)}{P_d(\Omega_r,\theta_r)}\right|^2 d\Omega d\theta\end{aligned} \tag{3.31}$$

where (Ω_r, θ_r) is the reference point. This expression can be changed into

$$J_{ef}(\mathbf{w}) = \mathbf{w}^H \mathbf{G}_{ef} \mathbf{w}\,, \tag{3.32}$$

where

$$\begin{aligned} \mathbf{G}_{ef} = \int_{\Omega_{pb}} \int_{\Theta} v(\Omega, \theta) \\ \left(\mathbf{d}(\Omega, \theta) - \mathbf{d}(\Omega_r, \theta_r) \frac{P_d(\Omega, \theta)}{P_d(\Omega_r, \theta_r)} \right) \\ \left(\mathbf{d}(\Omega, \theta) - \mathbf{d}(\Omega_r, \theta_r) \frac{P_d(\Omega, \theta)}{P_d(\Omega_r, \theta_r)} \right)^H d\Omega d\theta \end{aligned} \tag{3.33}$$

Consider a typical design case with desired sidelobe response equal to zero and response at look direction θ_0 given by $e^{-j\frac{J}{2}\Omega}$ equal to a pure delay; Ω_r and Ω_{pb} represent the reference frequency and passband frequency range, respectively, and α is the weighting factor for the mainlobe. The expression in (3.33) is modified accordingly for real-valued beamformer coefficients and given by

$$\begin{aligned} \mathbf{G}_{ef} = \alpha \int_{\Omega_{pb}} \mathbf{Re}[\Big(\mathbf{d}(\Omega, \theta_0) - e^{-j\frac{J}{2}(\Omega - \Omega_r)} \mathbf{d}(\Omega_r, \theta_r) \Big) \\ \Big(\mathbf{d}(\Omega, \theta_0) - e^{-j\frac{J}{2}(\Omega - \Omega_r)} \mathbf{d}(\Omega_r, \theta_r) \Big)^H] d\Omega \\ + (1 - \alpha) \int_{\Omega_{pb}} \int_{\Theta_{sl}} \mathbf{Re}[\mathbf{d}(\Omega, \theta) \mathbf{d}(\Omega, \theta)^H] d\Omega d\theta \end{aligned} \tag{3.34}$$

Then, the solution to the wideband beamformer design problem is given by

$$\min_{\mathbf{w}} \quad \frac{\mathbf{w}^H \mathbf{G}_{ef}(\Omega, \theta) \mathbf{w}}{\mathbf{w}^H \mathbf{w}} \tag{3.35}$$

Similar to the FIR filter design case, testing of the designed wideband beamformer through the eigenfilter method showed an inconsistent design performance. The design performed well for some look directions, while attained a very poor response for other look directions.

This variable nature of look direction response for the same set of specifications can again be traced back to the design formulation in (3.34), where the first part of the expression calculates the difference between the beamformer response at reference point (Ω_r, θ_r) and those at other frequencies in the look direction θ_0 . The term $e^{-j\frac{J}{2}(\Omega - \Omega_r)}$ compensates for the different phase shifts experienced by the wideband signal at different frequencies.

The formulation ensures minimzation of the relative error at the look direction for different frequencies, thus providing flat response at θ_0. However, just like the FIR filter case, there is a lack of control for exact response in the look direction which can lead to design failure.

3.3 Proposed Solution with an Additional Constraint

As shown in our analysis of the eigenfilter design for both FIR filters and wideband beamformers in Section 3.2, the key issue is its lack of control of the achieved response at the passband/look direction compared to the desired one in the formulation. To solve this problem, an additional constraint is added to the formulation to specify the required response explicitly at the reference point. Since the original formulation will minimize the variation of the achieved response in the passband/look direction, the explicit control of the response of the designed filter/beamformer at one reference point of the passband/look direction will guarantee the design reaches the desired response for the whole considered passband/look direction region with a minimum overall error.

Now, constraining the reference frequency response to unity by adding a linear constraint to (3.20) gives us the following modified design formulation

$$\min_{\mathbf{w}} \quad \mathbf{w}^H \mathbf{P} \mathbf{w} \text{ Subject to } \mathbf{C}^H \mathbf{w} = \mathbf{f}, \tag{3.36}$$

where the constraint matrix $\mathbf{C}$ and the response vector $\mathbf{f}$ provide the required constraint on the weight vector $\mathbf{w}$, so that the resultant design can have the required exact response at the reference frequency. The constraint matrix $\mathbf{C}$ in its most basic form corresponds to the real and imaginary parts of the reference frequency vector, where the response for this reference frequency vector in the passband of a filter or the look direction of a wideband beamformer is constrained to a fixed desired response with its real and imaginary parts contained in the response vector $\mathbf{f}$.

For example, consider the design of a lowpass filter. In order to provide correction for the original formulation flaw, a constraint is imposed for the filter passband response at the reference frequency to be equal to the desired response with unity gain magnitude

and linear phase. For a reference frequency $\omega_r = 0$, $\mathbf{c}(\omega)$ in (3.3) changes to

$$\mathbf{c}(\omega_r) = [1, 1, \cdots, 1]^T . \tag{3.37}$$

Then, the constraint matrix $\mathbf{C}$ just becomes a constraint vector with $\mathbf{C} = \mathbf{c}(\omega_r)$ with the response vector $\mathbf{f}$ containing the desired unity gain as the response of the filter at $\omega_r = 0$ represented by

$$\mathbf{c}(\omega_r)^H \mathbf{w} = \mathbf{f}, \tag{3.38}$$

which is simply

$$[1, 1, \cdots, 1]\mathbf{w} = 1 . \tag{3.39}$$

This constraint will make sure that the designed response of the filter at the reference frequency in the passband is equal to the desired response. As the original formulation will minimize the variation in the response achieved at other frequencies in the passband with respect to the reference frequency, the overall designed response in the passband will be equal to the desired response, thus solving the original formulation problem.

Note that other constraints can also be added to the formulation of $\mathbf{C}$ and $\mathbf{f}$ so that more flexible constraints can be imposed on the design. For example, a constraint can be added to make sure the resultant design has an exact zero response at some stopband frequencies.

The solution to (3.36) can be obtained by the Lagrange multipliers method and it is given by

$$\mathbf{w}_{opt} = \mathbf{P}^{-1}\mathbf{C}(\mathbf{C}^H\mathbf{P}^{-1}\mathbf{C})^{-1}\mathbf{f} \tag{3.40}$$

For the wideband beamformer design, the modified problem is given by

$$\underset{\mathbf{w}}{\text{Min}} \quad \mathbf{w}^H\mathbf{G}_{ef}\mathbf{w} \text{ Subject to } \mathbf{C}^H\mathbf{w} = \mathbf{f}, \tag{3.41}$$

where $\mathbf{C}$ and $\mathbf{f}$ again correspond to the constraint matrix and response vector, respectively. For the wideband beamformer case, just like the filter design scenario, this constraint matrix will correspond to the reference frequency steering vector, where $\mathbf{C} = \mathbf{d}(\Omega_r, \theta_r)$.

By constraining the response of the wideband beamformer at this reference frequency steering vector equal to the desired response $e^{-j\frac{J}{2}\Omega_r}$ as

$$\mathbf{d}(\Omega_r, \theta_r)^H \mathbf{w} = e^{-j\frac{J}{2}\Omega_r} , \tag{3.42}$$

the overall response of the wideband beamformer at the look direction for different frequencies will be equal to the desired response, thus mitigating the initial formulation problem. The solution to (3.41) is then given by

$$\mathbf{w}_{opt} = \mathbf{G}_{ef}^{-1}\mathbf{C}(\mathbf{C}^H\mathbf{G}_{ef}^{-1}\mathbf{C})^{-1}\mathbf{f} \tag{3.43}$$

Note that there are matrix inversion operations in (3.40) and (3.43), which can be computationally intensive for larger filters and beamformers. However, there are other approaches available in literature e.g. null space based methods to solve (3.36) and (3.41) avoiding the need to compute matrix inversion [1].

Now, the null space method is presented to solve the proposed constrained eigenfilter problem. Here the wideband beamformer perspective is considered to solve (3.41). The same concept can be applied to solve the FIR filter design case for the proposed method in (3.36). The solution of constrained eigenfilter problem in (3.41) can be obtained by first transforming the constraint $\mathbf{C}^H\mathbf{w} = \mathbf{f}$ into the form

$$\hat{\mathbf{C}}^H\mathbf{w} = \mathbf{0} \tag{3.44}$$

with:

$$\hat{\mathbf{C}} = \mathbf{C} - \frac{\mathbf{d}(\Omega_r, \theta_r)}{P(\Omega_r, \theta_r)}\mathbf{f}^H \tag{3.45}$$

To meet this constraint equation, $\mathbf{w}$ must lie in the null space of $\hat{\mathbf{C}}$. Suppose $\tilde{\mathbf{C}}$ is a unitary matrix with its columns being the bases of the null space. Then $\mathbf{w} = \tilde{\mathbf{C}}\tilde{\mathbf{w}}$ and the problem is reduced to finding the new unknown vector $\tilde{\mathbf{w}}$ in the following minimizing problem:

$$\underset{\tilde{\mathbf{w}}}{\text{Min}} \quad \tilde{\mathbf{w}}^H\tilde{\mathbf{C}}^H\mathbf{G}_{ef}\tilde{\mathbf{C}}\tilde{\mathbf{w}} \tag{3.46}$$

This is again a standard eigenfilter problem and the optimum $\tilde{\mathbf{w}}$ is the eigenvector corresponding to the smallest eigenvalue of the matrix $\tilde{\mathbf{C}}^H\mathbf{G}_{ef}\tilde{\mathbf{C}}$. By obtaining $\tilde{\mathbf{w}}$, the required weight vector is given by $\mathbf{w} = \tilde{\mathbf{C}}\tilde{\mathbf{w}}$.

3.4 Design Examples

In this section, design examples are provided to show the inconsistent performance produced by the original unconstrained eigenfilter design method. The examples are then re-designed through the proposed constrained eigenfilter method to show the improvement.

3.4.1 Unconstrained Eigenfilter Design

First, the lowpass filter design scenario is considered where the whole frequency range from $[0, \pi]$ was discretized into 400 points. The design specifications include the passband from [0, 0.5π] and stopband from [0.8π, π]. A 70-tap filter with trade-off parameter $\alpha = 0.97$ and reference frequency at 0.35π is then designed using the original formulation. The result is shown in Fig. 3.1 in blue colour (solid curve) with a clearly satisfactory design performance showing a passband to stopband ratio of 140 dB.

In the second case, the number of taps is changed to 76, while keeping all the other specifications the same as the first case. The result is shown in Fig. 3.1, highlighted in dashed curve with red colour. It can be seen that the passband response is out of control, with a flat response of around -118 dB, and the resulting ratio between passband and stopband is just around 19 dB (if ignoring the unacceptable response at the transition band), clearly highlighting the problem with the original formulation.

For highpass filters, again two cases are presented. For the first case, an 81-tap filter is considered, where the design specifications include a stopband from [0, 0.4π] and passband from [0.7π, π]. The tradeoff factor $\alpha = 0.71$ and the reference frequency is set to 0.74π. The result is depicted in Fig. 3.2 with solid curve and blue colour, where a very satisfactory design performance can be observed with a passband to stopband ratio of 150 dB.

For the second case, the reference frequency is changed to 0.94π and the result is shown in Fig. 3.2 with dashed red colour, which is without any doubt unacceptable, with a passband response at around -130 dB leaving a passband to stopbad ratio of only 15 dB. The results for lowpass and highpass filter design examples clearly demonstrate the magnitude of the problem at hand for different arbitrary design scenarios.

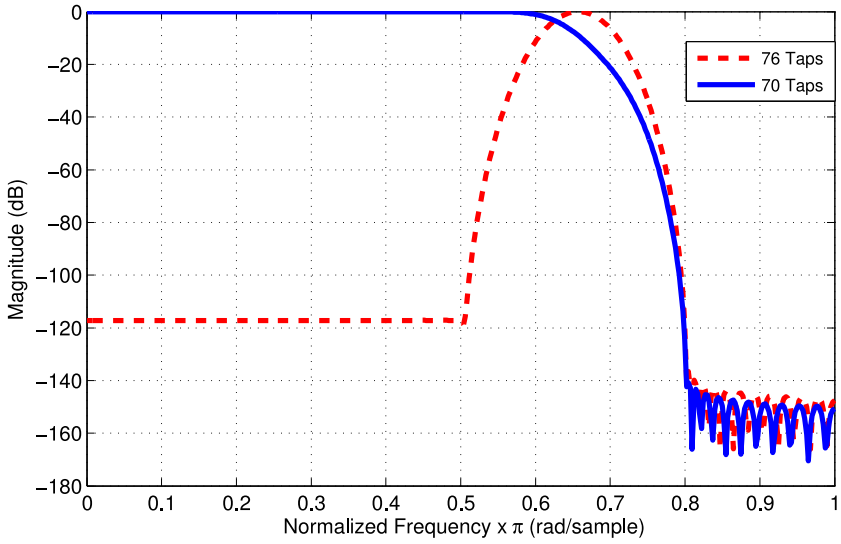

Figure 3.1: The designed lowpass FIR filters using the original formulation.

Now this observation can be extended to the design of bandpass filters to see if the same problem can be observed in those filters as well.

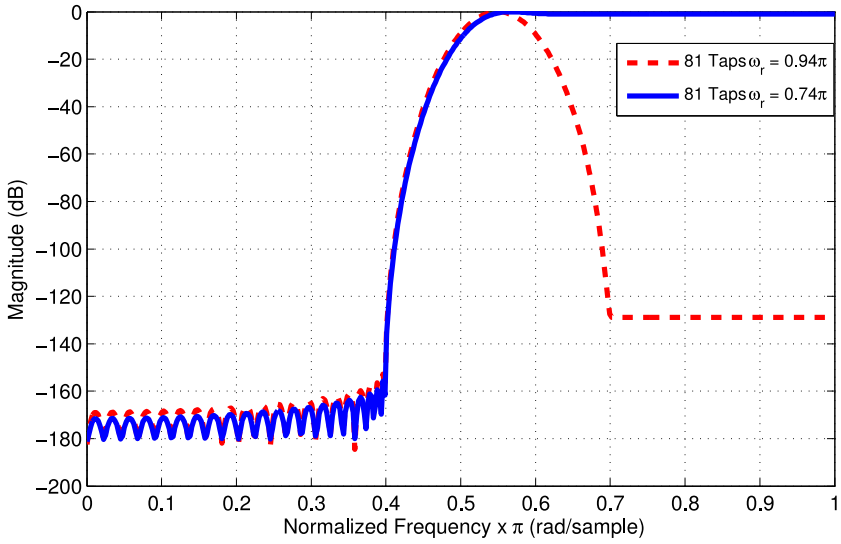

Figure 3.2: The designed highpass FIR filters using the original formulation.

For the bandpass filter design scenario, again two cases are considered for comparison. For the first case, 91 taps are considered, where the design specifications include the first stopband from $[0,\ 0.15\pi]$, passband from $[0.35\pi,\ 0.65\pi]$ and the second stopband from $[0.85\pi,\ \pi]$. The tradeoff factor $\alpha = 0.96$ and the reference frequency is set to 0.55π. The

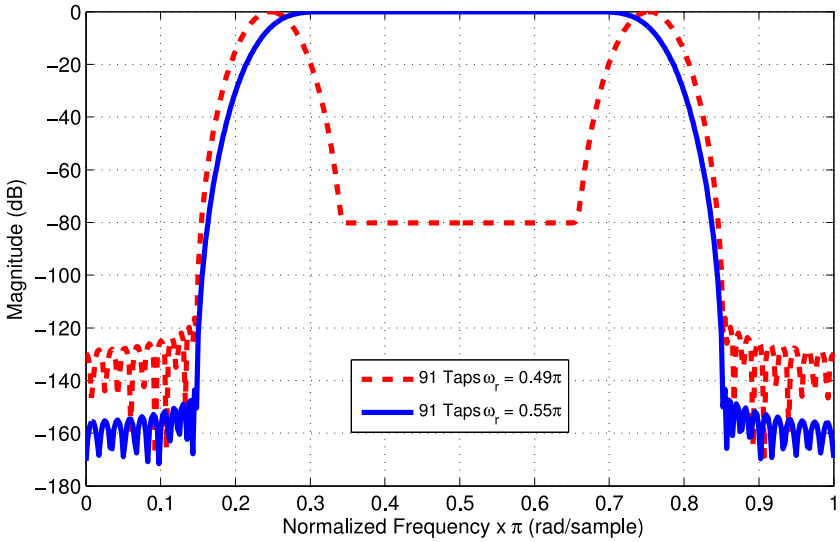

Figure 3.3: The designed bandpass FIR filters using the original formulation.

satisfactory design result is shown in Fig. 3.3 with solid curve and blue colour, where a suitable passband to stopband ratio of 145 dB can be observed.

For the second case, the reference frequency is changed to 0.49π, while keeping the remaining specifications similar to the first case and the result is shown with dashed red colour, where it can be seen that the flat passband again has dropped to a very low unacceptable magnitude of -80 dB with a passband to stopband ratio of 36 dB, providing further evidence for the kind of inconsistent results caused by the flawed design formulation.

For the wideband beamformer design, an array with 10 sensors is considered with a TDL length of 10 taps. The look direction is chosen as an off-broadside direction of $\theta_0 = 10^\circ$ with the desired response equal to $e^{-j5\Omega}$. The considered wideband signal has a frequency range of $\Omega_{pb} = [0.4\pi, \pi]$ with the reference frequency $\Omega_r = 0.7\pi$ and $\theta_r = 10^\circ$ chosen as the reference point. The weighting function is set to $\alpha = 0.6$ at the look direction and 0.4 at the sidelobe region, which runs from -90^0 to -10^0 and 30^0 to 90^0. The frequency range is discretized into 20 points, while the angle range is divided into 360 points.

The result is shown in Fig. 3.4(a), where a satisfactory design performance is achieved with the look direction to sidelobe ratio around 20 dB. The same scenario is again tested

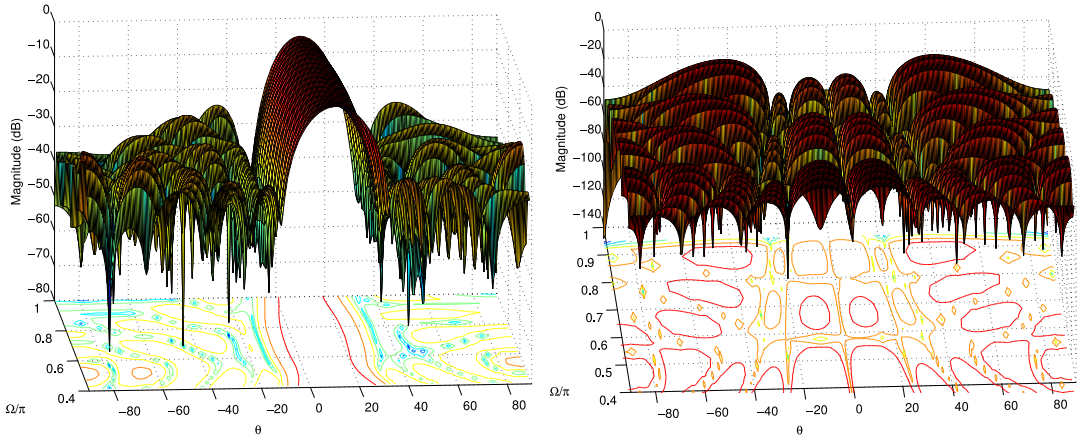

(a) $\theta_0 = 10^0$ **(b)** $\theta_0 = 0^0$

Figure 3.4: The designed wideband beamformer using the original formulation with 10 sensors and 10 taps.

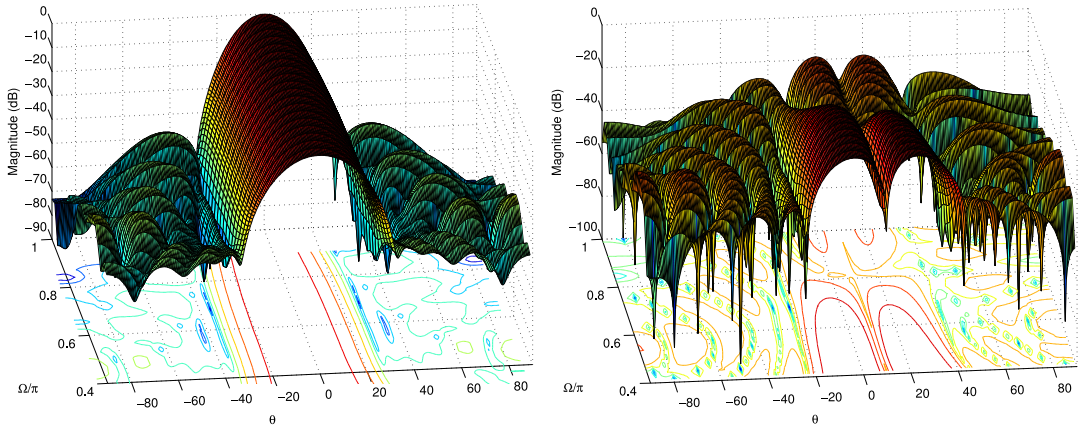

(a) $\theta_0 = 0^0$ **(b)** $\theta_0 = 10^0$

Figure 3.5: The designed wideband beamformer using the original formulation with 11 sensors and 10 taps.

by changing the look direction to the broadside of $\theta_0 = 0^0$ with the sidelobe region ranging from -90^0 to -20^0 and 20^0 to 90^0 with the remaining specifications unchanged. The result is shown in Fig. 3.4(b), where it can be observed that the look direction response plunges to -40 dB with a flat response attained, which is even lower than the sidelobes.

Another example is provided for a scenario where an 11-sensor array is considered with a TDL structure of 10 taps. For the first case, the look direction is chosen as the broadside direction with $\theta_0 = 0^\circ$ and the desired response equal to $e^{-j5\Omega}$. For the design specifications, the considered wideband signal has a frequency range of $\Omega_{pb} = [0.4\pi, \pi]$ with the reference frequency $\Omega_r = 0.7\pi$ and $\theta_r = 10^\circ$ chosen as the reference point. The weighting function is the same as the previous example and the sidelobe region is from -90^0 to -30^0 and 30^0 to 90^0. The result is shown in Fig. 3.5(a), where a satisfactory design response is achieved with a look direction to sidelobe response ratio of 40 dB. For the second case, the look direction is changed to an off-broadside direction of $\theta_0 = 10^\circ$ with the sidelobe ranging from -90^0 to -20^0 and 40^0 to 90^0 with the remaining specifications unchanged. The result is shown in Fig. 3.5(b), where the look direction response again has no absolute control and achieves flatness around -30 dB with the resulting look direction response even lower than the sidelobes, again demonstrating the presence of this problem in a wide range of design scenarios.

It is worth noting that the reference points in the eigenfilter based FIR filter and wideband beamformer design simulations are chosen by searching out the entire passband frequency range and different look directions (in the case of wideband beamformer) while observing any anomalies in the design results with no control in the magnitude of passband response.

3.4.2 Constrained Eigenfilter Design

Now the constrained eigenfilter formulation in (3.36) is applied to design the lowpass, highpass and bandpass filters presented using unconstrained design formulation. The new results are presented in Figs. 3.6, 3.7 and 3.8. Although there is still a noticeable bump in the transition band for the design results in Figs. 3.6 and 3.7 for lowpass and highpass, respectively, the overall response has improved significantly compared to the

results in Figs. 3.1 and 3.2. The bandpass filter designed with the new formulation in Fig. 6.3(c) achieves a very satisfactory response compared to the result in Fig. 3.3.

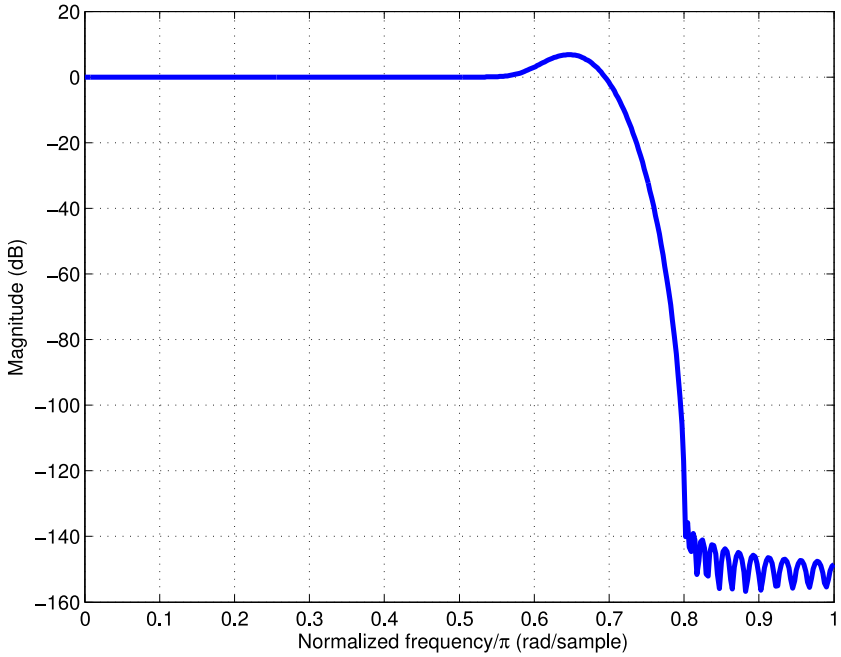

Figure 3.6: Lowpass FIR filter using the constrained design

The beamformer designs presented in Figs. 3.4(b) and 3.5(b) are re-designed using the constrained formulation in (3.41) and the result is provided in Figs. 3.9 and 3.10, where the look direction response has improved significantly with a decent look direction to sidelobe ratio achieved as per the desired specifications.

Various designs for different types of filters and wideband beamformers have been tried with varying design specifications and the proposed method has been found to perform consistently well in different scenarios.

3.5 Summary

The classic eigenfilter approach has been revisited and critically analyzed, where a formulation problem is highlighted in the passband/look direction part of the cost function which leads to an inconsistent design performance. A solution was then proposed by adding a linear constraint, explicitly setting the designed passband response at the refer-

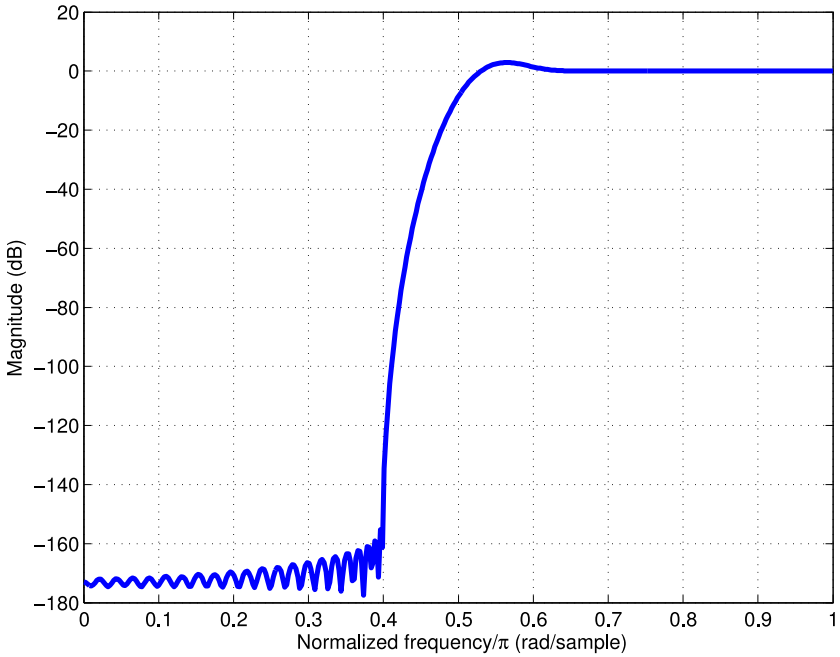

Figure 3.7: Highpass FIR filter using the constrained design

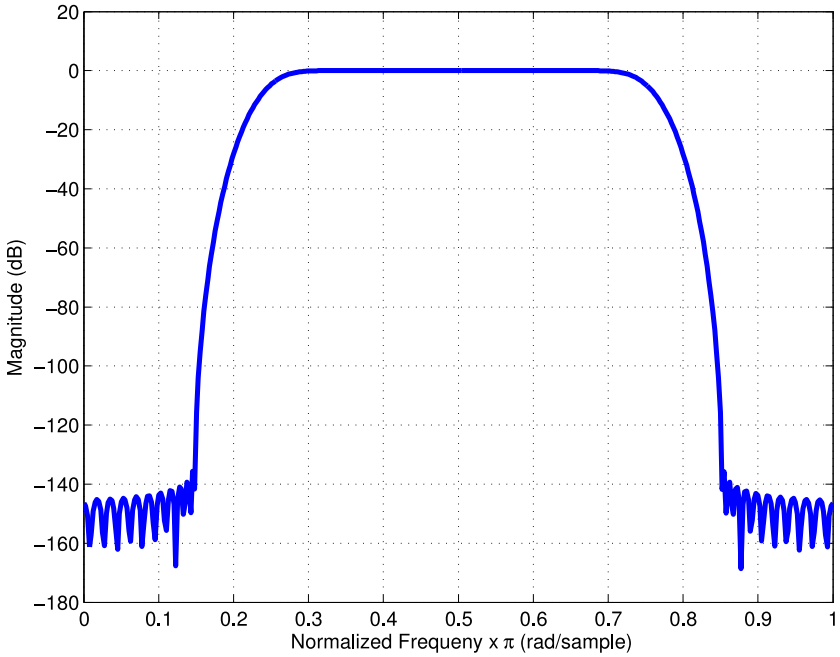

Figure 3.8: Bandpass FIR filter using the constrained design

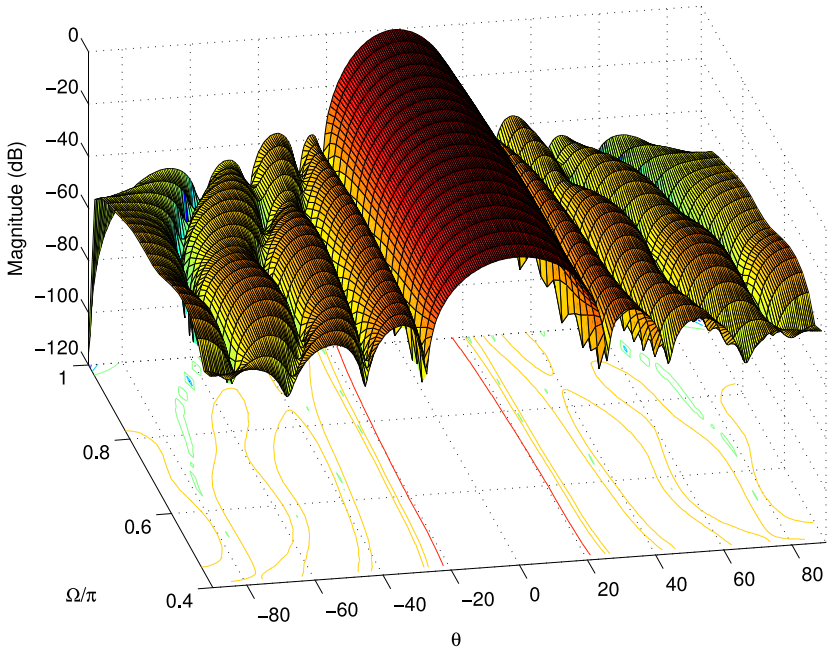

Figure 3.9: The designed wideband beamformer with $\theta_0 = 0^0$.

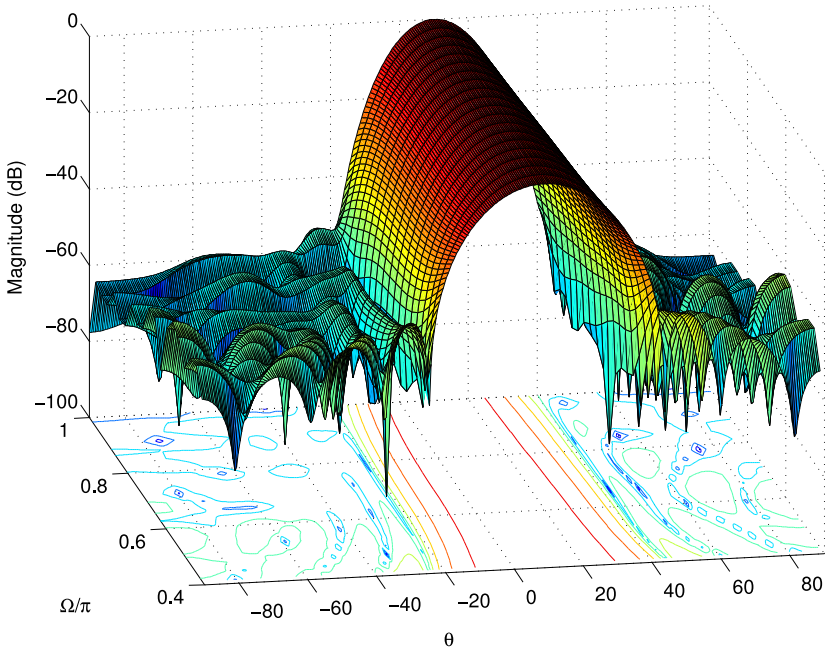

Figure 3.10: The designed wideband beamformer with $\theta_0 = 10^0$.

ence frequency point to the desired one. Results have been provided for different design scenarios based on FIR filter and wideband beamformer design to demonstrate the crucial issue of the original formulation and the satisfactory performance by the proposed one.

In the next chapter, the focus will be shifted from fixed wideband beamformer design with traditional arrays containing fixed inter-element spacing to sparse arrays where the inter-element spacing can vary from sensor to sensor and can be significantly larger than the spacing in traditional arrays. Such arrays have numerous applications especially in the area of DOA estimation where extensive research is being carried out. Although sparse arrays are a relatively little explored territory from the beamforming perspective, many types of sparse arrays with efficient difference co-arrays have been proposed for their application in DOA estimation. In Chapter 4, an overview of the difference co-array model, concepts of sparsity and a detailed review of existing sparse arrays will be presented.

Chapter 4

Review of Sparse Arrays and Difference Co-array Model

4.1 Introduction

Data received by the sensor arrays is very significant from signal processing perspective and can be used to compute different characteristics of the source signals like DOA and number of source signals [6]. DOA estimation determines the spatial spectra of the impinging electromagnetic waves on the sensor array. Different methods exist in the literature which are used to estimate the respective DOA of the impinging signals. The conventional subspace-based DOA estimation methods like MUSIC and ESPRIT resolve upto $N-1$ sources with an N-element array [17, 18]. The idea of detecting more sources than the number of sensors holds numerous applications and has received tremendous interest by the research community recently [87].

Towards that goal, higher number of degree of freedoms(DOFs) have been achieved by exploiting sparse arrays through their equivalent difference co-array model. In this chapter, difference co-array model and related terminologies stemming from it are explained in Section 4.2 with a perspective on mutual coupling in Section 4.3, followed by an extensive literature review on sparse arrays in Section 4.4.

4.2 Preliminaries of Difference Co-array Model

In this section, sparse arrays will be discussed from the point of view of difference co-array model and related terminologies will be defined for a better understanding of the concept.

4.2.1 Sparse Arrays

Sparse arrays differentiate themselves from the traditional arrays from the standpoint of inter-element spacing. Traditional arrays are defined by an inter-element spacing of $d = \frac{\lambda}{2}$ between the sensors, where λ is the minimum wavelength corresponding to maximum frequency content present in the incoming signal. This sensor spacing is aimed at avoiding the grating lobes, which start to appear in the beam pattern of the array in the form of peaks at spatial locations other than the main lobe if the inter-sensor spacing is greater than $\frac{\lambda}{2}$. An example of a 10-sensor normalized traditional ULA is provided with its sensor positions given by

$$\mathbb{S}_{TULA} = \{0, 1, 2, 3, 4, 5, 6, 7, 8, 9\} \tag{4.1}$$

Applications of traditional arrays are limited by the low aperture attained because of this closely packed arrangement of sensors in addition to mutual coupling problems. In comparison, sparse arrays work around this problem by having an increased sensor spacing much greater than $\lambda/2$ and achieve an increased aperture and enhanced degrees of freedom which can be utilized in applications like DOA estimation through their difference co-array model. For the ease of concept, a 10-sensor prototype coprime array, a type of sparse array which will be discussed in subsequent sections, has its sensor positions given by

$$\mathbb{S}_{CSA} = \{0, 5, 6, 10, 12, 15, 18, 20, 24, 25\} \tag{4.2}$$

which clearly shows the increased aperture and sparsity achieved by the array.

4.2.2 Difference Co-array Model

Definition 4.1 (Difference co-array $\mathbb{D}$)**.** Considering a sparse array with the position of its sensors specified by an integer set $\mathbb{S}$, its difference co-array $\mathbb{D}$ is defined as [88]

$$\mathbb{D} = \{n_1 - n_2 \mid n_1, n_2 \in \mathbb{S}\}$$

The difference co-array is based on computing the difference in position of one sensor relative to the remaining sensors in the sparse array. This difference is termed as lag and this process is repeated for every sensor in the array followed by constructing a set of lags for the whole array. These lags represent the points in the array at which the autocorrelation can be computed and represent degrees of freedoms (DOFs) of the difference co-array where autocorrelation is the correlation of the signal with a delayed copy of itself as a function of delay. It is the similarity between the observations as a function of time/spatial lag between them.

The difference co-array for the sparse array in (4.2) is given by

$$\mathbb{D}_{CSA} = \{-25, -24, -20, -19, -18, -15, -14, -13, -12, -10, -9, -8, -7, -6, -5, -4, -3, \\ -2, -1, 0, 1, 2, 3, 4, 5, 6, 7, 8, 9, 10, 12, 13, 14, 15, 18, 19, 20, 24, 25\}$$

4.2.3 Degrees of Freedom

Definition 4.2 (Degrees of freedom)**.** The number of degrees of freedom (DOF) of a sparse array is the cardinality of the difference co-array $\mathbb{D}$. [88]

The example shown above has 39 DOFs as per the number of entries in the corresponding difference co-array. For the sake of simplicity, DOF will be addressed as lag in the remaining part of this thesis.

4.2.4 Consecutive Lags

Definition 4.3 (Consecutive lags)**.** Given the difference co-array array $\mathbb{D}$, the largest set of consecutive entries in $\mathbb{D}$ identifies the number of consecutive lags provided by the difference co-array $\mathbb{D}$.

For consecutive lags of a sparse array equal to x, the number of uncorrelated signals that can be identified by SS-MUSIC is given by $\frac{x-1}{2}$. For the sparse array under consideration, it has consecutve entries from -10 to 10, thus providing 21 consecutive lags.

4.2.5 Unique Lags

Definition 4.4 (Unique lags)**.** Given the difference co-array $\mathbb{D}$, the number of distinct entries in $\mathbb{D}$ identifies the number of unique lags provided by the difference co-array $\mathbb{D}$.

The number of unique lags of a sparse array represents the number of uncorrelated signals that can be identified using compressive sensing (CS) based methods. The more the number of lags generated from the difference co-array, the more the available lags which can be exploited for DOA estimation. Again there are 39 distinct entries in the difference co-array for sparse array representing 39 unique lags.

4.2.6 Holes

Definition 4.5 (Holes)**.** Given a difference co-array $\mathbb{D}$, the missing points among the entries of the difference co-array $\mathbb{D}$ are termed as holes.

The holes represent the points in the difference co-array at which autocorrelation cannot be computed and represent the missing lags. It can be seen that the sparse array has holes at

$$\mathbb{H}_{CSA} = \{-23, -22, -21, -17, -16, -11, 11, 16, 17, 21, 22, 23\}$$

4.2.7 Restricted Arrays

Definition 4.6 (Restricted arrays)**.** A restricted array is an array whose difference co-array $\mathbb{D}$ is a ULA with adjacent elements separated by $\lambda/2$. In other words, there are no holes in the co-array domain. Thus the phrase "restricted array" is equivalent to "an array with a hole-free difference co-array." [88]

4.2.8 General Arrays

Definition 4.7 (General arrays)**.** If the difference co-array $\mathbb{D}$ of a sparse array $\mathbb{S}$ is not a ULA with inter-element spacing $\lambda/2$, then it is a general array. [88]

4.3 Mutual Coupling and Sparsity

The performance and output of sensors in an array are affected by their neighbouring sensors and this effect appears in the form of mutual electromagnetic coupling. The closer the sensors placed in the array, the more this scenario plays its part and affects the sensor output severely. Different methods in the literature target the decoupling or removal of effect of mutual coupling from the received data by incorporating mutual coupling models [89–98].

This effect is quantized in arrays with the help of weight functions which define the number of sensor pairs in the array with a certain value of inter-element spacing. This definition of weight functions is explained as follows.

Definition 4.8 (Weight functions)**.** The weight function $w(m)$ of an array $\mathbf{p}$ refers to the number of sensor pairs corresponding to a particular value of coarray index m (which is an indication of the separation between the underlined sensor pair), and is given by [88]

$$W(m) = \{(n_1, n_2) \in \mathbb{X}^2 \mid n_1 - n_2 = md\}, \tag{4.3}$$

$$w(m) = \text{Card}(W(m)), \tag{4.4}$$

where $md \in \mathbb{C}_{\mathbb{P}}$, (n_1, n_2) are the ordered pairs contributing to the co-array index m and $\text{Card}(A)$ returns the cardinality of the set A which is the number of elements in set A. The first 3 weights i.e. $w(1)$, $w(2)$ and $w(3)$ represent the number of sensor pairs in a sparse array having d, $2d$ and $3d$ inter-element spacing. These weights are very critical and point to the degree of sparsity achieved by the array and the potential of array to counter mutual coupling. Lower values of these weights lead to a sparser array design and better performance against mutual coupling.

4.4 Types of Sparse Arrays

In this section, different types of sparse arrays available in the literature will be reviewed. First in this line is the minimum redundancy array.

4.4.1 Minimum Redundancy Array

Minimum redundancy array (MRA) is a type of sparse array that maximizes the number of consecutive lags in the difference co-array for a fixed number of sensors [50]. The method of finding MRA's for a given number of sensors rests in minimizing the redundancy factor R which is a ratio of the number of possible pairs for a given number of sensors to the maximum available spacing that is the total aperture achieved by the array. The method involves exhaustive search to find the optimal arrays from the perspective of highest number of consecutive lags with a hole free co-array for a given number of sensors. The MRAs achieved thus have a hole-free co-array and belong to restricted arrays. A useful contribution on MRAs is provided by Ishiguro where MRAs for arbitrary number of antennas have been found after exhaustive search through different methods [57].

Although MRA for a given number of sensors is optimal from the perspective of highest number of consecutive lags, hole-free co-arrays and sparse structure, they are difficult to find. Extracting MRAs involves combinatorial search and table lookup, which is not scalable for a scenario especially where an array with a greater number of sensors has to be designed.

An example of a 12-sensor MRA is provided in Figure 4.1 with $49d$ aperture and $R = 1.347$ [57]. This array generates 99 lags from -49 to 49 with a hole-free co-array and able to detect and estimate 49 sources using the SS-MUSIC algorithm.

Figure 4.1: MRA with 12 sensors

The weight function plot of MRA is shown in Figure 4.2, where $w(1) = w(3) = 1$ and

$w(2) = 4$ indicating a very sparse structure.

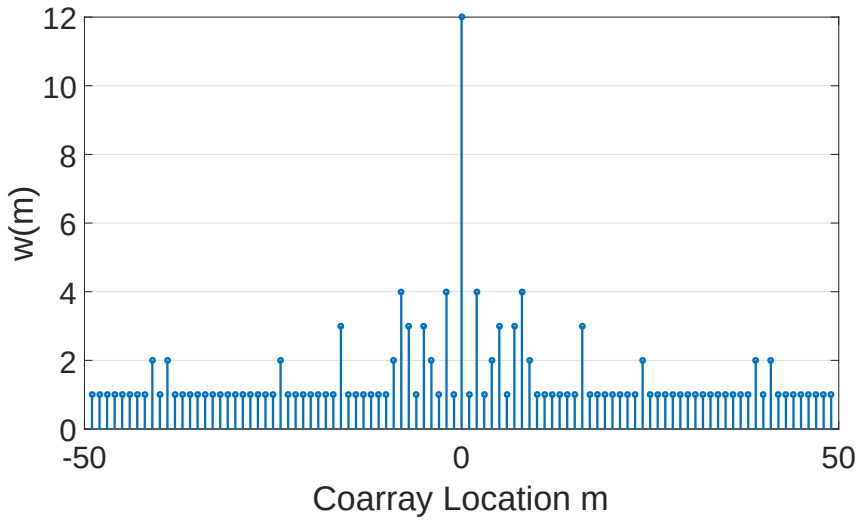

Figure 4.2: MRA weight functions

4.4.2 Minimum Hole Array

Another type of sparse array is a minimum hole array (MHA) which minimizes the number of holes in the difference co-array for a given number of sensors [58]. MHA's hold this property that all of differences in their co-array occur at most with a frequency of 1 except the difference of 0 which is a very desired characteristic from the mutual coupling perspective. Like MRA, MHA offers optimal array characteristics from the perspective of highest number of unique lags along with weight frequency of 1 for any lag for a given number of sensors but generating the sensor locations for an arbitrary number of sensors is an extremely complicated task [50, 99]. It doesn't have closed form expressions/analytical solutions for the array geometry and the sensor positions are normally extracted from the tabulated entries [50].

4.4.3 Nested Array

Another recently developed sparse array is the nested array. Nested arrays are composed of two uniform linear subarrays (ULAs) where one subarray is dense with unit inter-element spacing compared to the other one which is more sparsely spaced [26]. It has the

ability to resolve $\mathcal{O}(N^2)$ sources with N sensors where $\mathcal{O}(.)$ is the order of the function, and possess hole-free co-arrays. For given parameters N_1 and N_2, where N_1 denotes the number of sensors in the 1^{st} densely packed ULA with unit inter-element spacing $d = \frac{\lambda}{2}$ and N_2 denotes the number of sensors in the 2^{nd} ULA with sensors separated by $(N_1 + 1)d$, nested arrays obtain an aperture of $((N_1 + 1)N_2 - 1)d$ and produce $2(N_1 + 1)N_2 - 1$ consecutive lags from $-(N_1 + 1)N_2 - 1$ to $(N_1 + 1)N_2 - 1$. The total number of sensors in nested array is given by $N_1 + N_2$. In comparison to MRA and MHA, nested array is simple to construct and exact expressions are available for sensor locations and computing lags for a given number of sensors [26].

The drawback with the simple nested array design lies in the fact that as the sensor locations in one subarray are separated only by unit inter-element spacing, mutual coupling between neighbouring antennas becomes significant and affects DOA estimation performance [100]. An example of a nested array for $N_1 = 6$ and $N_2 = 6$ is shown in Figure 4.3.

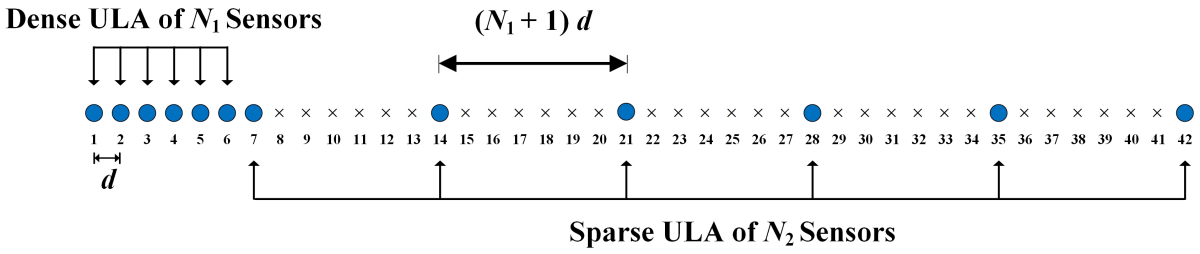

Figure 4.3: Nested array for $N_1 = N_2 = 6$

The weight function plot of the nested array in Figure 4.3 is shown in Figure 4.4, where $w(1) = 6$, $w(2) = 5$ and $w(3) = 4$, indicating significantly higher weight function values which make the array vulnerable to mutual coupling.

It can be seen that 6 pairs of sensors are separated from each other just by unit inter-element spacing which can significantly increase mutual coupling and increase estimation error. This array generates 83 consecutive lags available to be utilized for DOA estimation.

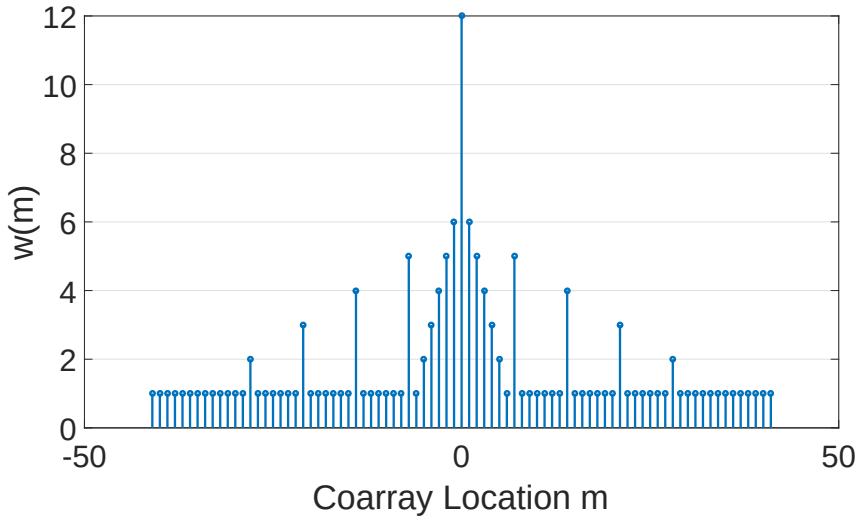

Figure 4.4: Nested array weight functions

4.4.4 Coprime Array/ Prototype Coprime Array

Coprime arrays are the sparse arrays developed to counter the mutual coupling problem present in the nested array with a much sparser array structure. There are a lot of configurations that have been proposed based on the coprime array structure. The very basic coprime array structure is called as prototype coprime array.

Prototype coprime arrays are composed of a pair of uniform linear subarrays where one subarray has M sensors separated by an inter-element spacing of N units, whereas the other subarray has N sensors separated by an inter-element spacing of M units where M and N are coprime integers. This coprime array structure is referred to as the prototype coprime array with $M+N-1$ sensors where the zeroth position sensor is shared between the two arrays [27]. These arrays possess holes in their co-arrays and therefore the analysis of their lags is based on the number of consecutive lags and unique lags present in the co-array. For a given M and N, these arrays possess $2(M+N)-1$ consecutive lags from $-M-N+1$ to $M+N-1$ and $MN+M+N-2$ unique lags. These arrays are able to resolve $\mathcal{O}(MN)$ sources with $M+N-1$ sensors. The aperture obtained by these arrays is given by $((M-1)N+1)d$.

An example of a 12-sensor prototype coprime array is provided for $M=6$ and $N=7$ in Figure 4.5. The weight function plot of prototype coprime array is shown in Figure

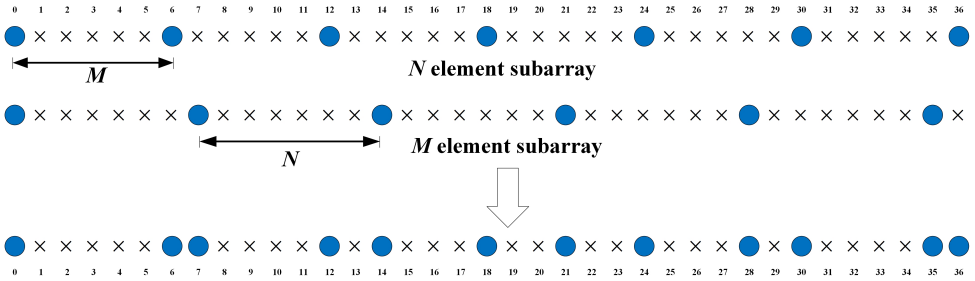

Figure 4.5: Prototype coprime array for $M = 6$ and $N = 7$

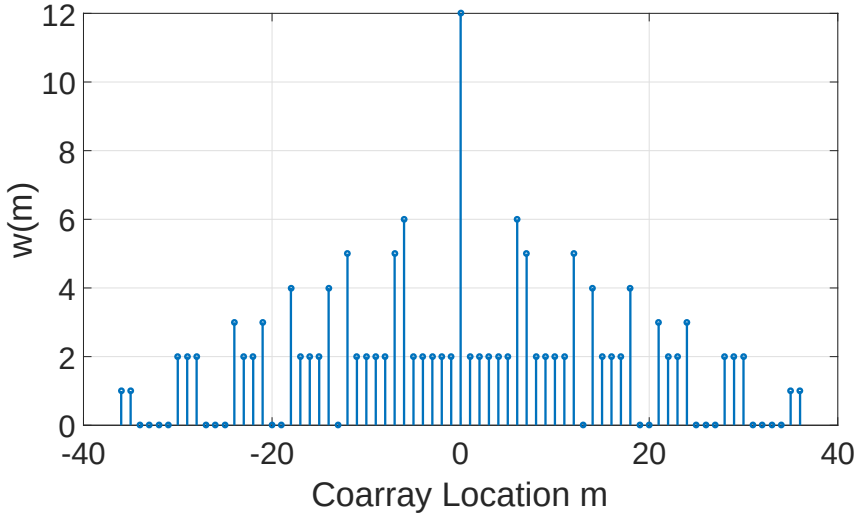

Figure 4.6: Prototype coprime array weight functions

4.6, where $w(1) = w(2) = w(3) = 2$. This array generates 25 consecutive lags from -12 to 12 and 53 unique lags which can be utilized appropriately for DOA estimation. In comparison to nested arrays for the same 12 sensors in Figure 4.3, the prototype coprime array only contains 2 pairs of sensors with unit inter-element spacing which is a great improvement to counter mutual coupling from neighbouring sensors. However, it lags the nested array in the provision of lags and aperture where the nested array is able to get an aperture of $41d$ and 83 lags. The prototype coprime array structure was improved by the introduction of conventional coprime array which provide a significant increase in the consecutive lags for application in SS-MUSIC based DOA estimation as shown later.

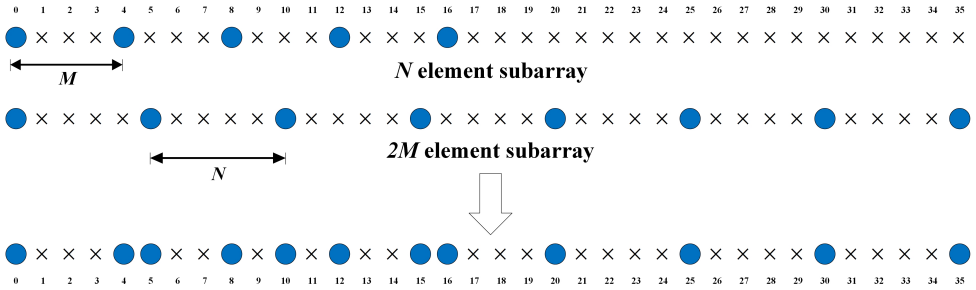

Figure 4.7: Conventional coprime array for $M = 4$ and $N = 5$

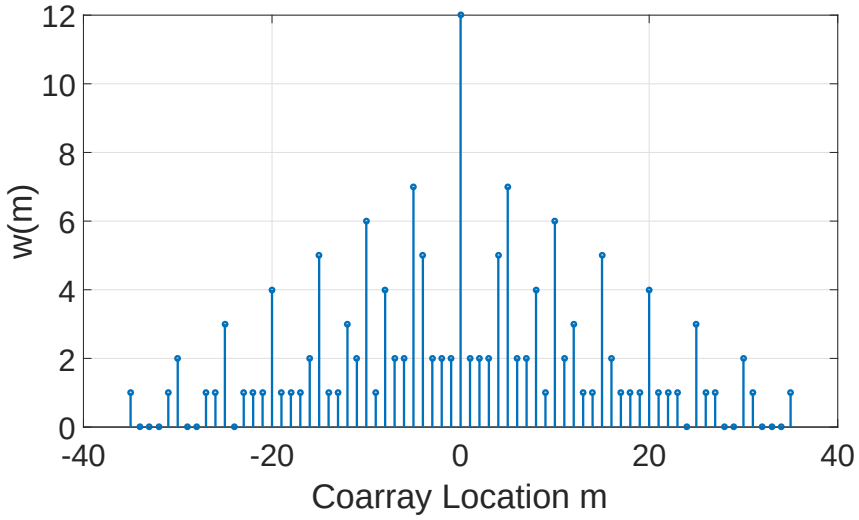

Figure 4.8: Conventional coprime array weight functions

4.4.5 Conventional Coprime Array

A modification to the prototype coprime array structure was proposed in [43] by doubling the number of elements in one subarray from M sensors to $2M$ sensors. It was shown by the authors that this structure of $2M + N - 1$ sensors resulted in increased consecutive lags in the difference co-array compared to the prototype coprime array of same number of sensors. For a given M and N, the co-array of $2M+N-1$ sensors generated $2MN+2M-1$ consecutive lags from $-MN - M + 1$ to $MN + M - 1$.

An example of a 12-sensor conventional coprime array is presented for $M = 4$ and $N = 5$ in Figure 4.7. The weight function plot of conventional coprime array is shown in Figure 4.8, where $w(1) = w(2) = w(3) = 2$, similar to the case of prototype coprime arrays. This array possesses 47 consecutive lags from -23 to 23 and 59 unique lags, which is a significant improvement over the prototype coprime array in Figure 4.5 which provides 25 consecutive lags. The conventional coprime array has 2 sensor pairs with unit inter-element spacing as prototype coprime and achieves nearly the same aperture but compared to nested arrays it still lags in consecutive lags and aperture.

Although the conventional coprime array provided improvement in the lags over prototype copirme array and more sparsity compared to nested array, it still had couple of sensor pairs separated by just the unit inter-element spacing. To suit the application of coprime arrays for the scenarios where the physical size of sensors is increased for larger directivity and are normally greater than half wavelength, another array configuration of coprime arrays was proposed in [101], where the minimum inter-element spacing was much greater than the typical half wavelength requirement. This configuration will be termed for our analysis as coprime arrays wih displaced subarrays (CADiS) version 1.

4.4.6 CADiS Version 1

This version of CADiS has the same $2M+N-1$ sensors as the conventional coprime array. It is different in the sense that the $2M-1$ sensor subarray is displaced from the N-sensor subarray by a spacing of Ld where $L \geq M$. The minimum inter-element spacing for this array is Md in comparison to d for the prototype and conventional coprime array. The

aperture obtained by the array for a fixed M and N was given by $(3MN - M - 2N + L)d$ which was considerably larger than the conventional coprime array.

It was shown in [101] that with an appropriate choice of $L = M + N$, this array was able to provide $MN + 2M + N - 1$ consecutive lags between $MN - M - N + 1$ and $2MN + M - 1$ which was slightly larger than half the conventional coprime array lags for SS-MUSIC to be exploited. Due to the displacement between the two subarrays in CADiS version 1, this array was able to provide increased unique lags given by $4MN + 2M - 1$ compared to $3MN + M - N$ of conventional coprime array.

To show the concept, a 12-sensor CADiS version 1 array for $M = 4$ and $N = 5$ is presened in Figure 4.9. The weight function plot of CADiS version 1 is shown in Figure 4.10, where $w(1) = w(2) = w(3) = 0$, providing good sparsity. This array possesses 32 consecutive lags compared to 47 lags for the conventional coprime array in Figure 4.7, but provides 87 unique lags compared to 59 for the conventional coprime case. It has a much longer aperture of $55d$ and contains the sparsest structure with minimum inter-element spacing equal to $4d$.

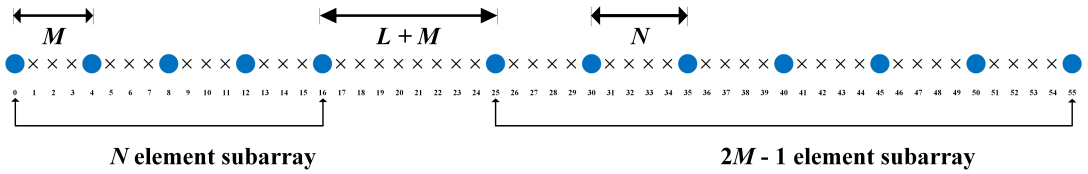

Figure 4.9: CADiS version 1 for $M = 4$ and $N = 5$

The authors presented generalizations of coprime arrays in [54] based on two different configurations. The 1^{st} configuration was based on compressing one subarray of prototype coprime array by an integer factor, resulting in a coprime array with compressed inter-element spacing (CACIS). The 2^{nd} type was based on applying the same compression principle in the 1^{st} type but on a CADiS structure with subarrays displaced from each other. These two configurations will be explored in detail in the following section.

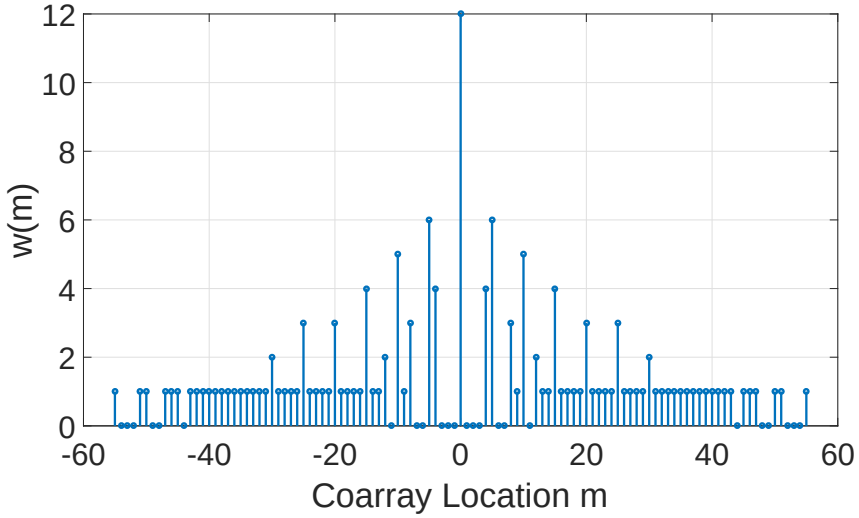

Figure 4.10: CADIS version1 weight functions

4.4.7 CACIS

Consider two subarrays with M and N sensors, where M and N are coprime integers. Unlike the prototype coprime array where coprime numbers are used for inter-element spacing of the respective subarrays, an integer compression factor p is introduced for changing the inter-element spacing of one subarray. Assuming that M can be expressed as a product of two positive integers p and $M^{'}$ i.e.

$$M = pM^{'} \tag{4.5}$$

where p takes a value between 2 and M. It can be easily confirmed that $M^{'}$ and N are also coprime since M and N do not have common factors other than unity. In this CACIS structure, the M-element subarray has an inter-element spacing of Nd whereas the N-element subarray is compressed by an inter-element spacing of $M^{'}d$ rather than Md which was the case in prototype coprime. All the CACIS arrays consist of the same $M+N-1$ physical sensors and provide $(M-1)N$ aperture irrespective of the value of p.

The authors showed that for a given M, N and $M^{'}$, CACIS provides $2MN-(M^{'}+1)(N-1)-1$ unqiue lags, out of which there are $2MN-2M^{'}(N-1)-1$ consecutive lags from $-MN+M^{'}(N-1)+1$ to $MN-M^{'}(N-1)-1$. An example of CACIS for $M=6$ and $N=7$ is presented in Figure 4.11. For $M=6$, there are 3 possible structures

of CACIS available to be explored respectively for $p = 2$, 3 and 6.

For $p = 2$, $M^{'} = 3$ which corresponds to a spacing of $3d$ for the N-element subarray as depicted in Figure 4.11 (a). This is the sparsest structure possible for $M = 6$ and provides 47 consecutive lags and 59 unique lags. There are 2 sensor pairs each with d and $2d$ spacing and 7 sensor pairs with $3d$ spacing.

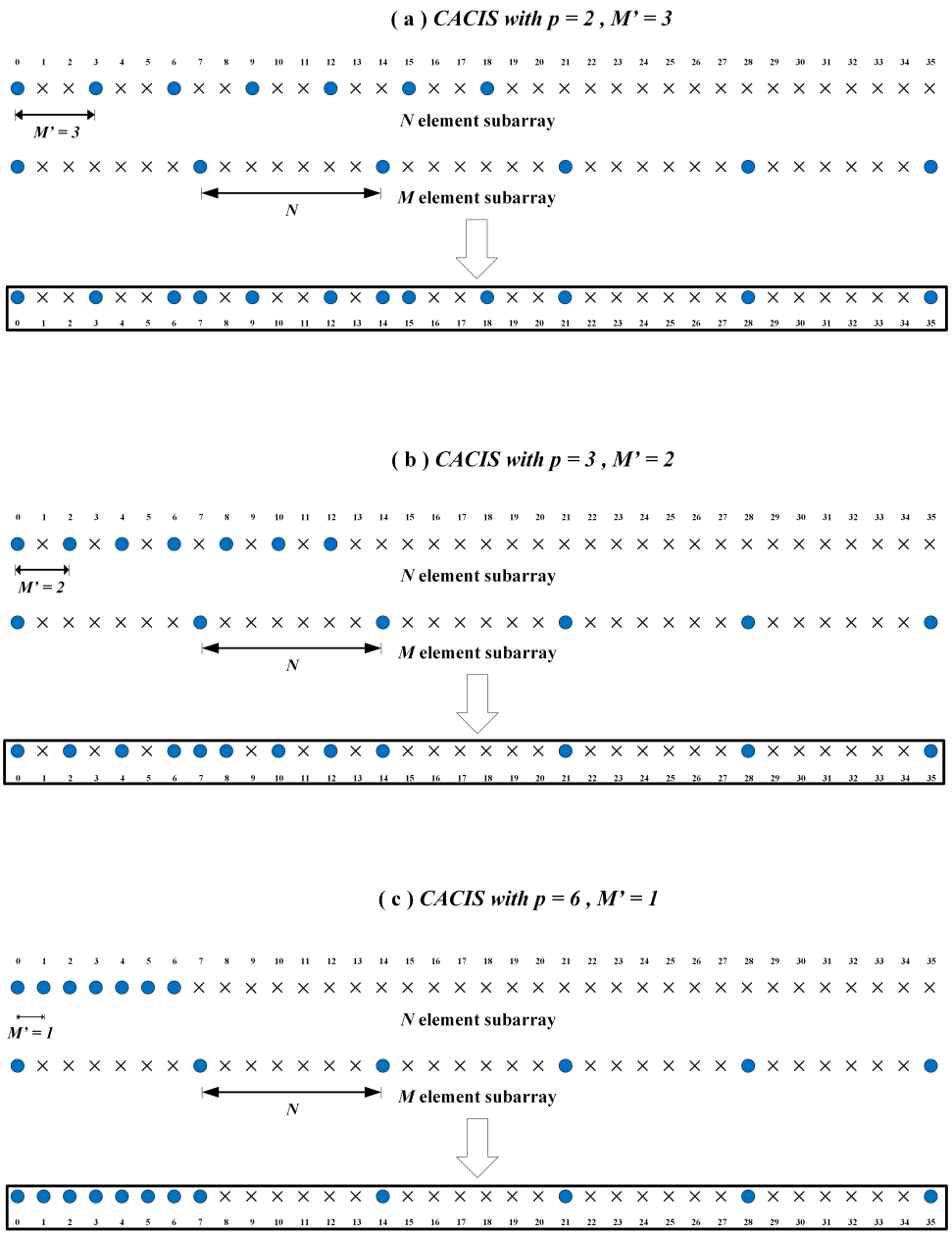

Figure 4.11: CACIS for $M = 6$ and $N = 7$

For $p = 3$, $M^{'} = 2$ which corresponds to a spacing of $2d$ for the N-element subarray

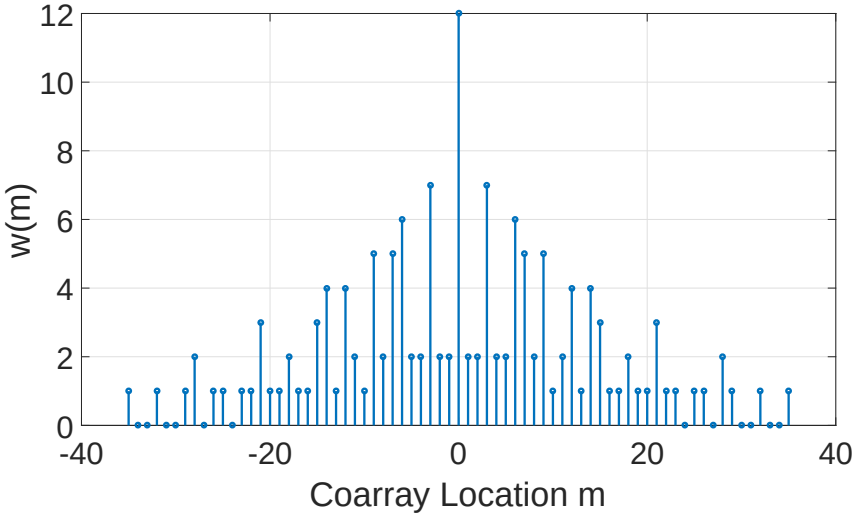

Figure 4.12: CACIS $p = 2$ weight functions

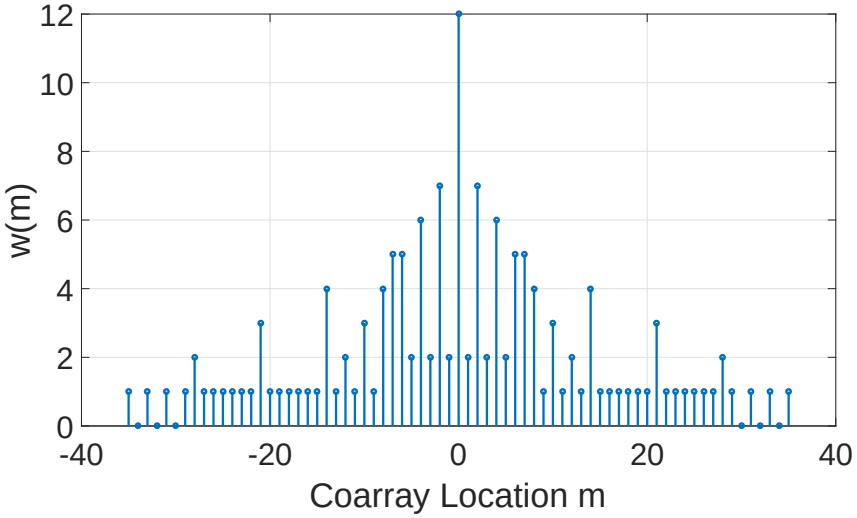

Figure 4.13: CACIS $p = 3$ weight functions

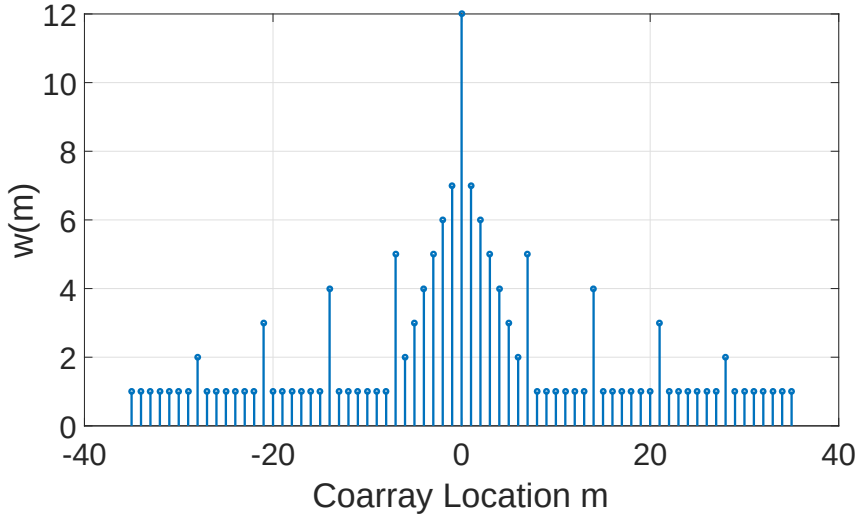

Figure 4.14: CACIS $p = 6$ (nested) weight functions

as depicted in Figure 4.11 (b). This structure provides 59 consecutive lags and 65 unique lags. There are 2 sensor pairs with d and $3d$ spacing and 7 sensor pairs with $2d$ spacing. By increasing the compression factor p, there is a noticeable increase in the consecutive and unique lags; however it comes at the cost of closer spacing among the elements of the array.

For $p = 6$, $M^{'} = 1$ with a nested CACIS structure, where the N-element subarray becomes a nested array for 7 sensors with d inter-element spacing as shown in Figure 4.11 (c). This structure provides the highest number of consecutive lags equal to 71 and provides a hole-free co-array. There are 7 sensor pairs with d spacing, 6 sensor pairs with $2d$ spacing and 5 sensor pairs with $3d$ spacing showing a visible problem of mutual coupling.

The weight function plots for $p = 2$, 3 and 6 for this CACIS configuration are shown in Figures 4.12, 4.13 and 4.14, respectively. The drawbacks of this CACIS structure are in its minimum unit inter-element spacing, higher frequency of sensor pairs with d, $2d$ and $3d$ spacing and lot of overlapping in self and cross lags which occurs due to collocation of the two subarrays. To counter this, a 2nd version of CADiS was proposed in [54] by introducing displacement between two subarrays of a prototype coprime array with the compression of one subarray resulting in an array with larger minimum inter-element spacing and higher number of unique lags. In this case, the number of consecutive lags

was reduced because the positive and negative lags were no longer connected due to larger minimum inter-element spacing. This array was termed as coprime array with displaced subarrays (CADiS) version 2.

4.4.8 CADiS Version 2

Consider two collinearly located uniform linear subarrays where one subarray consists of N sensors and the other subarray consists of $M-1$ sensors. The total number of sensors in the array is again $M+N-1$. Similar to CACIS, the sensors in N-element subarray are separated by inter-element spacing of $M^{'}d$ while the M-element subarray is separated by an inter-element spacing of Nd. The inter subarray displacement is represented by Ld where the authors showed that the choice of $L = M^{'} + N$ gives $2MN + 2M^{'} - 1$ unique lags and the highest number of consecutive lags from $(M^{'} - 1)(N - 1)$ to $MN + M^{'} - 1$, while the choice of $L > N(M - 2)$ yields the highest number of unique lags given by $2MN + 2M - 5$. For illustrative purpose, $L = M^{'} + N$ is used for analysis. An example of CADiS for $M = 6$ and $N = 7$ is presented in Figure 4.15. For $M = 6$, again there are 3 possible structures of CADiS available to be explored respectively for $p = 2$, 3 and 6.

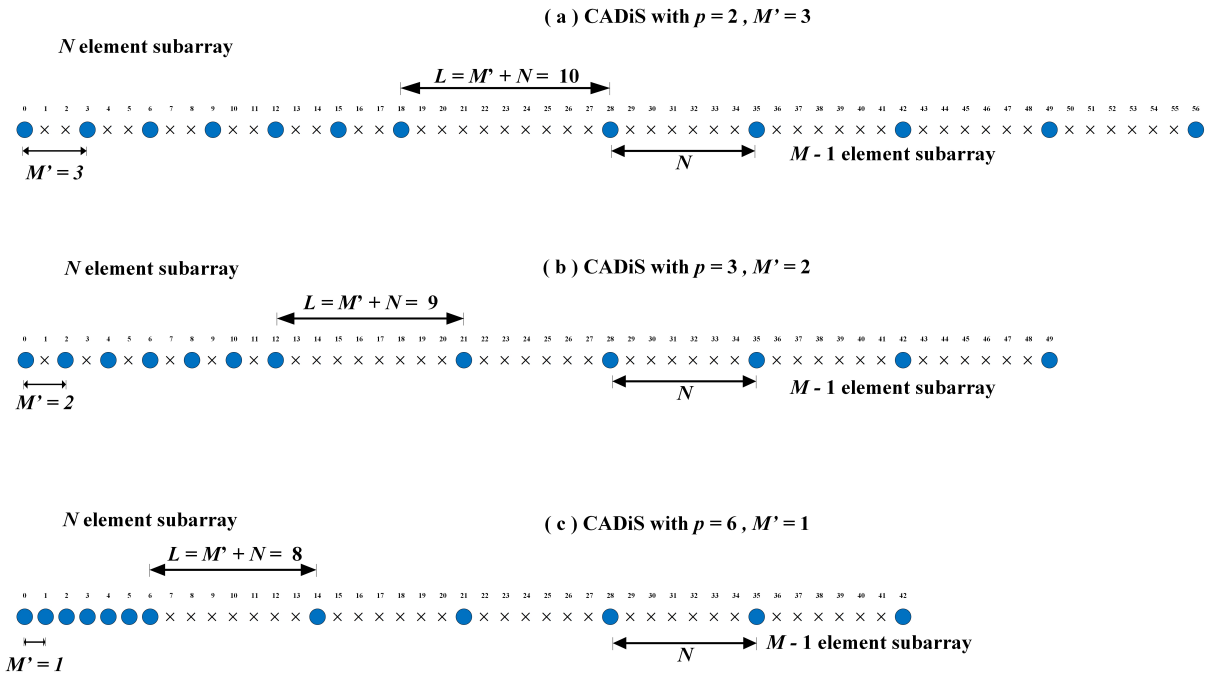

Figure 4.15: CADiS version 2 for $M = 6$ and $N = 7$

For $p = 2$, $M^{'} = 3$ which corresponds to a spacing of $3d$ for the N-element subarray as depicted in Figure 4.15 (a). This is the sparsest CADiS structure possible for $M = 6$. This structure provides 33 consecutive lags and 89 unique lags, a big increase from the CACIS structure. There are no sensor pairs with d and $2d$ spacing and 6 sensor pairs with $3d$ spacing proving to be a very good sparse structure to counter mutual coupling.

For $p = 3$, $M^{'} = 2$ which corresponds to a spacing of $2d$ for the N-element subarray as depicted in Figure 4.15 (b). This structure provides 48 consecutive lags and 87 unique lags. There are no sensor pairs with d and $3d$ spacing and 6 sensor pairs with $2d$ spacing.

Finally for $p = 6$, $M^{'} = 1$ for a nested CADiS structure, where the N-element subarray becomes a nested array for 7 sensors with d inter-element spacing as shown in Figure 4.15 (c). This structure provides the highest number of consecutive lags equal to 85 and provides a hole-free co-array. There are 6 sensor pairs with d spacing, 5 sensor pairs with $2d$ spacing and 4 sensor pairs with $3d$ spacing.

The weight function plots for $p = 2$, 3 and 6 for this CADIS configuration are shown in Figures 4.16, 4.17 and 4.18, respectively.

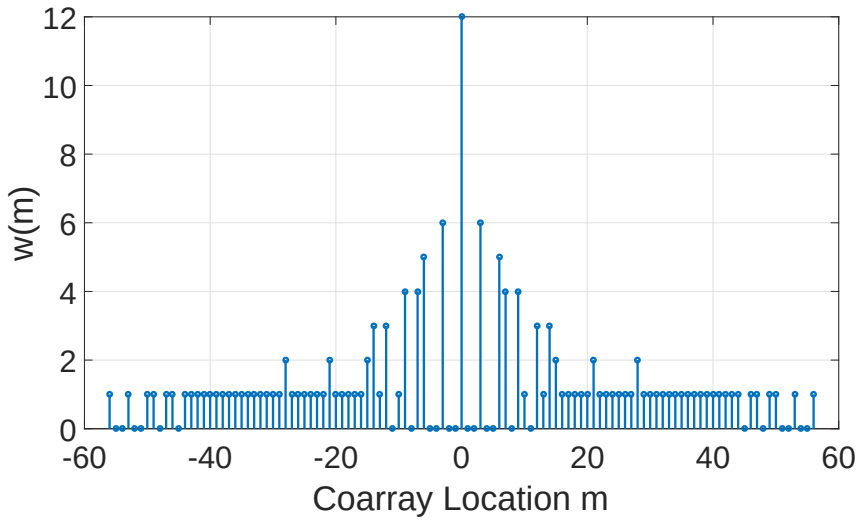

Figure 4.16: CACIS $p = 2$ weight functions

It was shown that CADiS structure yielded the highest number of unique lags which were all exploited using compressive sensing (CS) based DOA estimation method. In order to apply subspace based DOA estimation methods like SS-MUSIC, nested CADiS offered the highest number of consecutive lags and performed better than nested CACIS.

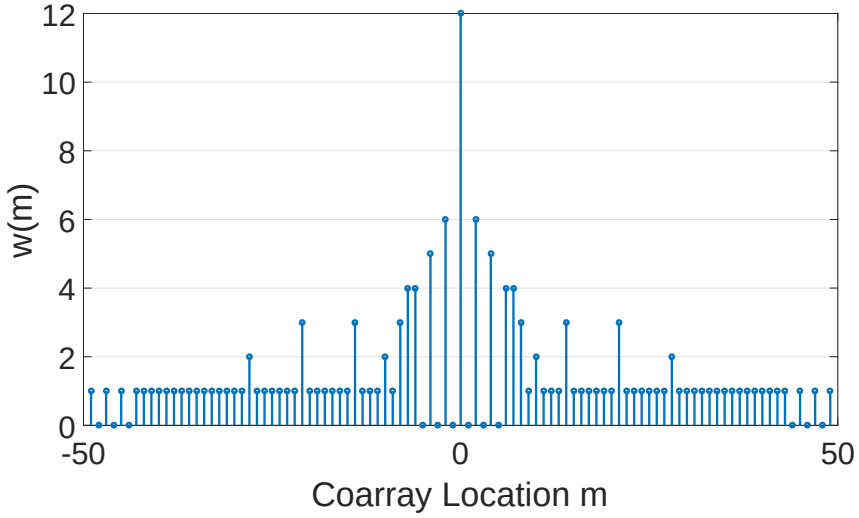

Figure 4.17: CADIS $p = 3$ weight functions

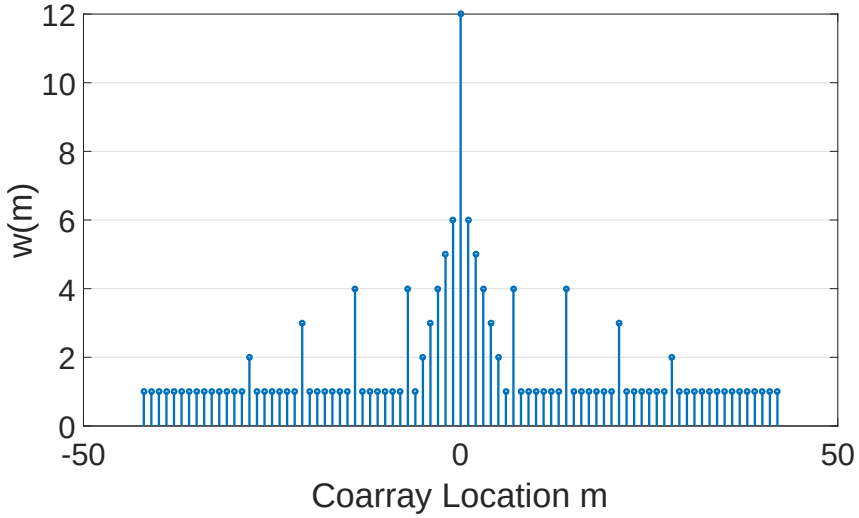

Figure 4.18: CADIS $p = 6$ (nested) weight functions

Although the nested CADiS offered the highest number of consecutive lags with a hole-free co-array, the mutual coupling problem still affected the DOA estimation performance.

The sparsest version of CADiS outperforms previously proposed sparse arrays from the perspective of high unique lags which can all be utilized by CS-based methods. Also the degree of sparsity achieved by these arrays is advantageous to counter the effects of mutual coupling along with an aperture with very decent resolution but it lacks in provision of consecutive lags which limits its use for SS-MUSIC based DOA estimation. The nested structures of CACIS and CADiS are able to provide hole-free co-arrays but at the cost of increased number of sensor pairs with d, $2d$ and $3d$ inter-element spacing.

4.4.9 Super Nested Array

An improvement to nested array design was proposed in [88], where the author showed that a hole-free co-array was achieved with a much sparser array structure. This array was called the super nested array (second order) [59] along with the higher order super nested arrays which were proposed later on [60]. It worked on the idea of a nested array where one subarray was densely packed with unit inter-element spacing while the other subarray was sparsely spaced. The author showed that by proper rearrangement of some of the sensors in the densely packed subarray, the overall array maintained all the properties of its parent nested array. The super nested array thus achieved had the same aperture, same hole-free co-array (number of consecutive lags) with lower number of sensor pairs with d, $2d$ and $3d$ spacing for reduced mutual coupling. The concept of super nested arrays is demonstrated with the help of an example as follows.

Consider N_1 and N_2 as integers satisfying $N_1 \geq 4$ and $N_2 \geq 3$. A second order super nested array is specified by the integer set $\mathbb{S}^{(2)}$ defined by

$$\mathbb{S}^{(2)} = \mathbb{X}_1^{(2)} \cup \mathbb{Y}_1^{(2)} \cup \mathbb{X}_2^{(2)} \cup \mathbb{Y}_2^{(2)} \cup \mathbb{Z}_1^{(2)} \cup \mathbb{Z}_2^{(2)} ,$$

where

$$\mathbb{X}_1^{(2)} = \{1 + 2l \mid 0 \leq l \leq A_1\},$$
$$\mathbb{Y}_1^{(2)} = \{(N_1 + 1) - (1 + 2l) \mid 0 \leq l \leq B_1\},$$
$$\mathbb{X}_2^{(2)} = \{(N_1 + 1) + (2 + 2l) \mid 0 \leq l \leq A_2\},$$
$$\mathbb{Y}_2^{(2)} = \{2(N_1 + 1) - (2 + 2l) \mid 0 \leq l \leq B_2\},$$
$$\mathbb{Z}_1^{(2)} = \{l(N_1 + 1) \mid 2 \leq l \leq N_2\},$$
$$\mathbb{Z}_2^{(2)} = \{N_2(N_1 + 1) - 1\},$$

The parameters A_1, B_1, A_2 and B_2 are defined as

$$(A_1, B_1, A_2, B_2) = \begin{cases} (r, r-1, r-1, r-2), & \textit{if } N_1 = 4r, \\ (r, r-1, r-1, r-1), & \textit{if } N_1 = 4r+1, \\ (r+1, r-1, r, r-2), & \textit{if } N_1 = 4r+2, \\ (r, r, r, r-1), & \textit{if } N_1 = 4r+3, \end{cases}$$

where r is an integer.

Consider a 12-sensor nested array for $N_1 = 6$ and $N_2 = 6$ from Figure 4.3 for the super nested array scenario. Setting $N_1 = N_2 = 6$, yields $A_1 = 2$, $B_1 = 0$, $A_2 = 1$ and $B_2 = -1$, and $\mathbb{X}_1^{(2)} = \{1, 3, 5\}$, $\mathbb{Y}_1^{(2)} = \{6\}$, $\mathbb{X}_2^{(2)} = \{9, 11\}$, $\mathbb{X}_1^{(2)} = \{\}$, $\mathbb{Z}_1^{(2)} = \{14, 21, 28, 35, 42\}$, $\mathbb{Z}_2^{(2)} = \{41\}$.

Another second order super nested array is considered for $N_1 = 5$ and $N_2 = 7$. Putting these values gives us parameters $A_1 = 1$, $B_1 = 0$, $A_2 = 0$ and $B_2 = 0$, and $\mathbb{X}_1^{(2)} = \{1, 3\}$, $\mathbb{Y}_1^{(2)} = \{5\}$, $\mathbb{X}_2^{(2)} = \{8\}$, $\mathbb{X}_1^{(2)} = \{10\}$, $\mathbb{Z}_1^{(2)} = \{12, 18, 24, 30, 36, 42\}$, $\mathbb{Z}_2^{(2)} = \{41\}$, which are the positions of the 12-sensor second order super nested arrays. The nested array and the two second order super nested arrays are shown for comparison in Figure 4.19 (a), (b) and (c) respectively. The respective weight function plots for nested array and two super nested arrays are presented in Figure 4.20, 4.21 and 4.22.

As evident in Figure 4.19, all the arrays attain equal aperture and their co-arrays also produce 83 consecutive lags but second order super nested arrays achieve much sparser configuration from the nested array among sensor spacing. The nested array has 6 sensor pairs with d spacing, 5 sensors pairs with $2d$ spacing and 4 sensor pairs with $3d$ spacing.

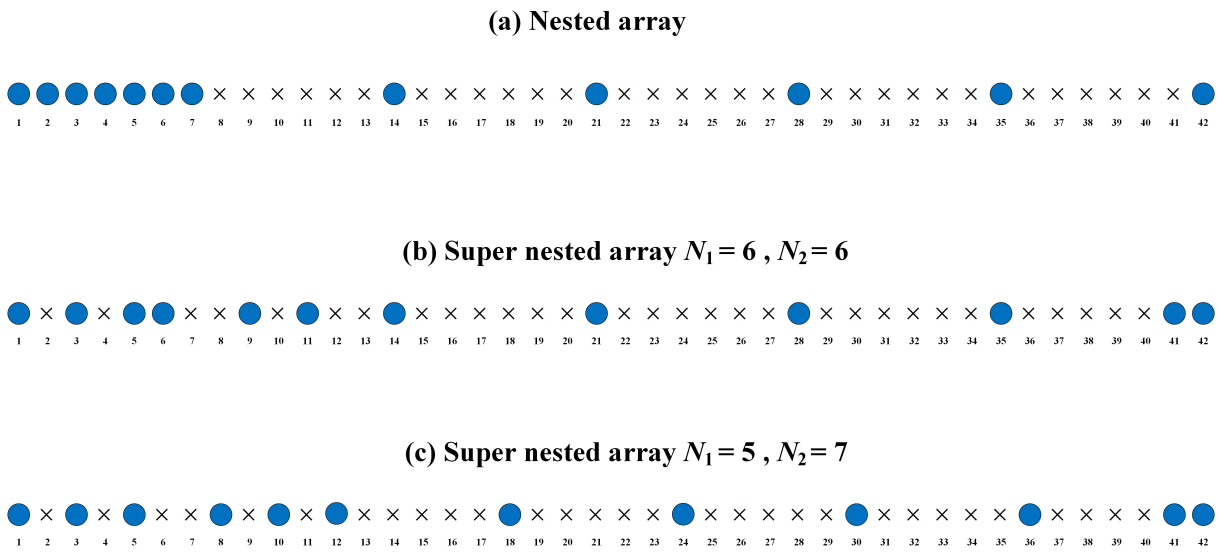

Figure 4.19: Comparison of 12 sensor nested and super nested array

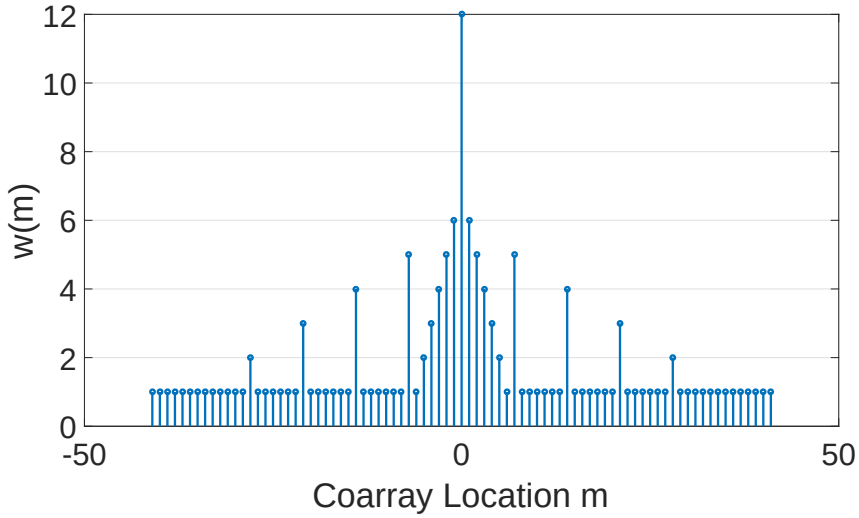

Figure 4.20: Nested array weight functions

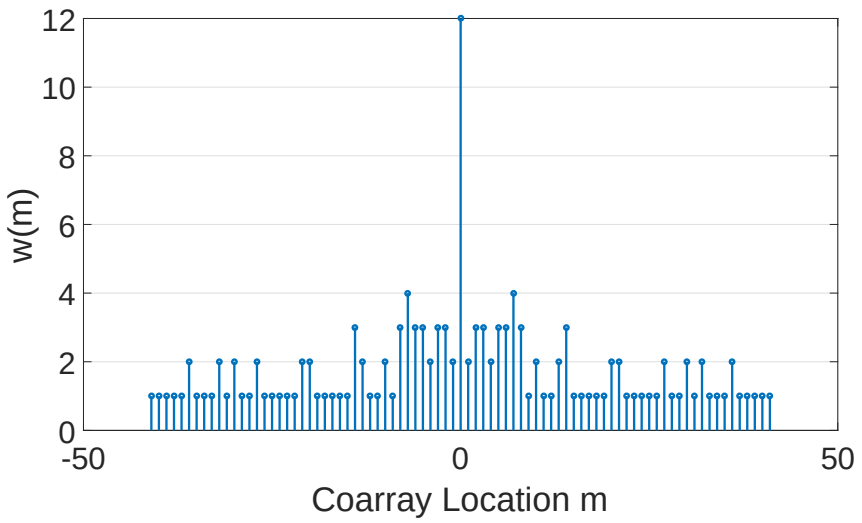

Figure 4.21: Super nested array $N_1 = N_2 = 6$ weight functions

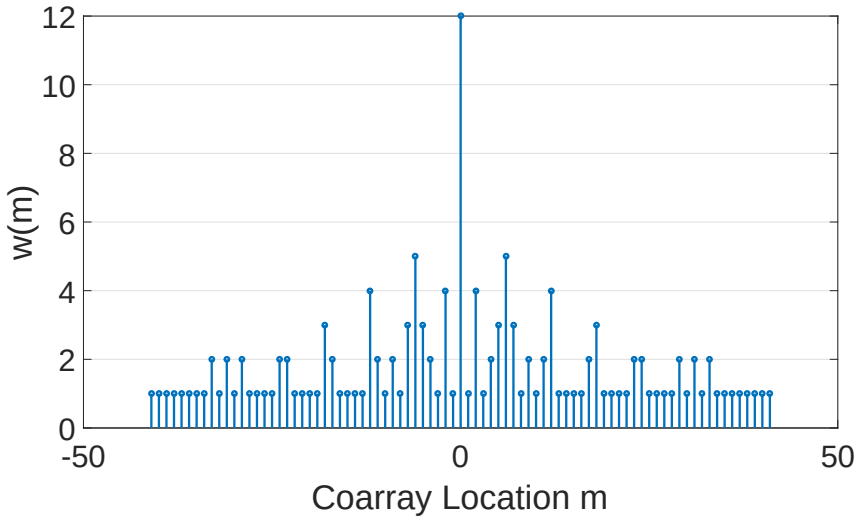

Figure 4.22: Super nested array $N_1 = 5$, $N_2 = 7$ weight functions

On the other hand, the first of the second order super nested arrays with even value of N_1 reduces the number of sensor pairs with 2 sensor pairs separated by d spacing, and 3 sensor pairs each with $2d$ and $3d$ spacing which is a significant improvement from the perspective of mutual coupling. The 2^{nd} super nested array with odd value of N_1 further improves the number of sensor pairs with d spacing by allowing just 1 sensor pair to have unit spacing followed by 4 sensor pairs with $2d$ spacing and 1 sensor pair with $3d$ spacing.

4.5 Summary

The foundations of difference co-array model have been laid down along with a mutual coupling perspective and its relationship to sparsity. This is followed by a detailed critical analysis of different types of sparse arrays. MRA's and MHA's are optimal arrays from the perspective of lags and their sparsity, but they are very difficult to obtain for a given design scenario. Nested arrays provide the ease of use with easy to follow closed form expression for its construction and provide hole-free co-array, but contain a lot of sensors packed densely with unit inter-element spacing which makes it vulnerable for mutual coupling.

Coprime arrays provide better response to mutual coupling with their sparse structure but possess holes in their co-arrays. Conventional coprime arrays are shown to have better performance with more consecutive and unique lags than prototype coprime arrays. The generalized configurations of coprime arrays provide very interesting results, where CADiS structure provided increased unique lags, aperture and sparsity while the nested CADiS provided the highest number of consecutive lags. However, the CADiS structure provided hole-free co-array at the cost of a nested structure with increased chances for mutual coupling.

Super nested arrays solve the problem of nested arrays with a hole-free co-array using a sparser structure than nested array, to provide a better line of defense against mutual coupling. Although super nested arrays and the CADiS structure of coprime array hold the best properties of sparse arrays at present, there is a need to investigate a sparse array design that maximizes the aperture, provides an increase in both consecutive and unique

lags along with an array structure that has the lowest number of sensor pairs with d, $2d$ and $3d$ spacing for the fixed number of sensors. Keeping these requirements in mind, a contribution in the shape of novel sparse array termed thinned coprime array which is based on conventional coprime array is presented in Chapter 5.

Chapter 5

Thinned Coprime Array for Second-Order Difference Co-Array Generation with Reduced Mutual Coupling

5.1 Introduction

As well known already, higher number of lags can be achieved by exploiting sparse arrays through the equivalent model of difference co-array [2, 87, 102]. These DOFs resulting from the difference in positions among different sensors represent the different lags at which the autocorrelation can be computed from the received data.

Two of the classic sparse array structures are the minimum redundancy array [50, 57] and, the minimum hole array [58]. However, MRA and MHA have a severe drawback in the sense that they do not possess closed-form expressions for the array geometry and the sensor positions are normally extracted from tabulated entries where closed form expression in the context of sparse arrays means that the positions of sensors for a given set of parameters or array size can be generated analytically (with the help of a formula) in a straight forward manner. Nested arrays in comparison are simple to construct and exact expressions are available for sensor locations and computing lags for a given number

of sensors but due to a densely packed subarray, they are prone to the effect of mutual coupling [100]. Another class of sparse arrays called coprime arrays can address this problem through a much sparser array design [27, 43]. Coprime and nested arrays offer certain advantages over MRAs and some other sparse array geometries. For example, depending on how they are processed, coprime arrays allow reduced peak sidelobe level compared to MRAs and MHAs [103].

A basic coprime array is a prototype coprime array with $M + N - 1$ sensors and provides $2(M + N) - 1$ consecutive lags. To increase the number of consecutive lags, a modification was proposed in [43] by increasing the number of elements in one subarray from M sensors to $2M$ sensors. This structure of $2M + N - 1$ sensors termed as conventional coprime array resulting in $2MN + 2M - 1$ consecutive lags can be exploited using subspace based DOA estimation methods such as MUSIC [17, 42, 43], where the number of sources should be estimated in advance [104, 105]. Generalized coprime array configurations exist in the form of CACIS and CADiS where it was shown that the CADiS structure performed much better than the CACIS structure for DOA estimation, and the compressive sensing (CS) based method can be employed for underdetermined DOA estimation without knowing the number of sources by forcing the sparsity across the potential incident angles based on the l_0 norm (which can be replaced by l_1 norm) [49, 54, 102, 106], where the non-zero entries are the detected DOAs based on the predefined search grids. However, the main drawback is the computational cost.

One factor not considered in many of the sparse array design schemes is the mutual coupling effect [33, 34]. As a result, performance degradation will result when this effect is strong. Two approaches can be adopted to tackle this problem. The first one tends to estimate the mutual coupling parameters along with the DOAs to get an improved estimate at the cost of extra computation and reduced lags [90, 96, 97, 107]. The second route tries to reduce mutual coupling by designing sparser arrays. In this direction, super nested arrays were developed recently which hold all the advantages of nested arrays [59, 60]. It was shown that the third order super nested array was most robust to the effects of mutual coupling and performed better than the second order one and other sparse arrays using MUSIC based DOA estimation methods. Most recently, an augmented

nested array structure was proposed with enhanced number of lags and reduced mutual coupling [108]. However, the mutual coupling of this structure could increase significantly with the increasing sensor number and even cause more mutual coupling than the super nested arrays.

As illustrated in [109], redundancy reduction in array structures require more snapshots to achieve a similar performance. Therefore, tradeoff has to be made between these two factors in sparse array design in different applications. In this chapter, main focus is on reducing the redundancy to improve the number of lags with reduced mutual coupling for a given number of sensors, and propose a new structure called thinned coprime array (TCA) by exploiting the redundancy in the difference co-array model of the conventional coprime array. As proved later in the chapter, the lag contribution from some of the sensors in the $2M$-element subarray of the conventional coprime array is generated by the rest of the sensors in the array and these sensors can therefore be removed without affecting the properties of the parent array. The proposed TCA holds the same number of consecutive lags, unique lags and aperture as the conventional coprime array, but with $\lceil \frac{M}{2} \rceil$ fewer sensors where $\lceil x \rceil$ returns the least integer greater than or equal to x. For a fixed number of sensors, thinned coprime array achieves more number of unique lags than the total lags (hole-free co-array) of a nested array, while generating close to 75 percent consecutive lags of those of a nested array, producing a much larger and sparser aperture than the nested array. The work presented here is a further extension of our conference publication [62] and investigates the performance of the new structure from the perspective of mutual coupling. As an indication of the mutual coupling effect, the weight functions are also derived along with the proof and some new properties, which shows that the proposed TCA is robust to high levels of mutual coupling. The performance of TCA is thoroughly investigated in comparison to MRA, super nested arrays and CADiS for DOA estimation in the presence of mutual coupling using CS-based DOA estimation method and spatial smoothing (SS)-MUSIC.

This chapter is organized as follows. The conventional coprime array model is reviewed in Section 5.2. The proposed TCA is detailed in Section 5.3. A comparison in terms of lags and mutual coupling between the TCA and other sparse arrays is provided in Sections

5.4 and 5.5 respectively. Simulations results are provided in Section 5.6.

5.2 Conventional Coprime Array Model

Consider a conventional coprime array with $2M + N - 1$ sensors as shown in Fig. 5.1, where M and N are coprime integers. The array sensors are positioned at

$$\mathbb{P} = \{Mnd \mid 0 \leq n \leq N-1\} \cup \{Nmd \mid 0 \leq m \leq 2M-1\}. \tag{5.1}$$

The positions of the sensors are given by the set $\mathbf{p} = [p_0, \ldots, p_{2M+N-2}]^T$ where $p_i \in \mathbb{P}, i = 0, \ldots, 2M+N-2$. The zeroth sensor in both subarrays is co-located at the zeroth position with $p_0 = 0$.

Consider the scenario where Q uncorrelated signals are impinging on the array from angles $\Theta = [\theta_1, \theta_2, \ldots, \theta_Q]$ and their sampled baseband waveforms are expressed as $s_q(t), t = 1, \ldots, T$, for $q = 1, \ldots, Q$. Then, the data vector received by the coprime array is given by

$$\mathbf{x}(t) = \sum_{q=1}^{Q} \mathbf{a}(\theta_q) s_q(t) + \mathbf{n}(t) = \mathbf{A}\mathbf{s}(t) + \mathbf{n}(t), \tag{5.2}$$

where

$$\mathbf{a}(\theta_q) = [1, e^{-j\frac{2\pi p_2}{\lambda}\sin(\theta_q)}, \ldots, e^{-j\frac{2\pi p_{2M+N-1}}{\lambda}\sin(\theta_q)}]^T \tag{5.3}$$

is the steering vector of the array corresponding to θ_q, $\mathbf{A} = [\mathbf{a}(\theta_1), \ldots, \mathbf{a}(\theta_Q)]$ and $\mathbf{s}(t) = [s_1(t), \ldots, s_Q(t)]^T$. The entries of the noise vector $\mathbf{n}(t)$ are white Gaussian with a covariance matrix given by $\sigma_n^2 \mathbf{I}_{2M+N-1}$, where σ_n^2 is the noise variance. The covariance matrix of data vector $\mathbf{x}(t)$ is given by

$$\begin{aligned} \mathbf{R}_{\mathbf{xx}} &= E[\mathbf{x}(t)\mathbf{x}^H(t)] = \mathbf{A}\mathbf{R}_{\mathbf{ss}}\mathbf{A}^H + \sigma_n^2 \mathbf{I}_{2M+N-1} \\ &= \sum_{q=1}^{Q} \sigma_q^2 \mathbf{a}(\theta_q)\mathbf{a}^H(\theta_q) + \sigma_n^2 \mathbf{I}_{2M+N-1}, \end{aligned} \tag{5.4}$$

where $\mathbf{R}_{\mathbf{ss}} = E[\mathbf{s}(t)\mathbf{s}^H(t)] = \text{diag}([\sigma_1^2, \ldots, \sigma_Q^2])$ is the source covariance matrix, with σ_q^2 denoting the signal power of the qth source. In practice, the covariance matrix is estimated from the T available samples.

$$\hat{\mathbf{R}}_{\mathbf{xx}} = \frac{1}{T} \sum_{t=1}^{T} [\mathbf{x}(t)\mathbf{x}^H(t)]. \tag{5.5}$$

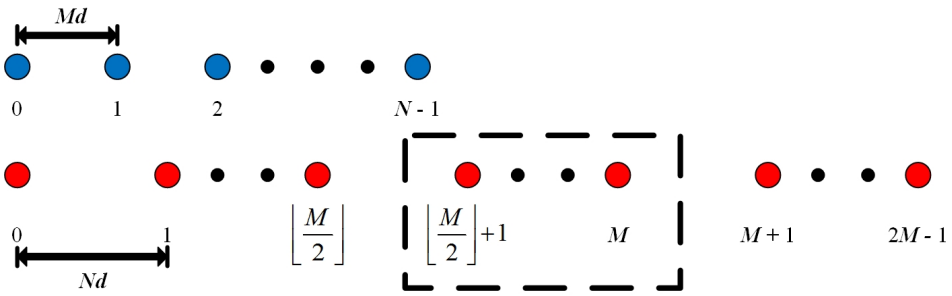

Figure 5.1: Conventional coprime array.

From the antennas located at the mth and nth positions in $\mathbf{p}$, the correlation $E[x_m(t)x_n^*(t)]$ results in the (m,n)th entry in $\mathbf{R_{xx}}$ with lag $p_m - p_n$. All the values of m and n, where $0 \leq m, n \leq 2M+N-2$, yield the lags or virtual sensors of the following difference co-array:

$$\mathbb{C}_{\mathbb{P}} = \{z \mid z = u - v, u \in \mathbb{P}, v \in \mathbb{P}\} \ . \tag{5.6}$$

5.3 Thinned Coprime Array

In this section it will shown that all of the sensors in the $2M$-element subarray enclosed within the dashed rectangle in Fig. 5.1 are redundant and therefore can be removed without affecting the lags of the difference co-array, leading to the proposed TCA structure.

Theorem 1. *The number of redundant sensors in a conventional coprime array with $M \geq 2$ for even M and $M \geq 5$ for odd M respectively are given by*

$$S_{red} = \left\lceil \frac{M}{2} \right\rceil, \tag{5.7}$$

where the starting index of these S_{red} contiguous redundant sensors in the $(2M-1)$-element subarray is given by $\lfloor \frac{M}{2} \rfloor + 1$.

Proof. The structure of the difference co-array can be divided into *self difference* i.e. diff($\mathbb{A}$, $\mathbb{A}$) and diff($\mathbb{B}$, $\mathbb{B}$) and *cross difference* i.e. diff($\mathbb{A}$, $\mathbb{B}$) and diff($\mathbb{B}$, $\mathbb{A}$), where $\mathbb{A}$ and $\mathbb{B}$ contain the sensor positions Mnd and Nmd respectively for the two subarrays with $0 \leq n \leq N-1$ and $0 \leq m \leq 2M-1$ while the diff operator stands for the difference between the positions of the sensors contained in the second set from the first set. In

detail,

$$\begin{aligned}
\text{diff}(\mathbb{A},\mathbb{A}) &= \{Mn_1d - Mn_2d \mid 0 \le n_1, n_2 \le N-1\},\\
\text{diff}(\mathbb{B},\mathbb{B}) &= \{Nm_1d - Nm_2d \mid 0 \le m_1, m_2 \le 2M-1\},\\
\text{diff}(\mathbb{A},\mathbb{B}) &= \{(Mn - Nm)d \mid 0 \le n \le N-1, 0 \le m \le 2M-1\},\\
\text{diff}(\mathbb{B},\mathbb{A}) &= \{(Nm - Mn)d \mid 0 \le n \le N-1, 0 \le m \le 2M-1\},
\end{aligned}$$

Since all the self difference co-arrays are included in the cross difference co-arrays [110], only the redundancies in diff($\mathbb{A}$, $\mathbb{B}$) need to be checked. For the cross difference diff($\mathbb{A}$, $\mathbb{B}$), the index (n, m) is used to represent the lag entry $Mn-Nm$. It was shown in [110] that the entries in the cross correlation matrix associated with indices (n_1, m_1) and (n_2, m_2) in diff($\mathbb{A}$, $\mathbb{B}$) are complex conjugate of each other when the indices satisfy the following relationship

$$(n_1 + n_2)M = (m_1 + m_2)N \tag{5.8}$$

with the sufficient condition for (5.8) given by

$$(n_1 + n_2 = N) \cap (m_1 + m_2 = M). \tag{5.9}$$

This condition dictates that if an index (n_1, m_1) with $0 \le m_1 \le \lfloor \frac{M}{2} \rfloor$ ($\lfloor x \rfloor$ returns the largest integer less than or equal to x) and $1 \le n_1 \le N-1$ is considered, then it will have a corresponding index (n_2, m_2) with $m_2 = M - m_1$ in the range $M - \lfloor \frac{M}{2} \rfloor \le m_2 \le M$ and $n_2 = N - n_1$ from $1 \le n_2 \le N-1$ with both indices satisfying (5.8). The corresponding entries of cross difference co-arrays with indices (n_1, m_1) and (n_2, m_2) satisfy the following relationship.

$$\begin{aligned}
\text{diff}(\mathbb{A},\mathbb{B})^{n_1,m_1} &= -\text{diff}(\mathbb{B},\mathbb{A})^{m_1,n_1} = -\text{diff}(\mathbb{A},\mathbb{B})^{n_2,m_2}\\
&= -\text{diff}(\mathbb{A},\mathbb{B})^{N-n_1,M-m_1}.
\end{aligned} \tag{5.10}$$

It thus follows that the lag entry corresponding to the index (n_2, m_2) of diff($\mathbb{A}$, $\mathbb{B}$) will be found in lag entry corresponding to index (m_1, n_1) of diff($\mathbb{B}$, $\mathbb{A}$), making the contribution of these lags from index (n_2, m_2) redundant.

Note that for index (n_1, m_1) with $m_1 = \lfloor \frac{M}{2} \rfloor = \frac{M}{2}$ when M is even, the corresponding redundant index (n_2, m_2) where $1 \le n_1, n_2 \le N-1$, will also have $m_2 = \frac{M}{2}$ with indices satisfying (5.8) and (5.10) respectively, and therefore $m = \frac{M}{2}$ for even M is not

a redundant sensor. As a result, for arbitrary M and $1 \leq n \leq N-1$, the redundant sensor indices in the second sub-array are $\phi_r = \{\lfloor \frac{M}{2} \rfloor + 1, \ldots, M\}$.

Then, the redundant sensors for $n = 0$ are considered in the cross difference co-arrays and only the positive co-arrays are analyzed due to its symmetric property. For any even $M \geq 2$, the lags from $(\frac{M}{2}+1)N$ to MN associated with ϕ_r can be generated by taking the self difference of the $(M+1)$th sensor from the sensor indices 1 to $\frac{M}{2}$ in $\mathbb{B}$. Therefore, after removing the sensors in ϕ_r for even M, all the lags can be generated by the remaining sensors which proves the existence of $\lceil \frac{M}{2} \rceil$ redundant sensors shown by dashed rectangle in Fig. 5.1.

For the scenario where M is odd, the value of n is set to 0 and to ensure the set ϕ_r still consists of redundant sensors, the lags from $\frac{M+1}{2}N$ to MN, related to the set ϕ_r are assumed to be generated by the remaining sensors. Considering the self difference of the $(M+1)$th sensor from sensor indices 1 to $\frac{M-1}{2}$, lags from $\frac{M+3}{2}N$ to MN can be generated. The $\frac{M+1}{2}N$ lag can be generated by taking difference of the $(M+1)$th sensor from the $(2M - \frac{M-3}{2})$th sensor where $(2M - \frac{M-3}{2}) = 3\frac{M+1}{2}$th sensor. Then the following relationship should be satisfied to ensure the existence of the $3\frac{M+1}{2}$th sensor:

$$3\frac{(M+1)}{2} \leq 2M - 1, \tag{5.11}$$

which solves for $M \geq 5$. This result also proves the existence of the redundant sensor set ϕ_r with $\lceil \frac{M}{2} \rceil = \frac{M+1}{2}$ sensors shown by dashed rectangle in Fig. 5.1. □

Instead of thinning redundant sensors from the conventional coprime array as mentioned in the proof, the TCA can be developed independently by a combination of three uniform linear subarrays in a straightforward way as follows.

Definition 5.1 (Thinned coprime arrays)**.** *Assume M and N are coprime integers with $M \geq 2$ for even M and $M \geq 5$ for odd M respectively, then the thinned coprime arrays are specified by the integer set $\mathbb{X}$, defined by*

$$\mathbb{X} = \mathbb{X}_1 \cup \mathbb{X}_2 \cup \mathbb{X}_3,$$

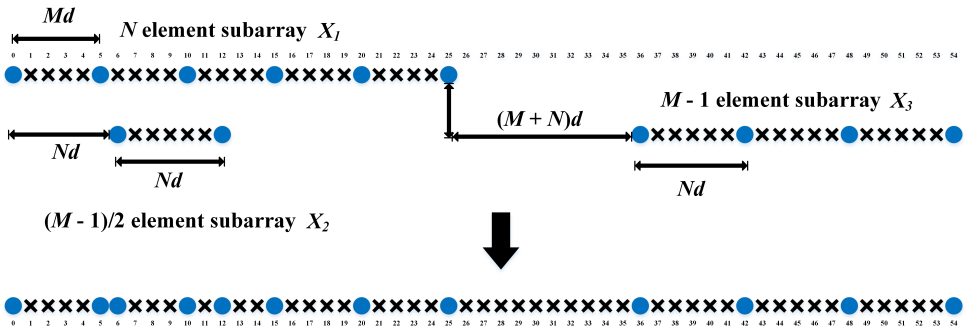

Figure 5.2: Thinned coprime sensor array for $M = 5$, $N = 6$.

where

$$\begin{cases} \mathbb{X}_1 = \{nMd \mid 0 \leq n \leq N-1\}, \\ \mathbb{X}_2 = \{mNd \mid 1 \leq m \leq \lfloor \frac{M}{2} \rfloor\}, \\ \mathbb{X}_3 = \{(m+M+1)Nd \mid 0 \leq m \leq M-2\}. \end{cases} \tag{5.12}$$

The sets $\mathbb{X}_1$, $\mathbb{X}_2$ and $\mathbb{X}_3$ represent the positions of sensors in the 1^{st}, 2^{nd} and 3^{rd} subarrays, respectively, which constitute the TCA. The total number of sensors is given by

$$S_{tcsa} = M + N + \lfloor \frac{M}{2} \rfloor - 1. \tag{5.13}$$

An example of the TCA with parameters $M = 5$ and $N = 6$ is shown in Fig. 5.2, where $\mathbb{X}_1 = \{0, 5, 10, 15, 20, 25\}d$, $\mathbb{X}_2 = \{6, 12\}d$ and $\mathbb{X}_3 = \{36, 42, 48, 54\}d$. The 3^{rd} subarray is displaced from the 1^{st} subarray by a spacing of $(M + N)d$ which in our case is $11d$ and is composed of $M - 1 = 4$ sensors separated by $Nd = 6d$. By combining these three subarrays, the total number of sensors in the TCA is given by $M + N + \lfloor \frac{M}{2} \rfloor - 1 = 12$.

5.4 Comparison of Number of Lags for Sparse Arrays

In this section the number of lags provided by the proposed TCA are compared to nested arrays, CADiS and its special cases for a fixed number of total sensors, where lags presented here represent two sided lags generated from the co-array structure of a sparse array.

Nested arrays for a given N_1 and N_2, where N_1 and N_2 represent the number of sensors in the two constituent subarrays, provide a hole-free co-array of $2N_2(N_1 + 1) - 1$ lags for

a total of $N_1 + N_2$ sensors. The CADiS structure in [54] brings two changes to the existing prototype coprime array. In the first change, the first subarray of N sensors is compressed by a factor p where $M = pM'$ for $2 \leq p \leq M$ with $1 \leq M' < M$ ($M' = 1$ is a special case for nested CADiS which will be discussed later). The resulting factors M' and N are still coprime. The elements of the first subarray then possess an inter-element spacing of $M'd$, while the second subarray of M sensors retains the original inter-element spacing of Nd. For the second change, it displaces the two subarrays by a factor Ld. It was shown in [54] that the CADiS configuration for $M' > 1$ achieves a maximum number of unique lags equal to $2MN + 2M - 5$ when $L > N(M-2)$, while the maximum number of consecutive lags is achieved when $L = M' + N$ with $MN - (M'-1)(N-2) + 1$ consecutive lags and $2MN + 2M' - 1$ unique lags. The number of unique lags increases with increasing M' while the consecutive lags decrease. Nested CADiS with $M' = 1$ provides a hole-free co-array of $2MN + 1$ lags. The proposed thinned coprime array retains all the properties of conventional coprime array, but with $\left\lceil \frac{M}{2} \right\rceil$ fewer sensors.

In the next step, the number of lags including consecutive and unique lags are generated for the sparse arrays under consideration. To further compare the sparsity of these array structures, the lag capacity beyond the redundancy [50] is defined as

$$\gamma(S) = \frac{S^2}{DOFs} \tag{5.14}$$

where S represents the total number of sensors in an array and $DOFs$ represents the number of lags measured by the number of consecutive lags or unique lags. The smaller the value of $\gamma(S)$, the higher the lag capacity with a specific number of sensors for that particular sparse array. Then the unique lags capacity for sparsest CADiS ($M' > 1$ with highest value of M' less than M and different cases of L), nested array, nested CADiS and TCA are plotted in Fig. 5.3, while the consecutive lags capacity are plotted in Fig. 5.4 with respect to the number of sensors from 12 to 40.

One potential problem in generating sparsest CADiS for any fixed number of sensors lies in the fact that sometimes the value of M available in combination with N to generate CADiS is a prime number itself (no factors for M other than 1), thus only offering the possibility of generating nested CADiS with $M' = 1$. For the analysis, all the available sparsest CADiS have been extracted, while nested arrays, nested CADiS and TCAs all

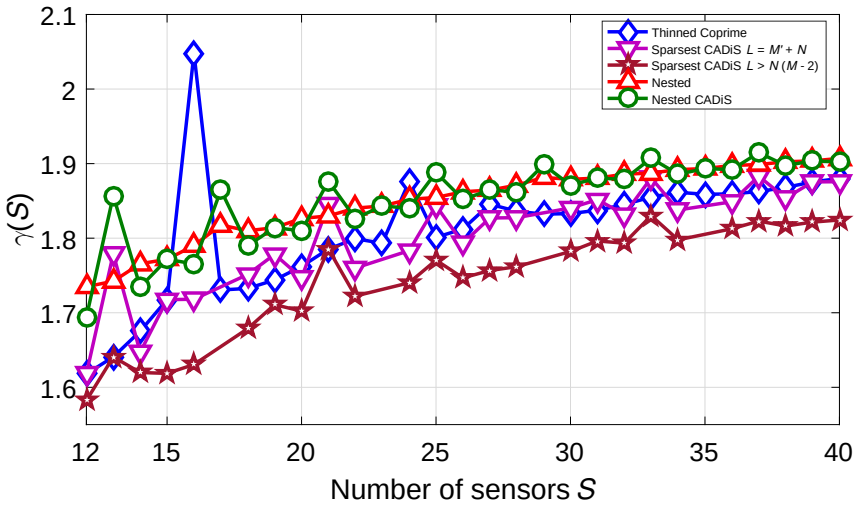

Figure 5.3: Unique lags capacity comparison for sparse arrays.

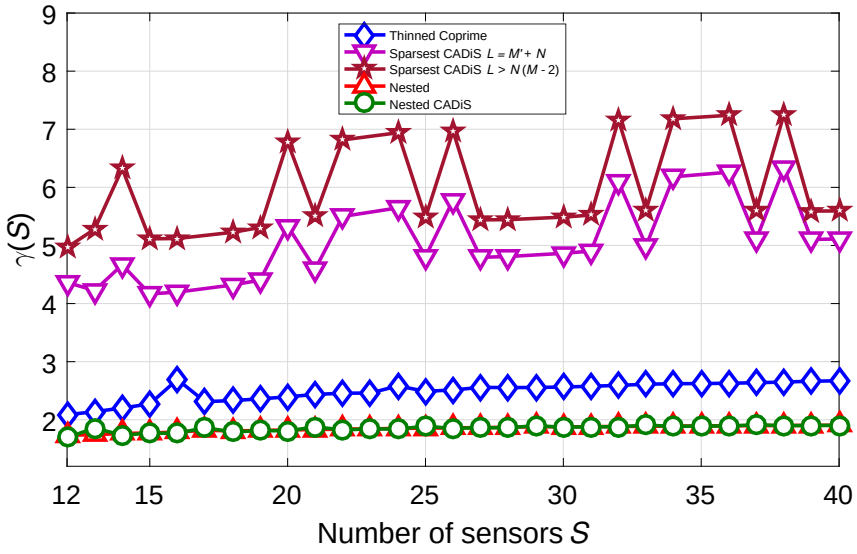

Figure 5.4: Consecutive lags capacity comparison for sparse arrays.

can be generated for the considered range of sensors. The combinations of parameters have been chosen to produce the highest possible number of lags. It can be seen in Fig. 5.3 that the unique lags of TCA are comparable to the unique lags of the sparsest CADiS with $L = M' + N$, while the sparsest CADiS with $L > N(M-2)$ generates the highest number of unique lags. The number of unique lags of TCA are greater than the hole-free structure of nested array and nested CADiS as depicted in Fig. 5.3. It is further examined by taking the ratio of the number of unique lags produced by TCA to the lags produced by nested array for each sensor size scenario and then taking the mean which comes out as 1.0283. For the case of consecutive lags in Fig. 5.4, nested array and nested CADiS produce the highest number of consecutive lags. The number of consecutive lags of TCA are around 75 percent to those of nested array which is calculated by taking the ratio of consecutive lags for TCA to the number of lags produced by nested array for each scenario of fixed number of sensors in the considered range of sensor array size and then calculating the mean of the ratio which comes out to be 0.7414, thus close to 75 percent. The sparse versions of CADiS produce the lowest number of consecutive lags in comparison to the TCA, nested array and nested CADiS.

Another interesting thing is the non-availability of sparsest CADiS for 4 different cases of fixed number of sensors i.e. 17, 23, 29 and 35 due to reasons mentioned earlier. The points in the lags curve where there is a spike in the value of $\gamma(S)$ corresponds to a relatively lower increase in the lags for that specific number of sensors and is attributed to the value of M'. A larger M' available for one scenario will generate lower number of lags with resulting increase in the value of $\gamma(S)$. If a smaller M' is available for the next sensor array size, it will generate higher number of lags with a smaller $\gamma(S)$, giving the presence of a spike in $\gamma(S)$ for the former case. On the whole, sparse versions of CADiS cannot be generated for any arbitrary number of sensors and possess very low number of consecutive lags to be exploited by MUSIC based DOA estimation methods. Their application lies directly in the CS-based methods, where their unique lags can be utilized. TCAs can be generated for any arbitrary number of sensors and the number of unique lags are much higher than most of the sparse arrays and even the consecutive lags generated by TCA are on average around 75 percent of the hole-free co-array generated

by nested arrays, which proves their application in both SS-MUSIC and CS-based DOA estimation methods.

5.5 Mutual Coupling Perspective

5.5.1 Mutual Coupling Model

Equation (5.2) of the received signal at the array assumes an interference free scenario between the sensors. In practice, the electromagnetic radiation received at each sensor is affected by the radiation from the neighbouring sensors. The closer the sensors spaced, the more significant the effect of this coupled radiation. Mutual coupling can be incorporated into the received signal as follows.

$$\mathbf{x}(t) = \mathbf{CAs}(t) + \mathbf{n}(t) \tag{5.15}$$

where $\mathbf{C}$ is the mutual coupling matrix, which for uniform linear arrays can be modelled by a B-banded symmetric Toeplitz matrix [59, 60, 97], where B is chosen to be a suitable inter-sensor spacing beyond which the effect of mutual coupling can be deemed negligible. The entries of the coupling matrix $\mathbf{C}$ in this case can be written as

$$\langle \mathbf{C} \rangle_{n_1,n_2} = \begin{cases} c_{|n_1-n_2|}, & \text{if } |n_1 - n_2| \leq B, \\ 0, & \text{otherwise} \end{cases} \tag{5.16}$$

where $n_1, n_2 \in \mathbf{p}$ and coupling coefficients $c_0, c_1, \ldots, c_B$ satisfy $1 = c_0 > |c_1| > |c_2| > \ldots |c_B|$. The magnitudes of coupling coefficients are assumed to be inversely proportional to their sensor separations [90] given by

$$|\frac{c_k}{c_l}| = \frac{l}{k} \tag{5.17}$$

5.5.2 Mutual Coupling and Thinned Coprime Array

The effect of mutual coupling can be quantified with the help of weight function parameter defined in [59]. The weight function $w(m)$ of an array $\mathbf{p}$ refers to the number of sensor

pairs corresponding to a particular value of co-array index m (which is an indication of the separation between the underlined sensor pair), given by

$$w(m) = \{(n_1, n_2) \in \mathbb{X}^2 \mid n_1 - n_2 = md\}, \qquad md \in \mathbb{C}_{\mathbb{P}}$$

The weight function values corresponding to small values of m would be of great interest as they contribute primarily towards mutual coupling in the array due to sensors separated by small multiples of inter-element spacing. In this subsection, the weight functions of TCA are presented along with the proof.

Theorem 2. *Let $\mathbb{X}$ be a thinned coprime array with $M \geq 2$* for even *M and $M \geq 5$* for odd *M* respectively. *Its weight functions $w(m)$ for $m = 1$, 2 and 3 are given by*

$$\begin{cases} w(1) = \begin{cases} 2, & M = 2, \\ 1, & M \geq 4, \end{cases} \\ w(2) = \begin{cases} N-1, & \textit{if } M = 2, \\ \frac{3M-5}{2}, & \textit{if } N = 2, \\ 2, & \textit{if } M = 4, \\ 1, & \textit{otherwise,} \end{cases} \\ w(3) = \begin{cases} \frac{3M-4}{2}, & \textit{if } N = 3 \textit{ for any even } M, \\ \frac{3M-5}{2}, & \textit{if } N = 3 \textit{ for any odd } M, \\ 2, & \textit{if } (M = 2, N \geq 5) \textit{ or } M = 6, \\ 1, & \textit{otherwise,} \end{cases} \end{cases} \tag{5.18}$$

Proof. It is clear that the displacement between the third sub-array of the TCA and the others is at least more than $5d$ since M and N are coprime. Then only the case when $\lfloor \frac{M}{2} \rfloor$ sensors of $\mathbb{X}_2$ interact with N sensors of $\mathbb{X}_1$ is considered. For any sensor of $\mathbb{X}_2$, there will be two sensors of $\mathbb{X}_1$ on either side of this sensor, resulting in 2 interactions per sensor with 2 lags less than the spacing Md for $\mathbb{X}_1$. For $\lfloor \frac{M}{2} \rfloor$ sensors of $\mathbb{X}_2$, this will result in

a total of $2\lfloor\frac{M}{2}\rfloor$ lags contributed to the cross-difference set. Consider an arbitrary sensor of $\mathbb{X}_2$ located at iNd (d is ignored in the following analysis for simplification), where $1 \leq i \leq \lfloor\frac{M}{2}\rfloor$, and then the distance of this sensor relative to the nearest sensor of $\mathbb{X}_1$ lesser in value than iN is given by

$$S_i = \text{mod}(iN, M), 1 \leq i \leq \left\lfloor \frac{M}{2} \right\rfloor \tag{5.19}$$

where mod refers to the modulo operator and returns the remainder of $\frac{iN}{M}$. Likewise, the distance of any arbitrary sensor of $\mathbb{X}_2$ relative to the nearest sensor of $\mathbb{X}_1$ greater in value than iN is given by

$$\hat{S}_i = M - \text{mod}(iN, M), 1 \leq i \leq \left\lfloor \frac{M}{2} \right\rfloor \tag{5.20}$$

The lags generated from the interaction of any arbitrary sensor of $\mathbb{X}_2$ relative to two sensors of $\mathbb{X}_1$ surrounding it take the form $(S_i, \hat{S}_i)$. It can be shown that the lags in sets S_i and $\hat{S}_i$ repeat with a period of M. Substituting i with $i + M$ in (5.19)

$$S_{i+M} = \text{mod}((i + M)N, M)$$

$$= \quad \text{mod } (iN, M) + \text{mod}(MN, M) = \text{mod}(iN, M) \tag{5.21}$$

Similarly for $\hat{S}_i$,

$$\hat{S}_{i+M} = M - \text{mod}((i + M)N, M)$$

$$= M - \text{mod}(iN, M) - \text{mod}(MN, M)$$

$$= M - \text{mod}(iN, M) \tag{5.22}$$

As each lag in sets S_i and $\hat{S}_i$ repeats with a period M, this proves the unique nature of lags present within both sets S_i and $\hat{S}_i$ for $1 \leq i \leq \lfloor\frac{M}{2}\rfloor$. To analyze the scenario when the lag from one set also appears in the other set, the condition is found when $S_i = \hat{S}_j$

$$\text{mod } (iN, M) = M - \text{mod}(jN, M), 1 \leq i, j \leq \left\lfloor \frac{M}{2} \right\rfloor \tag{5.23}$$

$$\text{mod } (iN, M) + \text{mod}(jN, M) = M \tag{5.24}$$

Applying modulo on both sides yields

$$\text{mod}\ (iN + jN, M) = \text{mod}(M, M) = 0 \tag{5.25}$$

Since M and N are coprime, the solution is given by

$$(i + j) = kM, k \in \mathbb{Z} \tag{5.26}$$

Since $1 \leq i, j \leq \lfloor \frac{M}{2} \rfloor$, the condition $(i + j) = kM$ cannot be satisfied for odd M. Then for even M, there exists $i = j = \frac{M}{2}$ that satisifes (5.26) with only one replicate lag at the $\frac{M}{2}$th sensor. As the lag values are of the form $(S_i, \hat{S}_i)$, this corresponds to values of these lags given as $(k, M - k)$, where $1 \leq k \leq M - 1$. For $k = \lfloor \frac{M}{2} \rfloor$, the lag pair will be equal to $(\lfloor \frac{M}{2} \rfloor, \lceil \frac{M}{2} \rceil)$. For even M, $i = j = \frac{M}{2}$ which implies that the repitition of lag for even M will occur at index $\frac{M}{2}$. To find the repeated value of lag pair at index $\frac{M}{2}$, this sensor in $\mathbb{X}_2$ is assumed to be displaced from its corresponding two sensors of $\mathbb{X}_1$ by $\frac{M}{2}$. This corresponds to the position of the outer sensor of $\mathbb{X}_1$ relative to the $\frac{M}{2}$th sensor of $\mathbb{X}_2$ at $\frac{MN}{2} + \frac{M}{2} = \frac{M(N+1)}{2}$. Then the condition is found when $\frac{N+1}{2} \leq N - 1$ (the outermost index of $\mathbb{X}_1$), which solves for $N \geq 3$. This proves that the repeated lag pair for even M occuring at index $\frac{M}{2}$ has a value equal to $\frac{M}{2}$. This value of repeated lag can also be alternatively checked by analyzing the case when for even M, lag pair $(\lfloor \frac{M}{2} \rfloor, \lceil \frac{M}{2} \rceil)$ reduces to $(\frac{M}{2}, \frac{M}{2})$. As a result $w(\frac{M}{2}) = 2$ for even M.

Now different weight scenarios for even $M \geq 4$ and $N > 3$ are considered. Starting with $M = 4$, two sensors in $\mathbb{X}_2$ contribute four lags in total with values 1, 3 and two lags with values 2 proving $w(2) = 2$ and $w(1) = w(3) = 1$. For $M = 6$, three sensors in $\mathbb{X}_2$ contribute six lags in total with vaules 1, 5, 2, 4 and two lags with values 3 proving $w(3) = 2$ and $w(1) = w(2) = 1$. For $M > 6$ and $N > 3$, $w(1) = w(2) = w(3) = 1$ as the repeated lag for even M i.e. $\frac{M}{2} > 3$. For odd valued M with $N > 3$, the resulting lag pairs are all unique as shown above.

Now some special cases of weight functions are considered starting with the case when $N = 3$ and M is even. It is clear that $\frac{M}{2} - 1$ pairs of sensors in $\mathbb{X}_2$ will be separated by a spacing of 3 in adddition to $M - 2$ pairs of sensors in $\mathbb{X}_3$. Adding the one unique lag equal to 3 from the interaction between the zeroth sensor of $\mathbb{X}_1$ and the first sensor of $\mathbb{X}_2$,

then for any even M and $N = 3$, $w(3) = \frac{3M-4}{2}$. For the case of odd M and $N = 3$, the only difference is that $\frac{M-1}{2} - 1 = \frac{M-3}{2}$ pairs of sensors in $\mathbb{X}_2$ separated by 3 which will give an overall $w(3) = \frac{3M-5}{2}$. The case of odd M with $N = 2$ will also have $w(2) = \frac{3M-5}{2}$.

Finally the weights scenario is considered when $M = 2$, resulting in one sensor contained in $\mathbb{X}_2$. This sensor through interaction with two sensors of $\mathbb{X}_1$ that are separated by a spacing of 2, contributes two lags in total with values 1 proving $w(1) = 2$. The value $w(2)$ depends on N as $N - 1$ sensor pairs in the N-element subarray will be separated by inter-element spacing of 2 generating $w(2) = N - 1$. For $w(3)$, the case is considered when $N \geq 5$, then one sensor in $\mathbb{X}_2$ generating $w(1) = 2$ by falling in the middle of the two sensors of $\mathbb{X}_1$ will always be at a distance of 3 from the outer two sensors surrounding the two sensors of $\mathbb{X}_1$ on each side that generated $w(1)$, yielding $w(3) = 2$ for $M = 2$, $N \geq 5$.

As arrays with odd M provide $2\lfloor \frac{M}{2} \rfloor = 2\frac{M-1}{2} = M - 1$ unique lags and the even valued M provide $M - 2$ unique and two same valued lags with value $\frac{M}{2}$, it implies $w(1) = 1$ for $M \geq 4$. As $w(2) = 2$ only for $M = 4$, it proves $w(2) = 1$ otherwise. Likewise, $w(3) = 2$ for $M = 2$, $N \geq 5$ and $M = 6$ while $w(3) = 1$ otherwise, thus completing the proof. It is interesting to note that for odd $M \geq 5$ and $M > 6$ for even M, with $N > 3$, TCA possesses $w(1) = w(2) = w(3) = 1$. □

5.5.3 Array Profile Comparison and Mutual Coupling

In this subsection different types of sparse arrays are considered in the presence of mutual coupling. For that purpose, the consdered 12-sensor sparse arrays comprise of two second order super nested arrays for the parameters $N_1 = N_2 = 6$ and $N_1 = 5$, $N_2 = 7$, one 3^{rd} order super nested array for $N_1 = 5$, and $N_2 = 7$, MRA as

$$\{0, 1, 6, 14, 22, 30, 38, 40, 42, 45, 47, 49\}d$$

[57], sparse versions of CADiS for $M = 6$, $N = 7$, $p = 2$ and 3, and TCA for $M = 5$ and $N = 6$. The mutual coupling model is based on (5.16) with $c_1 = 0.4e^{j\pi/3}$, $B = 10$ and $c_l = c_1 e^{-j(l-1)\pi/8}/l$ for $2 \leq l \leq B$. The analysis of these sparse arrays from different perspectives is provided in Fig. 5.5 where the weight functions $w(m)$ are provided in the

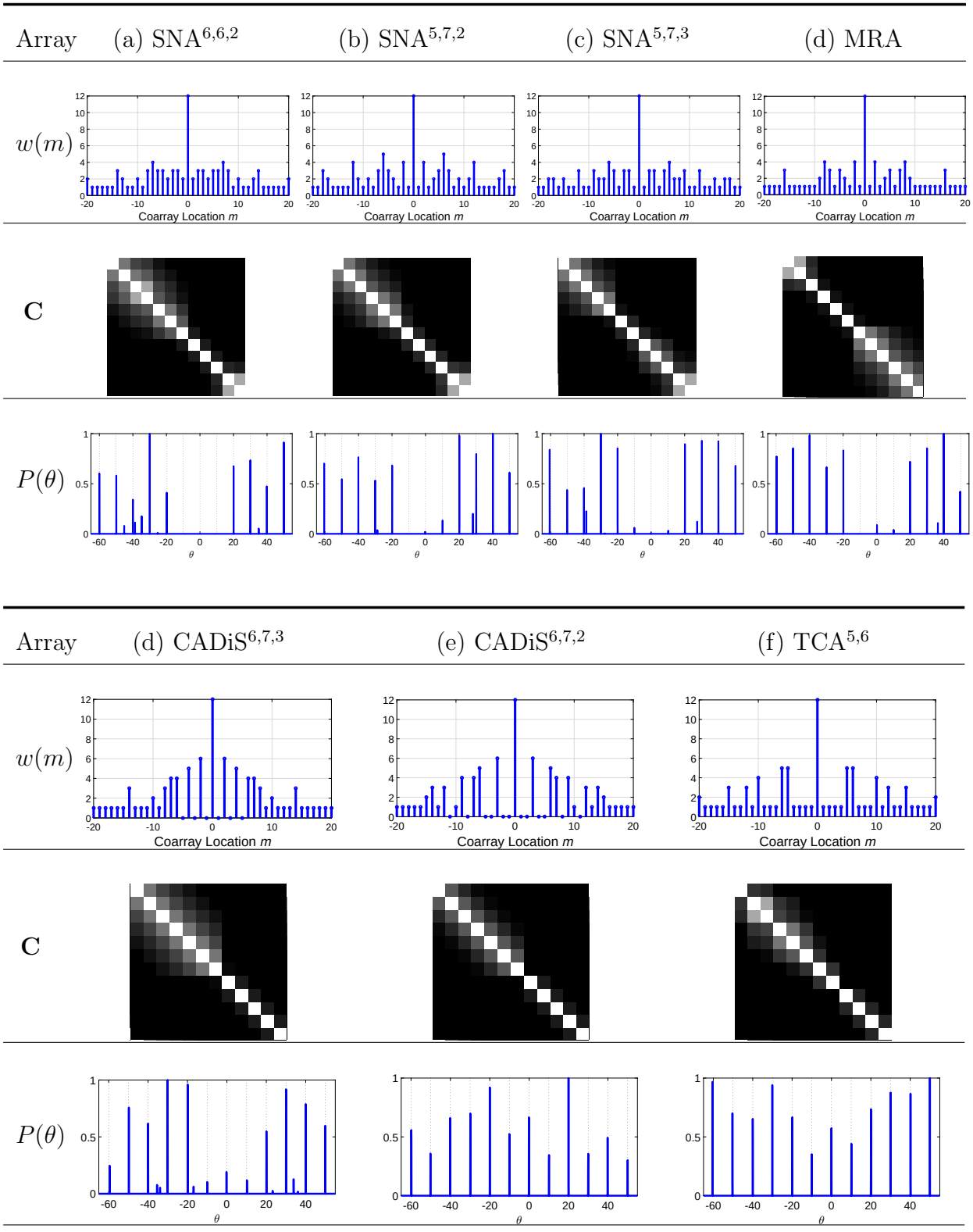

Figure 5.5: Comparison among 12 sensors 2nd order super nested array, 3rd order super nested array, MRA, sparse CADiS and TCA in the presence of mutual coupling.

Array	$\text{SNA}^{6,6,2}$	$\text{SNA}^{5,7,2}$	$\text{SNA}^{5,7,3}$	$\text{CADiS}^{6,7,2}$	$\text{CADiS}^{6,7,3}$	$\text{TCA}^{5,6}$	MRA
Aperture	41	41	41	49	56	54	49
Uni. Lags	83	83	83	87	89	89	99
Con. Lags	83	83	83	38	33	69	99
Max. sources SS-MUSIC	41	41	41	18	16	34	49
$w(1)$	2	1	1	0	0	1	1
$w(2)$	3	4	3	6	0	1	4
$w(3)$	3	1	3	0	6	1	1

Table 5.1: Sparse array characteristics for 12 sensors.

second and sixth row of Fig. 5.5 and $|[\mathbf{C}]_{i,j}|^2$ is shown on log scale in the third and seventh row. The regions in dark indcate less energy for that particular entry and it is important to note that the off-diagonal entries of the matrix, i.e, the entries showing the interaction between different sensors characterize the amount of mutual coupling for the sparse array. The darker these off-diagonal entries, the less the mutual coupling experienced by the particular sparse array. Looking at the coupling matrix structure, it is visible that the TCA and CADiS have less off-diagonal energy and more sparsity than the super nested arrays.

The array profile for these arrays is shown in Table 5.1, highlighting different array characteristics like aperture, unique and consecutive lags, maximum number of detectable sources using SS-MUSIC and number of smaller weight functions like $w(1)$, $w(2)$ and $w(3)$. It is clear that the MRA contains the highest number of lags with a hole-free co-array of 99 lags. Sparsest CADiS for $p = 2$ and thinned coprime array both attain unique lags equal to 89 which can all be used in CS-based DOA estimation techniques followed by sparse CADiS for $p = 3$ with 87 lags and then the super nested arrays with 83 lags for a hole-free structure. Talking from the SS-MUSIC perspective which halves the available number of consecutive lags for application in DOA estimation, the sparsest structure of CADiS with $p = 2$ results in the lowest number of consecutive lags with only 16 number

of sources able to be identified and resolved. As the segment of consecutive lags for CADiS are not centered around zero, for application of SS-MUSIC, the largest portion of consecutive lags is extracted from the available segments of consecutive lags in the co-array followed by the spatial smoothing technique to generate the covariance matrix based on the extracted co-array segment before applying MUSIC. In comparison to sparse CADiS, thinned coprime array, super nested arrays and MRA have a capacity to solve up to 34, 41 and 49 sources respectively.

5.6 Simulation Results for DOA Estimation

In this section, the considered sparse arrays are investigated with respect to their DOA estimation performance under the effect of mutual coupling. For the analysis, both the CS-based DOA estimation technique as well as the subspace based SS-MUSIC will be used.

The DOA estimation results in this Chapter are obtained by modelling narrowband uncorrelated sources impinging on an array comprising of a number of sensors with mutual coupling model incorporated. The covariance matrix is constructed by using the received data on the array for a number of snapshots. As the performance of considered sparse arrays is investigated from the perspective of DOA estimation using both compressive sensing (CS) based method and spatial smoothing (SS) based MUSIC, different steps are required to obtain the DOA spectrum.

The power received at the array from different sources is concentrated at few locations given by the source DOAs which implies that the received signal power is sparse in the angular domain. It is also supported by the fact that the DOA spectrum of signals is usually sparse. This motivates the use of compressive sensing (CS) for DOA estimation. DOA estimation is usually done by constructing the covariance matrix from the received data. The covariance matrix is vectorized to simulate a longer virtual array used to received the data. A sensing matrix/dictionary consisting of searching steering vectors is constructed for the virtual array on a finite grid and the sparse DOA spectrum with peaks corresponding to the DOA of the estimated sources is obtained by solving the l_1-norm

minimization problem which balances the sparsity of the spectrum with the parameter estimation error. This technique makes it possible to utilize all unique lags generated from the difference co-array of a sparse array. The details of CS-based DOA estimation method will be presented later in this Chapter.

To utilize the lags originating from the difference co-array of a particular array, the covariance matrix is vectorized. However, the vectorization step makes the received data from uncorrelated sources impinging on a physical array appear as data received by a longer virtual array from correlated sources which unables the application of MUSIC algorithm to find DOA. To utilize the MUSIC algorithm [17], rank enhancement is required for the matrix constructed from the vectorized data. Spatial smoothing is one such step which creates a positive semidefinite matrix with suitable rank [42, 43]. To perform spatial smoothing, all the consecutive lags resulting from the difference co-array are extracted and the vectorized covariance matrix is processed and sorted so that all the consecutive lag entries are available in the right sequence. Then the spatial smoothing step is performed to create a new covariance matrix with full rank on which MUSIC algorithm can be performed. The resulting peaks in the MUSIC spectrum correspond to the estimated peaks of the source DOAs. Then the error performance for both CS-based and SS-MUSIC based DOA estimation is evaluated by calculating the respective root mean square error (RMSE) for the parameter estimates for different sparse arrays.

To make use of all unique lags provided by the difference co-array of a sparse array, the CS-based DOA estimation method is utilized [62] which is briefly reviewed as follows.

Referring to (5.4), CS-based DOA estimation method involves vectorizing the covariance matrix $\mathbf{R_{xx}}$ given by

$$\mathbf{z} = vec(\mathbf{R_{xx}}) = \tilde{\mathbf{A}}\mathbf{b} + \sigma_n^2\tilde{\mathbf{I}} = \mathbf{B}\mathbf{r}\,, \tag{5.27}$$

where $\tilde{\mathbf{A}} = [\tilde{\mathbf{a}}(\theta_1), ..., \tilde{\mathbf{a}}(\theta_Q)]$, $\tilde{\mathbf{a}}(\theta_q) = \mathbf{a}^*(\theta_q) \bigotimes \mathbf{a}(\theta_q)$, $\mathbf{b} = [\sigma_1^2, ..., \sigma_Q^2]^T$, $\tilde{\mathbf{I}} = vec(\mathbf{I}_S)$. The distinct rows of $\tilde{\mathbf{A}}$ behave like the steering vector of a longer array whose sensor locations are given by the difference in positions of the sensors of the physical array which corresponds to the difference co-array of the physical array. The matrix $\mathbf{I}_S$ has a dimension equal to the number of sensors in the array. Additionally, $\mathbf{B} = [\tilde{\mathbf{A}}, \tilde{\mathbf{I}}]$ while

$\mathbf{r} = [\mathbf{b}^T, \sigma_n^2]^T = [\sigma_1^2, ..., \sigma_Q^2, \sigma_n^2]^T$.

Estimating the DOA spectrum of sources $\mathbf{r}$ which represents the power of Q sources in addition to the noise power estimate in (5.27) can be achieved by solving the following optimization problem:

$$\min \quad \|\mathbf{r}^\circ\|_1 \quad \text{s.t.} \quad \|\mathbf{z} - \mathbf{B}^\circ \mathbf{r}^\circ\|_2 < \epsilon \tag{5.28}$$

Although the signal model is sparse in a continuous angular domain, to apply the CS framework we need to construct a finite dictionary by sampling this domain with a predefined sampling grid i.e., the angle space is divided into a large number of sampling points (grids) where the source directions of interest are assumed to exactly lie on some of the grids. In the optimization problem, $\mathbf{B}^\circ$ is the dictionary composed of searching steering vectors and $\tilde{\mathbf{I}}$, whereas $\mathbf{r}^\circ$ is a vector of sparse entries to be determined from the search grid. The sensing matrix/dictionary $\mathbf{B}^\circ$ and the DOA spectrum estimate vector $\mathbf{r}^\circ$ are defined over a finite grid $\theta_1^g, ..., \theta_G^g$ where $G \gg Q$. The last entry of $\mathbf{r}^\circ$ represents the estimate of σ_n^2, whereas the positions and values of the nonzero entries in other elements of $\mathbf{r}^\circ$ represent the estimated DOAs and the corresponding signal powers, respectively. The sensing matrix/dictionary composed of searching steering vectors satisfies the restrictive isometry property (RIP) and incoherence required for successful recovery of DOA spectrum.

The regularisation/trade-off parameter in the optimization problem is given by ϵ or the λ function where this regularisation parameter is a user specific bound which is chosen after repeated trials as the best value for a particular simulation scenario which gives a clean DOA spectrum (good sparsity) along with a reasonable parameter estimation error. The value of the trade-off parameter ϵ can be increased to provide more sparsity (less number of non-zero entries) at the cost of increased least square error in the estimates.

It is worth mentioning the difference between the trade-off parameter ϵ or the λ function and the weight function used in sparsity. The weight function $w(m)$ is used to quantify the sparsity of an array by showing the number of sensor pairs for a certain degree of separation (lag). The lower the value of weight functions like $w(1)$, $w(2)$ and $w(3)$ corresponding to smaller separation between sensors d, $2d$ and $3d$, where d is the wavelength of the signal for the highest frequency component, the sparser an array. This

sparsity also leads to reduced mutual coupling between sensors. Overall, ϵ or the λ function deals with the sparsity of the DOA spectrum while the weight function quantifies the sparsity of an array.

For simulation, the parameters considered here are 5 dB SNR (signal to noise ratio which measures signal strength relative to background noise and is given by $10 * log\frac{S}{N}$ where S and N represent signal and noise voltages in volts respectively), 1000 snapshots, 12 uncorrelated sources evenly spaced between $-60°$ and $60°$ with ϵ chosen empirically for a clear and fine DOA estimate. A search grid of 3601 angles is formed in the full angle range with a step size of $0.05°$. The estimation results are shown in the fourth and eighth rows of Fig. 5.5.

It can be seen that the 2^{nd} order super nested array with $N_1 = N_2 = 6$ is missing 3 sources while the 2^{nd} and 3^{rd} order super nested array with $N_1 = 5$ and $N_2 = 7$ and MRA are all missing at least one source with the other two sources at extremely low powers and being buried under the accompanying noise in the spectrum. Sparse CADiS with $p = 3$ has a noisy spectrum with the power of three sources being degraded while both the sparsest CADiS with $p = 2$ and thinned coprime array are able to resolve the 12 sources with a fine DOA spectrum in the presence of mutual coupling.

The three missing peaks for the 2^{nd} order super nested array with $N_1 = N_2 = 6$ are attributed to a higher $w(1)$ i.e. $w(1) = 2$ compared to $w(1) = 1$ for the other two super nested arrays and MRA which limits the use of this particular super nested array for lower values of $|c_1|$. The sparser structure of TCA and sparsest CADiS hold promising potential to counter mutual coupling using CS-based DOA estimation techniques.

To give a better understanding of the benefits of the proposed TCA, another scenario is considered with different set of parameters to check the performance of these arrays under the effect of mutual coupling. Here a signal processing case is encountered where a 17 sensor array is required for DOA estimation of 20 incoming signals in an environment with moderate SNR and heavy mutual coupling. All of the 20 sources considered here are narrowband uncorrelated sources with a peak amplitude of unity. The paremeters set for such a scenario are modeled as 10 dB SNR, 1000 snapshots and a mutual coupling coefficient with its magnitude $|c_1|$ assumed to be equal to 0.4 with the remaining

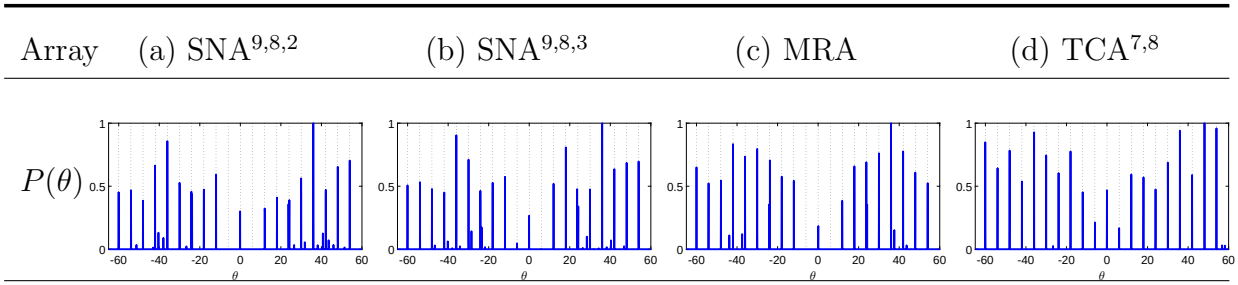

Figure 5.6: Comparison among 17 sensors 2nd order super nested array, 3rd order super nested array, MRA and thinned coprime array in the presence of mutual coupling.

parameters the same as above. It is obvious that for a 17 sensor array, it is not possible to generate sparse CADiS as described in Section 5.4. For other sparse arrays, second and third order super nested arrays for the choice of $N_1 = 9$ and $N_2 = 8$, MRA as $\{0, 1, 8, 18, 28, 38, 48, 58, 68, 78, 80, 82, 84, 87, 89, 91, 93\}d$ [57], and thinned coprime array for $M = 7$ and $N = 8$ can be generated.

MRA and super nested arrays have hole-free co-arrays with 187 and 159 consecutive lags respectively, while thinned coprime array generates 125 consecutive lags and 167 unique lags respectively. The critical part of the analysis is the weight functions for these arrays. The second order super nested array has the highest $w(2)$ among all the arrays equal to 8 with $w(1) = w(3) = 1$, while $w(1) = 1$, $w(2) = 6$, $w(3) = 1$ for MRA, and $w(1) = 1$, $w(2) = 5$, $w(3) = 2$ for the 3rd order super nested array. Thinned coprime array again provides attractive set of weight functions with $w(1) = w(2) = w(3) = 1$. The estimation results are shown in Fig. 5.6, where it can be clearly seen that the super nested arrays and MRA are unable to distinguish all 20 sources and have a degraded spectrum with missing sources and lots of spurious peaks, while the TCA, due to its improved sparsity, is able to detect all sources with a fine spectrum showcasing its potential to counter heavy mutual coupling when other sparse arrays are simply not available or not able to cope with the conditions.

In the previous scenarios, the DOAs of all sources were assumed to be evenly spaced between -60 and 60 degrees with sufficient separation between them. However, there can be many practical scenarios where the source DOAs are quite close to each other. To investigate the DOA estimation of sources with close spacing, 20 sources considered in

Array	(a) SNA^{9,8,2}	(b) SNA^{9,8,3}	(c) MRA	(d) TCA^{7,8}

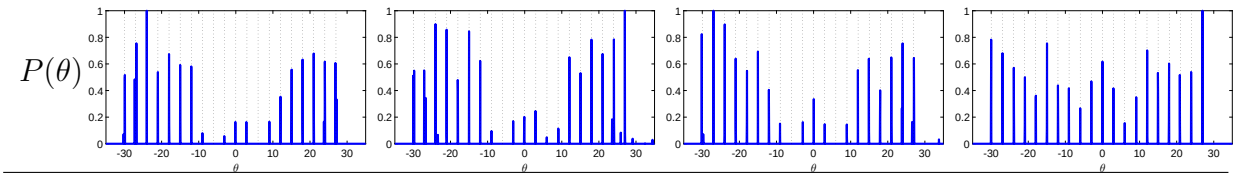

Figure 5.7: Comparison among 17 sensors 2nd order super nested array, 3rd order super nested array, MRA and thinned coprime array in the presence of mutual coupling with closely spaced sources.

Figure 5.6 are evenly spaced between -30 and 30 degrees with half the source spacing as the previous case and the estimation results using same parameters as Figure 5.6 are shown in Figure 5.7. It can be seen that the second order super nested array, third order super nested array and MRA are all missing sources with lots of spurious peaks in a heavy mutual coupling scenario with $|c_1|= 0.4$ due to a higher $w(2)$ while the thinned coprime array is able to estimate all 20 sources with a clean spectrum.

In the next step, a comparison of weight functions for these sparse arrays is provided in Table 5.2 as mentioned in [54, 59, 60]. Although super nested arrays (both second order and higher orders) have smaller $w(1)$ and $w(3)$, their $w(2)$ is dependent on N_1 and thus increases with the array size, which ia a significant challenge in tackling mutual coupling.

Sparse CADiS on the other hand has a zero-valued $w(1)$ and depending on the value of M, subsequently $M^{'}$, can have either $w(2)$ or $w(3)$ equal to $N- 1$ which will also increase with increasing array size but overall maintain good level of sparsity. The proposed TCA has its weights $w(1)$, $w(2)$ and $w(3)$ independent of the array size and maintains $w(1) = w(2) = w(3) = 1$ for odd $M \geq 5$ and $N > 3$, which makes it a promising array structure in combating the ills of mutual coupling.

Investigating the DOA estimation error performance of sparse arrays involves testing the considered arrays under a different range of scenarios with a number of variables. The more the diverse range of scenarios considered, the better the overall analysis of the strengths and weaknesses of different arrays. As mutual coupling is inevitable between the sensors of an array, there is a need to model the mutual coupling intensity which

Array	SNA $Q = 2$ $N_1 \geq 4$, $N_2 \geq 3$	SNA $Q \geq 3$, (Odd N_1) $N_1 \geq 3 \times 2^Q - 1$, $N_2 \geq 3Q - 4$	SNA $Q \geq 3$, ($Even$ N_1) $N_1 \geq 2 \times 2^Q + 2$, $N_2 \geq 3Q - 4$
$w(1)$	$\begin{cases} 2, & N_1 \textit{ is even,} \\ 1, & N_1 \textit{ is odd,} \end{cases}$	1	2
$w(2)$	$\begin{cases} N_1 - 3, & N_1 \textit{ is even,} \\ N_1 - 1, & N_1 \textit{ is odd,} \end{cases}$	$2 \lfloor \frac{N_1}{4} \rfloor + 1$	$\begin{cases} \frac{N_1}{2} + 1, & N_1 = 8k - 2, \\ \frac{N_1}{2} - 1, & N_1 = 8k + 2, \\ \frac{N_1}{2}, & \textit{otherwise}, k \in \mathbb{Z} \end{cases}$
$w(3)$	$\begin{cases} 3, & N_1 = 4, 6, \\ 4, & N_1 \textit{ is even}, N_1 \geq 8, \\ 1, & N_1 \textit{ is odd,} \end{cases}$	2	5

Array	Sparse CADiS $M = pM'$, $2 \leq p \leq M$, $1 \leq M' < M$	TCA $M \geq 2$ (even M), $M \geq 5$ (odd M)
$w(1)$	0	$\begin{cases} 2, & M = 2 \\ 1, & M \geq 4, \end{cases}$
$w(2)$	$\begin{cases} N - 1, & \textit{if } M' = 2, \\ 0, & \textit{otherwise}, \end{cases}$	$\begin{cases} N - 1, & \textit{if } M = 2, \\ \frac{3M-5}{2}, & \textit{if } N = 2, \\ 2, & \textit{if } M = 4, \\ 1, & \textit{otherwise} \end{cases}$
$w(3)$	$\begin{cases} N - 1, & \textit{if } M' = 3, \\ 0, & \textit{otherwise}, \end{cases}$	$\begin{cases} \frac{3M-4}{2}, & \textit{if } N = 3 \textit{ for any even } M. \\ \frac{3M-5}{2}, & \textit{if } N = 3 \textit{ for any odd } M. \\ 2, & \textit{if } (M = 2, N \geq 5) \textit{ or } M = 6, \\ 1, & \textit{otherwise,} \end{cases}$

Table 5.2: Weight functions comparison for sparse arrays.

can be done by varying the mutual coupling coefficient for different strengths of mutual coupling by fixing other variables like signal-to-noise ratio (SNR), number of snapshots and then checking the error in the parameter estimation. Investigating the performance of arrays in changing channel conditions for different noise levels also gives a clear picture of how different structures cope with the noisy channel. This can be done by varying SNR and fixing other variables like mutual coupling intensity and number of snapshots. Number of snapshots is a significant variable and in practical scenarios, often few number of snapshots are available due to limited hardware and processing capabilities. Thus an investigation with varying number of snapshots gives an idea of the robustness and the practical capability of the arrays. This can be achieved by varying snapshots while fixing mutual coupling intensity and SNR.

From the perspective of mutual coupling, most of the well-known sparse arrays like MRA and super nested arrays show an increase in the number of sensor pairs with smaller multiples of inter-element spacing like d, $2d$ and $3d$ with increased array size. These weight functions $w(1)$, $w(2)$ and $w(3)$ contribute directly to the intensity of mutual coupling experienced by a particular sparse array. As a result, it is important to evaluate the performance of the proposed thinned coprime array with these sparse arrays for an increased array size.

The simulation scenarios in this Chapter are designed to investigate the RMSE performance of the considered sparse arrays from the perspective of both CS and SS-MUSIC based DOA estimation methods. As the CS-based DOA estimation method is able to utilize all available lags (unique lags) resulting from the difference co-array of the arrays, the increased range of parameter values for which these arrays can be tested provides for more diverse simulation scenarios. In comparison, the SS-MUSIC method due to the application of spatial smoothing halves the number of extracted consecutive lags which limits the range of simulation scenarios. For a fair comparison of the performance of the sparse arrays in these two methods, different set of simulation scenarios will be chosen to assess RMSE for varying mutual coupling intensity, SNR and number of snapshots.

To investigate the DOA estimation error performance of these sparse arrays under the effect of mutual coupling, the root mean square error (RMSE) curves are calculated for

varying intensity of mutual coupling coefficient $|c_1|$, varying number of snapshots T and across a range of different values of SNR where the accuracy of DOA estimation in this thesis is quantified by root mean square error (RMSE) which is given by

$$\text{RMSE} = \sqrt{\frac{\sum_{i=1}^{I}\sum_{q=1}^{Q}\left(\hat{\theta}_q(i) - \theta_q\right)^2}{IQ}} \tag{5.29}$$

where I independent simulation runs are performed to calculate the root mean square error between the estimate $\hat{\theta}_q(i)$ and the actual DOA θ_q for each of the Q sources.

For the RMSE analysis, 10 narrowband sources impinge on a 12-sensor array where the considered sparse arrays include MRA, super nested array, TCA and sparse CADiS. First, the CS-based results are presented and the performance from the perspective of varying mutual coupling intensity is investigated where for CS-based DOA estimation, all the unique lags offered by the arrays are utilized. The parameters considered are 5 dB SNR, 1000 snapshots and $|c_1|$ varied from 0 to 0.7 which model a practical noisy channel with varying mutual coupling and moderate number of snapshots. The results are presented in Fig. 5.8 where each point is an average of 200 independent simulation runs. It can be observed that although MRA and super nested arrays possess lower error than CADiS and TCA, they are only capable of detecting all the sources in low to medium level of mutual coupling. For higher levels of mutual coupling, super nested arrays suffer heavily from missing sources, spurious peaks and degraded spectrum. Sparsest CADiS and TCA are able to tolerate severe mutual coupling with minimum loss to the spectrum. Thinned coprime array detects all sources till $|c_1|= 0.7$ while sparsest CADiS suffers from two source peaks degraded by the severe mutual coupling, making TCA the most robust of all the arrays due to its improved sparsity.

The RMSE results against the number of snapshots and SNR for $|c_1|= 0.3$ with remaining parameters same as before are shown in Figs. 5.9 and 5.10, respectively, where it can be seen that the MRA possesses the lowest RMSE due to high number of lags. MRA and super nested arrays with $w(1) = 1$ are able to tolerate medium levels of mutual coupling and achieve better estimation performance compared to sparse CADiS and the TCA. As the mutual coupling gets stronger, these arrays start missing sources, having the

spectrum contaminated with spurious peaks and eventually lose their applicability and that is where sparse CADiS and TCA come into play as shown by the results in Fig. 5.8.

Next, the SS-MUSIC based results are presented. Fig. 5.11 shows the RMSE for varying mutual coupling intensity in the range of $|c_1|= 0$ to 0.2 with 10 dB SNR and 1000 snapshots. The shorter range of mutual coupling is assumed relative to the CS case keeping in mind the corresponding reduction in the number of lags when using SS-MUSIC. It can be observed that the TCA, despite having lower number of lags compared to MRA and super nested arrays, matches the performance of these arrays as the mutual coupling levels rise. This is entirely made possible due to the attractive levels of sparsity offered by their structure. Sparse CADiS suffers from an increased error due to a dramatic reduction in the available number of lags for SS-MUSIC with only 18 and 16 for the sparse versions of CADiS considered. For RMSE curves against the number of snapshots and SNR, $|c_1|=$ 0.1 is considered and the results are presented in Figs. 5.12 and 5.13 respectively, where it can be seen that the TCA possesses a lower RMSE than super nested arrays and MRA especially at low to medium levels of mutual coupling due to a relatively sparser array structure.

Speaking from a practical point of view, assuming equal SNR for all the sources is unrealistic. In real world, different sources impinging on an array are coming from different directions and from different distances with varying channel conditions, resulting in different SNR values for each of the sources. The way forward is to assume a 10 dB dynamic range of SNR for the considered sources for DOA estimation in the presence of mutual coupling where the SNR of each source is uniformly distributed in the range [0,10] dB. The RMSE curves against varying mutual coupling for CS and SS-MUSIC in Figs. 5.8 and 5.11 are reproduced for dynamic range of SNR in Fig. 5.14 and Fig. 5.15 respectively. Analyzing Fig. 5.14, due to the 10 dB dynamic range of SNR with more noisy conditions compared to fixed 5 dB in the previous case, the overall operational range of mutual coupling in the new results has reduced from $|c_1| = 0.7$ to 0.6. The results again show the robust nature of the proposed TCA. Although the array incurs increased error compared to super nested arrays and MRA, it is able to outperform all other sparse arrays in tackling heavy levels of mutual coupling. Further more, even the sparsest among sparse

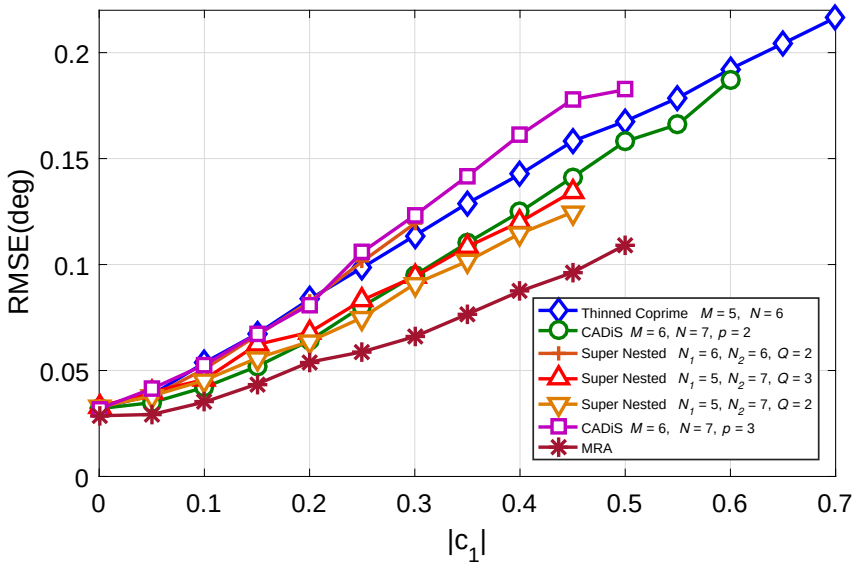

Figure 5.8: RMSE versus mutual coupling coefficient $|c_1|$ for CS.

CADiS loses its application at $|c_1| = 0.5$. In Fig. 5.15, it is clear that the error for sparse CADiS has increased a lot. It is directly in line with the use of dynamic range SNR as the low SNR for certain sources increases the overall error in the estimates and this effect is magnified by the lower number of lags available for sparse CADiS for SS-MUSIC. TCA again shows that it can match the performance of super nested arrays and MRA at low to medium levels of mutual coupling using SS-MUSIC.

In the light of the findings above, a general character comparison of the considered sparse arrays is presented in Table 5.3 where certain characteristics like availability for any array size, compatibility with CS, SS-MUSIC and relationship of critical weights functions with array size are described. Sparse CADiS finds its limitations in the use of SS-MUSIC as a few number of lags are left for use. It is also not available for any array size as mentioned before, although it is good at tackling mutual coupling. Super nested arrays and MRA are good at SS-MUSIC and CS but both have a problem of increasing critical weight $w(2)$ with array size, even for the sparsest of them, the third order super nested array as a function of N_1 which can create challenges to tackle heavy levels of mutual coupling. MRA is also limited by the fact that arrays for more than 20 sensors are still not defined in [50, 57] due to the increase in complexity of the search mechanism and longer computation time to obtain MRA. The proposed TCA is available for any array

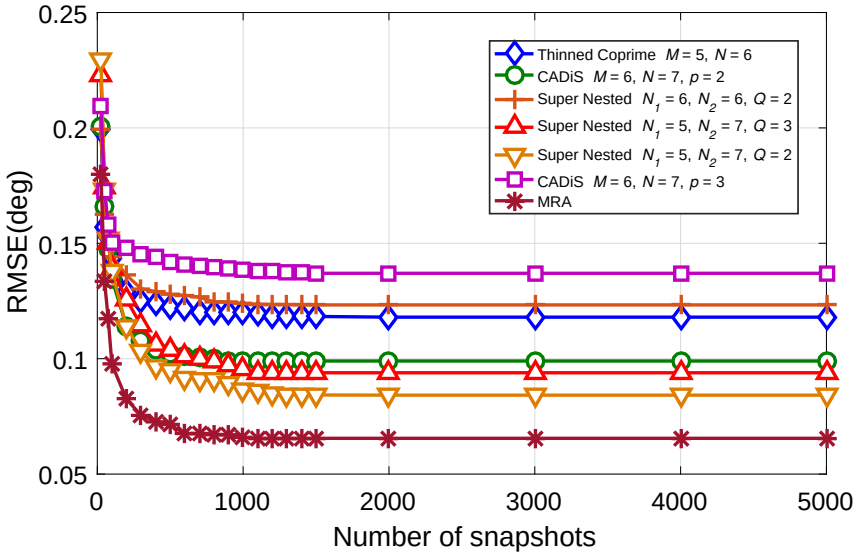

Figure 5.9: RMSE versus number of snapshots for CS with $|c_1|= 0.3$.

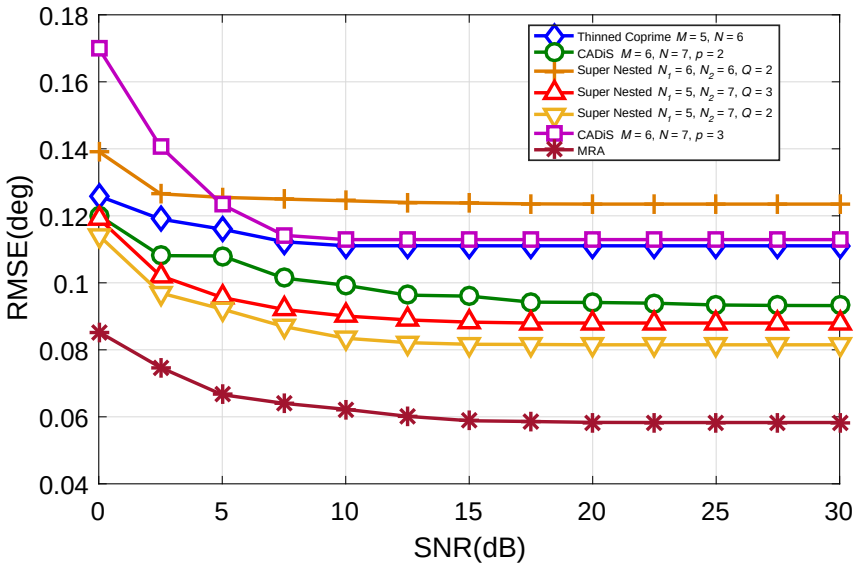

Figure 5.10: RMSE versus SNR for CS with $|c_1|= 0.3$.

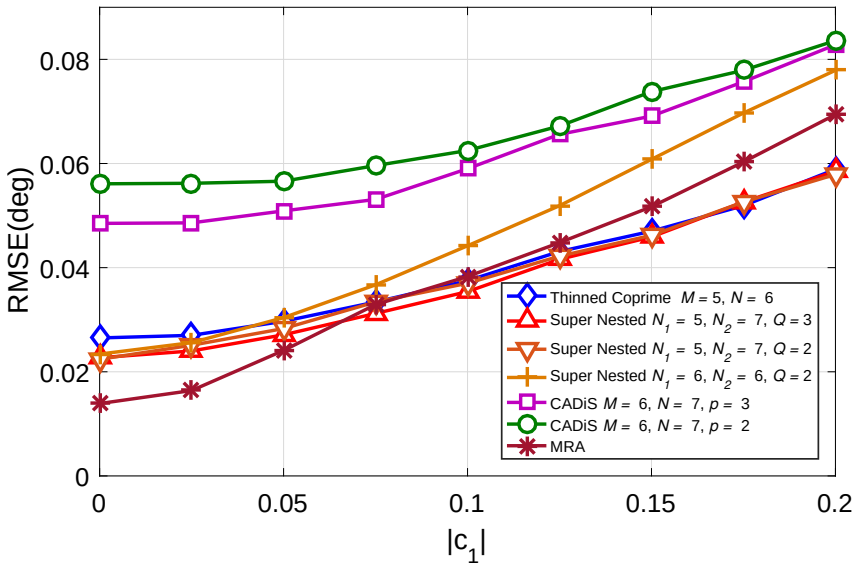

Figure 5.11: RMSE versus mutual coupling coefficient $|c_1|$ for MUSIC.

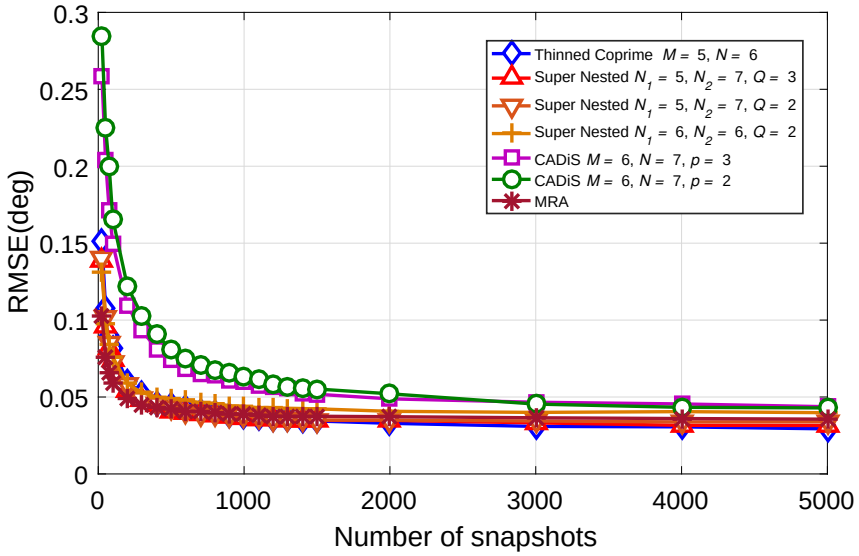

Figure 5.12: RMSE versus number of snapshots for MUSIC with $|c_1|= 0.1$.

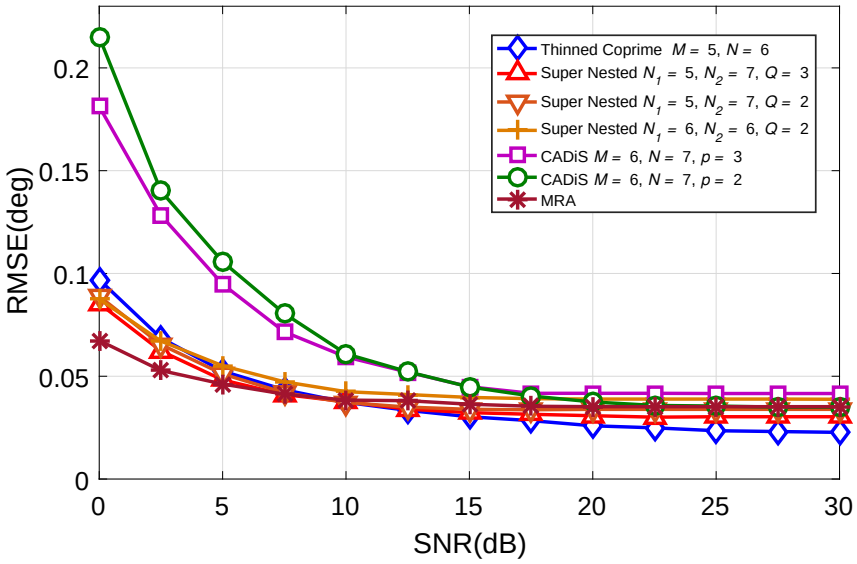

Figure 5.13: RMSE versus SNR for MUSIC with $|c_1|= 0.1$.

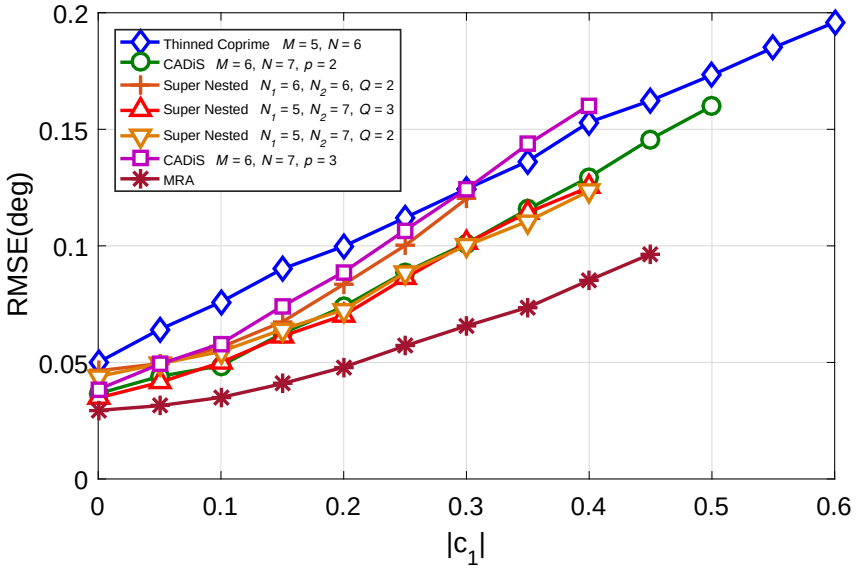

Figure 5.14: RMSE versus mutual coupling coefficient $|c_1|$ with 10 dB dynamic range SNR for CS.

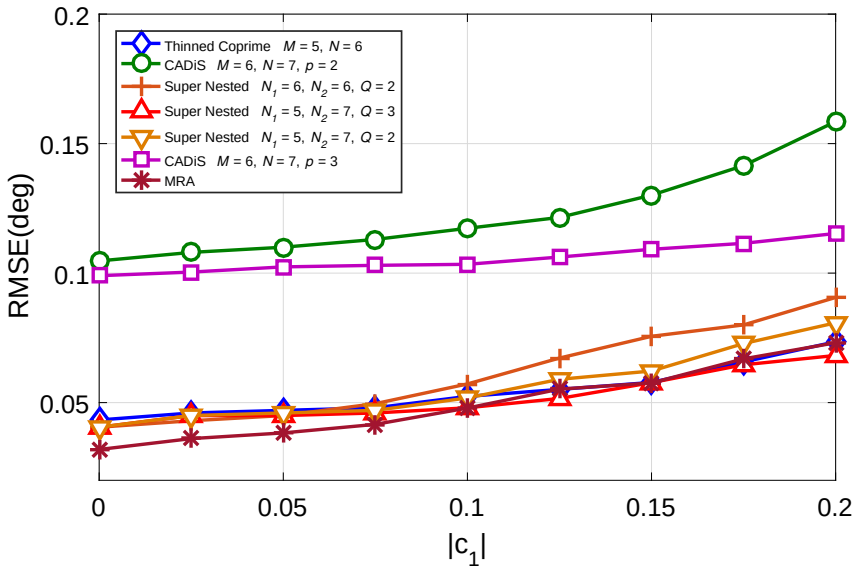

Figure 5.15: RMSE versus mutual coupling coefficient $|c_1|$ with 10 dB dynamic range SNR for MUSIC.

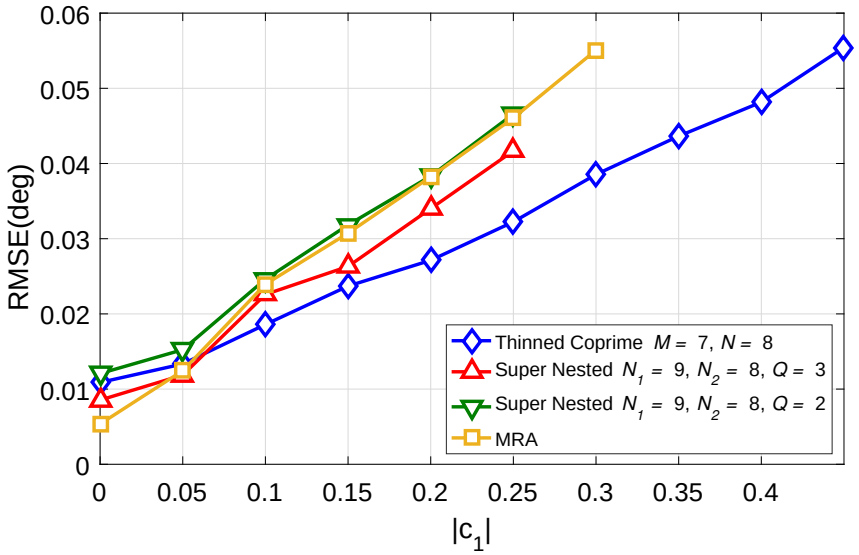

Figure 5.16: RMSE versus mutual coupling coefficient $|c_1|$ with 17 sensors for CS.

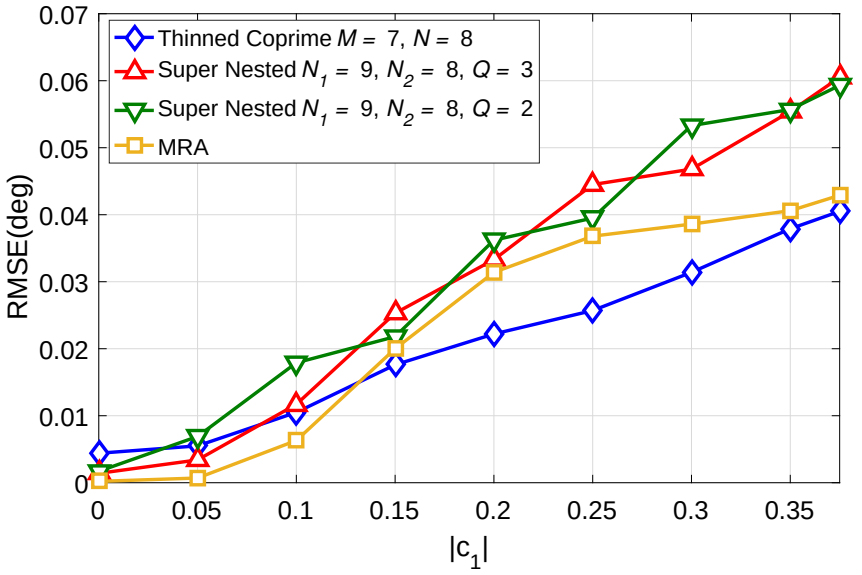

Figure 5.17: RMSE versus mutual coupling coefficient $|c_1|$ with 17 sensors for MUSIC.

size, applicable to both CS and SS-MUSIC as it provides a decent balance of consecutive and unique lags. This is further complimented by the fact that for $M \geq 5$ and $N > 3$, $w(1) = w(2) = w(3) = 1$, which makes them good at tackling even heavy levels of mutual coupling when other sparse arrays fail.

To investigate the estimation performance with large array size, 17-sensor sparse arrays are considered, the same as the scenario shown in Fig. 5.6. For this array size, all the sparse arrays are available except for sparse CADiS. For CS-based scenario, the considered simulation parameters include 20 sources, 10 dB SNR and 1000 snapshots with mutual coupling coefficient $|c_1|$ varied from 0 to 0.45 and the result is presented in Fig. 5.16. It can be seen that TCA achieves the lowest RMSE and is also able to tolerate high levels of mutual coupling. In comparison the operation range of super nested arrays is limited to $|c_1|= 0.25$ where the third order super nested array has the lowest error compared to second order super nested array and MRA due to its sparsity. This result shows that the error performance trend in the presence of mutual coupling varies significantly with increasing array size. As the lags rise in accordance with the array size, so do the critical weights for super nested arrays, MRA and even sparse CADiS. Thinned coprime array due to its consistent critical weights of $w(1) = w(2) = w(3) = 1$ being independent of the array size is able to estimate sources with the best performance as the array size increases

Array	SNA	CADiS	TCA	MRA
Availability	Yes	Not available for 17, 23, 29 and 35 sensors	Yes	Not available for more than 20 sensors
SS-MUSIC Compatibility	Yes	No	Yes	Yes
CS Compatibility	Yes	Yes	Yes	Yes
Relationship between weights and array size	$w(2)$ increases with array size	$w(2)$ or $w(3)$ increases with array size but $w(1) = 0$	$w(1) = w(2) = w(3) = 1$ for odd $M \geq 5$ and even $M > 6$ with $N > 3$	$w(2)$ increases with array size

Table 5.3: Character comparison of sparse arrays.

while relatively higher errors are incurred by the super nested arrays and MRA due to a significant increase in $w(2)$.

Then the performance of these arrays is investigated for SS-MUSIC. The considered simulation parameters include 10 sources, 10 dB SNR, 1000 snapshots, $|c_1|$ varied from 0 to 0.375 with the result presented in Fig. 5.17. It can be seen again that the TCA despite havng 63 lags to estimate 10 sources in comparison with 80 and 94 for super nested arrays and MRA respectively, is able to estimate the sources with the lowest error with increasing mutual coupling levels. This result compliments the results acheived with CS and shows the real application of TCA.

The simulations used in the thesis involved assuming the source signals evenly spaced between -60 and 60 degrees. For the endfire zone, where source signals impinge on the array from directions close to the axis of the array, it has been observed that the root mean square error (RMSE) generally increases for all the considered sparse arrays like MRA, sparse CADiS, super nested arrays and thinned coprime array. For source signals impinging from directions close to -70 and 70 degrees, there is not much difference in the

error compared to -60 and 60 degrees. However, as the source signal DOAs reach -80 degrees and 80 degrees, significant error increase has been observed for all sparse arrays.

Overall, the results have shown that the TCA offers a set of desirable properties compared to other sparse arrays. The most important advantage is that, the TCA is able to tolerate heavy levels of mutual coupling compared to super nested arrays, MRA and sparse CADiS. Due to consistent availability of few sensor pairs with d, $2d$ and $3d$ spacing, the TCA provides better error performance than super nested arrays and MRA with increasing array size especially using CS based method. Although MRA and super nested arrays have hole-free co-arrays with high DOFs which can be efficiently utilized using subspace based methods like SS-MUSIC, the increased value of weights $w(1)$, $w(2)$ and $w(3)$ with array size increases their estimation error in the presence of mutual coupling using both SS-MUSIC and CS based methods. TCA has shown some attractive traits and promise in scenarios of heavy mutual coupling, DOA estimation with arbitrary array size where certain sparse arrays like CADiS are not available and estimation with large number of sensors required for increase aperture to provide better resolution while mitigating the effects of mutual coupling at the same time. Among all the extensions based on coprime array proposed till now, the proposed TCA is a better solution that can be effectively used with both CS and SS-MUSIC based DOA estimation in the presence of mutual coupling.

5.7 Summary

Thinned coprime array has been proposed, which retains all the properties of the conventional coprime array, but with $\lceil \frac{M}{2} \rceil$ fewer sensors. For the same number of sensors, TCAs possess greater number of unique lags than the hole-free structure of the nested array and nested CADiS, and comparable number of unique lags to the sparsest CADiS. The number of consecutive lags of the TCAs are around 75 percent to those of nested arrays which showcases their application in both subspace and CS-based DOA estimation methods. Moreover, they can be easily constructed for an arbitrary number of sensors.

TCAs have a significantly sparser array structure with robustness against severe mutual coupling especially when using CS-based DOA estimation. With increasing array

size, TCAs also offer better error performance in parameter estimates compared to super nested arrays and MRA for both CS and SS-MUSIC based methods in the presence of mutual coupling. The key characteristic of TCA is the consistency in its attractive sparsity available for any array size compared to other sparse arrays, which implies that TCAs remain robust against mutual coupling irrespective of the array size.

Although TCA has good sparsity and robustness to mutual coupling, the number of unique lags provided by TCA remains close to the sparsest CADiS, hole-free co-array of nested arrays and significantly low compared to the co-array of MRA raising an intriguing question. How can the structure of TCA be exploited to increase the unique lags while maintaining or improving the sparsity offered by TCA to further reduce the DOA estimation error? Chapter 6 investigates the design of such a novel sparse array termed displaced thinned coprime array with additional sensor.

Chapter 6

Displaced Thinned Coprime Arrays with Additional Sensor for DOA Estimation

6.1 Introduction

In Chapter 5, TCA was proposed which showed robustness against mutual coupling through an attractive sparse structure. TCA provides weight functions $w(1) = w(2) = w(3) = 1$ for odd $M \geq 5$ and even $M > 6$, with $N > 3$. TCA is applicable for a variety of DOA estimation methods due to increased consecutive and unique lags and available for arbitrary array size with closed-form expressions. It was shown that TCA achieves lower RMSE compared to super nested arrays and MRA with increasing array size for SS-MUSIC and CS-based DOA estimation methods. Although TCA holds numerous desirable features, the number of unique lags offered by TCA are close to the sparsest CADiS and nested array and significantly lower than MRA which limits the estimation error performance offered by TCA through CS-based methods. With the continued search for improved sparse arrays, the structure of TCA is studied to explore the possibility of an array which can provide significantly higher number of unique lags with improved sparsity while maintaining a minimum inter-element spacing of half-wavelength to avoid spatial aliasing. An array of sensors can detect a plane wave signal at a wrong bear-

ing/direction of arrival if the signal wavelength is shorter than twice the distance between the closest adjacent sensors. In other words, when the minimum inter-sensor spacing is more than half-wavelength where wavelength corresponds to the shortest wavelength present in the incident signal, it can result in spatial ambiguities causing estimation error in the bearing/direction-of-arrival of the signal. This phenomenon is termed as spatial aliasing and it is recommended to keep the minimum inter-element spacing of the array to half-wavelength [111].

In this chapter, displaced thinned coprime array with additional sensor (DiTCAAS) is proposed based on TCA with a two-step design, where the first step involves a displacement of $(2M-2)N$ of subarrays $\mathbb{X}_2$ and $\mathbb{X}_3$ spaced by Nd, from their original positions [112]. This displacement results in the maximum number of unique lags possible for displaced TCA. Due to a significantly larger minimum inter-element spacing equal to integer multiples of half-wavelength which can cause spatial aliasing, an additional sensor at a distance of half-wavelength from one of the sensors of displaced subarray $\mathbb{X}_3$ is added in the second stage. Two locations are proposed for the placement of the additional sensor with significantly higher number of unique lags obtained. The resulting structure has more unique lags than the hole-free co-array of MRA for the same number of sensors. It will be shown that DiTCAAS due to its higher unique lags and sparsity has the best estimation error performance among other sparse arrays in the presence of mutual coupling when CS-based DOA estimation is applied.

This chapter is organized as follows. Theoretical foundations for DiTCAAS are developed in Section 6.2. The comparison of number of lags of DiTCAAS with other sparse arrays is presented in Section 6.3. The sparsity of DiTCAAS is discussed in Section 6.4. Simulations results using the CS-based DOA estimation method are provided in Section 6.5.

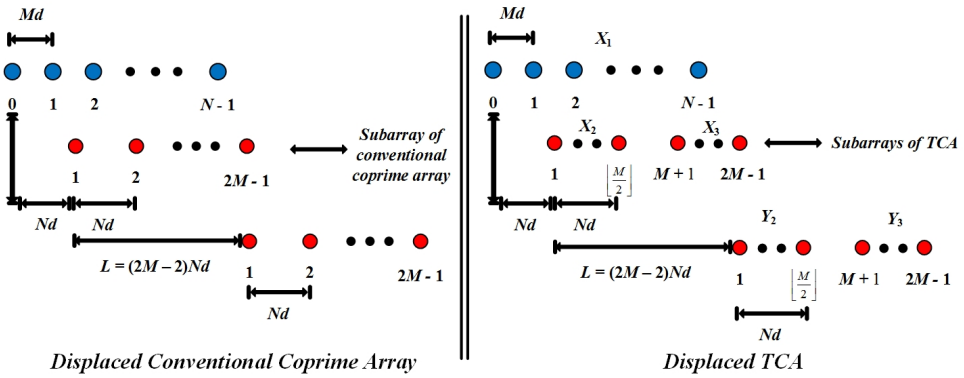

Figure 6.1: Displaced conventional coprime array and TCA

6.2 Theoretical Foundations for DiTCAAS

6.2.1 Stage 1 - Displaced Thinned Coprime Array

Definition 1 (Displaced thinned coprime arrays)**.** *Assume M and N are coprime integers with $M \geq 4$ and $N \geq 3$, then the displaced thinned coprime arrays are specified by the integer set* $\mathbb{X}$, defined by

$$\mathbb{X} = \mathbb{X}_1 \cup \mathbb{Y}_2 \cup \mathbb{Y}_3,$$

where

$$\begin{cases} \mathbb{X}_1 = \{nMd \mid 0 \leq n \leq N-1\}, \\ \mathbb{Y}_2 = \{(2M-2+m)Nd \mid 1 \leq m \leq \lfloor \frac{M}{2} \rfloor\}, \\ \mathbb{Y}_3 = \{(3M-1+m)Nd \mid 0 \leq m \leq M-2\}. \end{cases} \tag{6.1}$$

where $\mathbb{Y}_2$ and $\mathbb{Y}_3$ represent the displaced versions of $\mathbb{X}_2$ and $\mathbb{X}_3$ in TCA respectively. Next some properties of displaced thinned coprime arrays are presented.

Lemma 1. *For displaced TCA, no repitition in cross lags exist between the 1st subarray and the latter two subarrays at displacement $L = (2M-2)N$.*

Proof. First, the displaced coprime array is considered as shown in the left half of Fig. 6.1. By displacing the $2M-1$ element subarray by $L = (2M-2)Nd$, the new sensor positions of displaced coprime array are given by

$$\mathbb{F} = \mathbb{C} \cup \mathbb{D} \tag{6.2}$$

$$\mathbb{C} = \{Mnd \mid 0 \leq n \leq N-1\} \tag{6.3}$$

$$\mathbb{D} = \{(2M-2+m)Nd \mid 1 \leq m \leq 2M-1\} \tag{6.4}$$

As shown in [62, 110], the repeated lags in the cross difference co-arrays Diff($\mathbb{D}$, $\mathbb{C}$) are additive inverses of each other, where Diff($\mathbb{D}$, $\mathbb{C}$) represents the differences in sensor positions of $\mathbb{C}$ from $\mathbb{D}$. These repeated lags exist due to colocation of the two subarrays. By displacing the 2nd subarray sufficiently, the conjugate pairs of cross lags cease to exist and the only repitition of lags occurs when some cross lags equal to self lags.

Only the positive lags ae analyzed for convenience. The self lags of the two subarrays $\mathbb{C}$ and $\mathbb{D}$ themselves are of the form

$$\text{Diff}(\mathbb{C}, \mathbb{C}) = nM \tag{6.5}$$

$$\text{Diff}(\mathbb{D}, \mathbb{D}) = m'N \tag{6.6}$$

where $0 \leq n \leq N-1$ and $0 \leq m' \leq 2M-2$. Then the cross differences of the last two sensors of $\mathbb{C}$ from the first two sensors of $\mathbb{D}$ is taken, expressed as

$$\text{Diff}((2M-1)N, (N-1)M) = (M-1)N + M \tag{6.7}$$

$$\text{Diff}((2M-1)N, (N-2)M) = (M-1)N + 2M \tag{6.8}$$

$$\text{Diff}(2MN, (N-1)M) = M(N+1) \tag{6.9}$$

$$\text{Diff}(2MN, (N-2)M) = M(N+2) \tag{6.10}$$

With (6.7) and (6.8), cross differences of sensor at $(2M-1)N$ with sensors in $\mathbb{C}$ are of the form $(M-1)N + sM$, $1 \leq s \leq N$. As the two coprime numbers M and N cannot be a factor of $(M-1)N + sM$, self lags in (6.5) and (6.6) are not generated. Similarly, for lags in (6.9) and (6.10), cross differences related to the sensor at $2MN$ are of the form $M(N+s)$, which proves that all cross lags from sensors beyond $2MN$ in the 2nd subarray with sensors in $\mathbb{C}$ will be greater than the aperture of subarray $\mathbb{C}$ and therefore are unique compared with the self lags in (6.5) and (6.6), proving the unique nature of cross lags. As TCA is a redundant version of coprime array, Lemma 1 is equally applicable to displaced TCA, thus completing the proof. □

Theorem 1. *The total number of unique lags for a displaced TCA with* $M \geq 4$ and $N \geq 3$ *is given by*

$$T_{umax} = \begin{cases} 3MN + 4M - 5, & \textit{for even } M \\ 3MN + 4M - N - 5, & \textit{for odd } M \end{cases} \tag{6.11}$$

Proof. Consider displaced TCA as shown in the right half of Fig. 6.1 where the first sensor of $\mathbb{Y}_2$ starts from $(2M-1)Nd$. For even M, $\mathbb{X}_1$ has N sensors while $\mathbb{Y}_2$ and $\mathbb{Y}_3$ have a total of $\frac{M}{2} + M - 1 = \frac{3M-2}{2}$ sensors. A total of N sensors in $\mathbb{X}_1$ generate $N-1$ unique self positive lags for non-zero positions. As shown in [62], $\frac{3M-2}{2}$ sensors of $\mathbb{Y}_2$ and $\mathbb{Y}_3$ are able to generate all of the $2M-2$ unique lags like the $(2M-1)$-element subarray in conventional coprime array. As the cross lags between displaced subarrays $\mathbb{Y}_2$, $\mathbb{Y}_3$ and $\mathbb{X}_1$ are all unique as per Lemma 1, the total number of positive unique lags for displaced TCA with even M are given by

$$T_{ulep} = (N-1) + (2M-2) + \frac{3M-2}{2}N = \frac{3MN}{2} + 2M - 3 \tag{6.12}$$

Then the total number of unique lags (adding negative lags and zero lag) for a displaced TCA with even M is

$$T_{ule} = 3MN + 4M - 5 \tag{6.13}$$

which proves the first part of (6.11).

For odd M, the the total number of sensors in $\mathbb{Y}_2$ and $\mathbb{Y}_3$ is given by $\frac{M-1}{2} + M - 1 = \frac{3M-3}{2}$. Like even M case, the total number of positive unique lags for displaced TCA with odd M is

$$T_{ulop} = \frac{3MN}{2} + 2M - \frac{N}{2} - 3 \tag{6.14}$$

Then the total number of unique lags (adding negative lags and zero lag) for a displaced TCA with odd M is

$$T_{ulo} = 3MN + 4M - N - 5 \tag{6.15}$$

□

6.2.2 Stage 2 - Additional Sensor at Half-Wavelength

Although displaced TCA results in increased unique lags, the minimum interelement spacing becomes an integer multiple of half-wavelength, leading to the well-known spatial aliasing problem. To mitigate this problem, the addition of another sensor at half-wavelength from a sensor in the displaced TCA is investigated to make sure that the minimum interelement spacing of displaced TCA remains $\frac{\lambda}{2}$. The additional sensor also needs to be placed so that the overall structure has significantly higher number of unique lags. The new structure will be termed as displaced thinned coprime array with an additional sensor (DiTCAAS).

First, the conventional coprime array is analyzed to find out the positions of sensors in one subarray which are separated from their nearest sensor in the other subarray by a given distance for an arbitrary M and N. A general result in this direction is presented in Lemma 2.

Lemma 2. *The sensor of* $(2M-1)$*-element subarray leading/lagging the nearest sensor of* $N-$*element subarray by distance* n *where* $1 \leq n \leq M-1$*, is located at index* i and k*, given by the relationships* (6.16) *and* (6.17) *respectively*

$$i \bmod (N, M) = n + jM \tag{6.16}$$

$$M - k \bmod (N, M) = n - jM \tag{6.17}$$

where $1 \leq i, k \leq 2M-1$*,* $j \geq 0$ *and* $\text{mod}(N, M)$ *refers to the modulo operator and returns the remainder of* $\frac{N}{M}$*.*

Proof. The distance between a sensor of $(2M-1)$-element subarray located at iN and its nearest sensor of N-element subarray lesser in value than iN is given by

$$S_i = \text{mod}(iN, M) = \text{mod}(i \bmod (N, M), M) \tag{6.18}$$

As $\text{mod}(n, M) = \text{mod}(n + jM, M)$ where $1 \leq n \leq M-1$ and $j \geq 0$, index i for a particular n can be found by solving

$$i \bmod (N, M) = n + jM \tag{6.19}$$

Similarly, the distance of a sensor of $(2M-1)$-element subarray located at kN relative to the nearest sensor of N-element subarray greater in value than kN is given by

$$\hat{S}_k = M - \text{mod}(kN, M) = M - \text{mod}(k \bmod (N, M), M) \tag{6.20}$$

As $\text{mod}(n, M) = \text{mod}(n - jM, M)$, index i for a particular n can be found by solving

$$M - k \bmod (N, M) = n - jM \tag{6.21}$$

□

Please note that for TCA, (6.16) and (6.17) represent index of physical sensors for index range $1 \leq i, k \leq \left\lfloor \frac{M}{2} \right\rfloor$. For $n = 1$ corresponding to half-wavelength distance, (6.16) and (6.17) change to

$$i \bmod (N, M) = 1 + jM \tag{6.22}$$

$$M - k \bmod (N, M) = 1 - jM \tag{6.23}$$

It will be shown now that index i and k are related to each other. Equating S_i with $\hat{S}_k$ and rearranging the terms,

$$\text{mod}\ (iN, M) + \text{mod}(kN, M) = M \tag{6.24}$$

Applying modulo on both sides yields

$$\text{mod}\ (iN + kN, M) = \text{mod}(M, M) = 0 \tag{6.25}$$

Since M and N are coprime, the solution is given by

$$i + k = pM, p \in \mathbb{Z} \tag{6.26}$$

where p =1 since $1 \leq i, k \leq \left\lfloor \frac{M}{2} \right\rfloor$:

$$i + k = M \tag{6.27}$$

In the next step, two suitable locations for the additional sensor are presented which can significantly increase unique lags.

Theorem 2. *The total number of unique lags for* DiTCAAS *with additional sensor located at* $3M - 2 + iN - 1$ *or* $3M - 2 + kN + 1$ *with* $M \geq 4$ and $N \geq 3$ *is given by*

$$T_{umax} = \begin{cases} 3MN + 7M + 2N - 9, & \textit{for even } M \\ 3MN + 7M + N - 10, & \textit{for odd } M \end{cases} \tag{6.28}$$

Proof. For the two proposed locations $(3M-2)N+iN-1$ and $(3M-2)N+kN+1$, $(3M-2)N$ represents the redundant sensor at MN in TCA after displacement of $(2M-2)N$. This reference position is chosen to maximize the number of unique lags for additional sensor as shown later.

The starting sensor of $\mathbb{Y}_2$ at $(2M-1)N$ is equidistant from the additional sensor and a respective sensor of $\mathbb{X}_1$ which will be shown as follows. The differences in position of the additional sensor placed at $(3M-2)N+iN-1$ or $(3M-2)N+kN+1$ relative to $(2M-1)N$ (the first sensor in $\mathbb{Y}_2$) denoted by S_1 and S_2 are given by

$$S_1 = (M+i-1)N-1 \tag{6.29}$$

$$S_2 = (M+k-1)N+1 \tag{6.30}$$

Then by taking the difference of S_1 and S_2 from $(2M-1)N$, denoted by S_3 and S_4 respectively and according to (6.27),

$$S_3 = (M-i)N+1 = kN+1 \tag{6.31}$$

$$S_4 = (M-k)N-1 = iN-1 \tag{6.32}$$

For index i and k corresponding to $n=1$, $iN-1$ and $kN+1$ represent the positions of the sensors of $\mathbb{X}_1$ in TCA which proves that the sensor at $(2M-1)N$ is equidistant from the additional sensor and sensor of $\mathbb{X}_1$. The additional sensor will contribute the same set of lags by interacting with $\mathbb{Y}_2$ and $\mathbb{Y}_3$ as the sensor in (6.31) or (6.32) of $\mathbb{X}_1$ will do with $\mathbb{X}_2$ and $\mathbb{X}_3$ in TCA. As TCA and displaced TCA differ from each other only by the displacement $(2M-2)N$ for the displaced subarrays, their cross difference coarrays also differ from each other by a factor of $(2M-2)N$. As a result, with the exception of one repitition of the equidistant lag, the interaction between the additional sensor and $\mathbb{Y}_2$ and $\mathbb{Y}_3$ will generate unique lags. Now, the interaction of additional sensor with $\mathbb{X}_1$ is considered. As the additional sensor is placed at $iN-1 or \mathrm{kN}+1$ respectively from $(3M-2)N$, and represents displacement equal to multiples of M, it will generate part of the set of lags generated by the position $(3M-2)N$ relative to $\mathbb{X}_1$ given by

$$S_5 = (3M-2)N - lM, 0 \leq l \leq N-1 \tag{6.33}$$

in addition to i or k lags equal to S_5+qM where $1 \leq q \leq i$ or $1 \leq q \leq k$. Since $(3M-2)N$ in displaced TCA represents the displaced position of a redundant sensor in conventional coprime array at MN, missing in TCA, all the set of lags generated by the additional sensor through interaction with $\mathbb{X}_1$ will be unique. This proves that the additional sensor at these two locations through interaction with the displaced TCA generates only one repeated lag with all remaining lags as unique lags. As a result, this extra sensor brings $2(H-1)$ new unique lags for a displaced TCA with H sensors, for a total number of $H+1$ sensors for DiTCAAS. Now the total number of unique lags for DiTCAAS for cases of even and odd M are calculated. For even M, the total number of sensors for displaced TCA is given by $\frac{3M}{2} + N - 1$. The contribution of unique lags for additional sensor is

$$S_{add_{even}} = 2 \times (\frac{3M}{2} + N - 2) = 3M + 2N - 4$$

Then, the total number of unique lags for DiTCAAS with even M for $\frac{3M+2N}{2}$ sensors is given by

$$S_{DiTCAAS_{even}} = 3MN + 7M + 2N - 9 \tag{6.34}$$

Similarly for odd M, the total number of sensors for displaced TCA is given by $\frac{3M+2N-3}{2}$. The contribution of unique lags for additional sensor is given by

$$S_{add_{odd}} = 2 \times (\frac{3M + 2N - 3}{2} - 1) = 3M + 2N - 5$$

Then the total number of unique lags for DiTCAAS with odd M for $\frac{3M+2N-1}{2}$ sensors is

$$S_{DiTCAAS_{odd}} = 3MN + 7M + N - 10 \tag{6.35}$$

□

6.2.3 Demonstration of DiTCAAS with an Example

In this subsection, the concept of DiTCAAS is presented with the help of an example. For this scenario, a 15-sensor DiTCAAS is chosen for parameters $M = 5$ and $N = 8$, which will be constructed in a three-step process. The first step involves the construction of a TCA for the chosen M and N, which will comprise of 14 sensors with three subarrays $\mathbb{X}_1$,

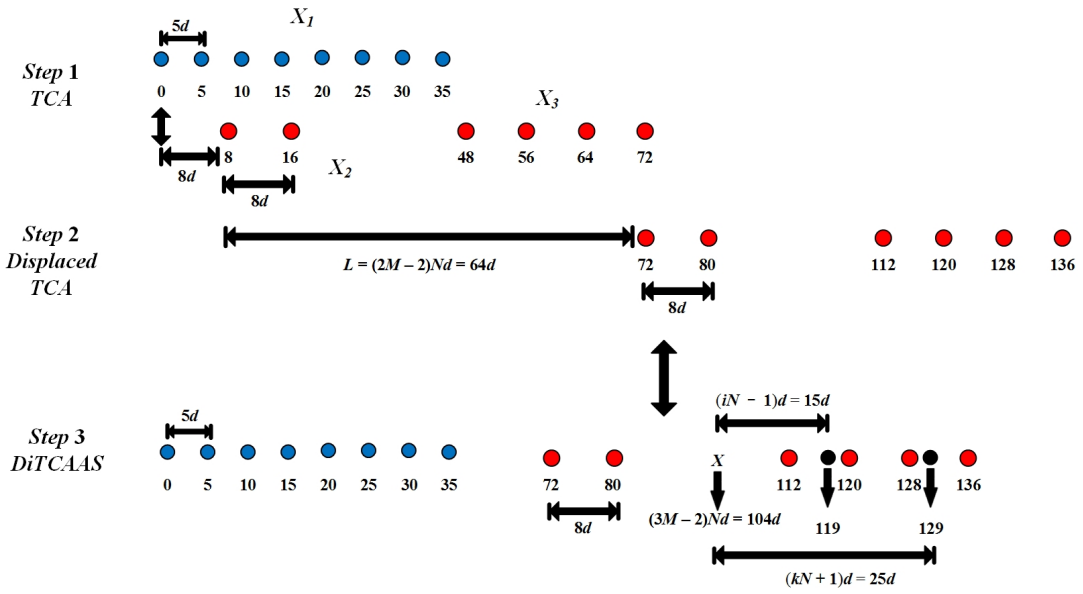

Figure 6.2: DiTCAAS for $M = 5$ and $N = 8$

$\mathbb{X}_2$ and $\mathbb{X}_3$, respectively, where $\mathbb{X}_1$ consists of 8 sensors spaced by $5d$. On the other hand, the subarrays $\mathbb{X}_2$ and $\mathbb{X}_3$ consist of 2 and 4 sensors respectively with spacing $8d$. The second step involves displacing $\mathbb{X}_2$ and $\mathbb{X}_3$ by $(2M-2)Nd = 64d$. The resulting structure is a displaced TCA. In the third and final step, an additional sensor is placed at half wavelength from one of the sensors of the displaced $\mathbb{X}_3$, selected from the two suitable choices with positions given by $(3M-2)N + iN - 1$ or $(3M-2)N + kN + 1$.

For $M = 5$ and $N = 8$, index i and k are calculated. To find i,

$$i \bmod (N, M) = 1 + jM \tag{6.36}$$

Plugging in the known parameters,

$$3i = 1 + 5j \tag{6.37}$$

which can be solved for $i = 2$ and $j = 1$. Using Lemma 6, $k = M - i = 5 - 2 = 3$. The index values $i = 2$ and $k = 3$, for a conventional coprime array represent the index of sensors of $2M-$element subarray which exceed or lag their nearest sensor from $N-$ element subarray by distance equal to 1. For TCA, $i = 2$ represents the index of a physical sensor belonging to $\mathbb{X}_2$ while $k = 3$ which is greater than $\left\lfloor \frac{M}{2} \right\rfloor = \left\lfloor \frac{5}{2} \right\rfloor = 2$, represents the redundant sensor position. In both cases of conventional coprime and TCA, $iN - 1$ and $kN + 1$ represent

sensors of $N-$element subarray and $\mathbb{X}_1$, respectively. Now, the two available locations for the additional sensor are given by $(3M-2)N+iN-1$ and $(3M-2)N+kN+1$, which come out to be $104+15=119$ and $104+25=129$, respectively. It can be seen that the first sensor of displaced $\mathbb{X}_2$ given by $(2M-1)N=72$ is equidistant from 119 and 25 as well as from 129 and 15, as proved in Theorem 2. These three steps of construction of DiTCAAS with two possible solutions are shown in Fig. 6.2.

6.3 Comparison of Number of Lags for Sparse Arrays

In this section the number of lags are compared, specifically the number of unique lags of different sparse arrays for a fixed number of total sensors.

For comparison, the proposed DiTCAAS, TCA, nested array, nested CADiS, MRA and sparse CADiS are considered. Nested array, nested CADiS and MRA generate hole-free co-arrays, while sparse CADiS, TCA and DiTCAAS, all generate co-arrays with holes resulting in consecutive and unique lags. Here the focus is on the applicability of these sparse arrays for CS-based DOA estimation which utilizes all the unique lags generated by a sparse array. As far as the availability of sparse arrays for arbitrary number of sensors is concerned, MRA in literature is available for a maximum of 20 sensors [57], while sparse CADiS maye not be available for a specific number of sensors. On the other hand, nested array, nested CADiS, TCA and DiTCAAS can all be generated for any number of sensors. In this analysis, the unique lags for a fixed number of sensors in the range 13 to 40 sensors are generated. Sparse CADiS with two variants depending on the separation parameter L between the two subarrays which maximizes either consecutive lags or unique lags are both inlcuded in the analysis.

Then, the unique lags capacity for sparse CADiS for different cases of L, nested array, nested CADiS, MRA, TCA and DiTCAAS utilizing (5.14) are plotted in Fig. 6.3 for the number of sensors from 13 to 40. It is clear from the plot that DiTCAAS has the highest lag capacity with a big difference compared to other sparse arrays, thus generating the highest number of unique lags for a fixed number of sensors. Only for the case of 17 sensors, MRA has more lags than DiTCAAS, as DiTCAAS derived from a 16 sensor TCA

generates relatively lower number of unique lags for the respective M and N. Overall, the proposed DiTCAAS holds strong potential to achieve significantly lower DOA estimation error with CS based methods than other sparse arrays, even better than the MRA [112].

6.4 DiTCAAS - Sparsity and Weight Functions

In this section, the sparsity of DiTCAAS is analyzed and critical weight functions are provided with the help of a proof.

Theorem 3. *For a DiTCAAS with* $M \geq 4$ and $N \geq 3$, *its weight functions* $\mathrm{w}(m)$ *for* $m = 1$, 2 *and* 3 *are given by*

$$\begin{cases} w(1) = \quad 1, \\ w(2) = \begin{cases} 1, & \text{if } N = 3, \\ 0, & \text{otherwise,} \end{cases} \\ w(3) = \begin{cases} \frac{3M-6}{2}, & \text{if } N = 3 \text{ for any even } M, \\ \frac{3M-7}{2}, & \text{if } N = 3 \text{ for any odd } M, \\ 1, & \text{if } N = 4, \\ 0, & \text{otherwise,} \end{cases} \end{cases} \tag{6.38}$$

Proof. DiTCAAS for $M \geq 4$ is a displaced version of TCA with one additional sensor placed at half wavelength spacing from its neighbouring sensor in the displaced $\mathbb{X}_3$ on any one of the two available locations, and is able to significantly increase the number of unique lags for a given number of sensors. Due to the displacement of $\mathbb{X}_2$ and $\mathbb{X}_3$ by $(2M-2)N$, the distance between $\mathbb{X}_1$ and displaced $\mathbb{X}_2$ is given by

$$S_{subdist} = (2M-1)N - (N-1)M \tag{6.39}$$

$$S_{subdist} = MN + M - N \tag{6.40}$$

Then the condition is found when $MN + M - N > M$ or N. First, the condition is found when $MN + M - N > M$, which solves for $M > 1$. For the condition when

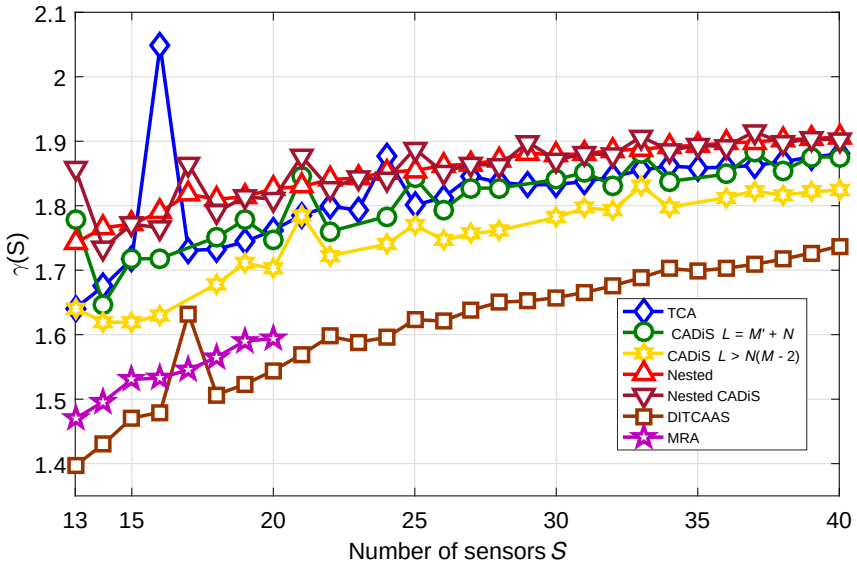

Figure 6.3: Unique lags capacity comparison for sparse arrays

$MN + M - N > N$, $M > \frac{2N}{N+1}$ which also solves for $M > 1$ for any value of N. As $M \geq 4$ and $N \geq 3$ for DiTCAAS, $MN + M - N$ will always be greater than M or N. As $\mathbb{X}_1$ is separated by Md spacing and the displaced $\mathbb{X}_2$ and $\mathbb{X}_3$ are separated by Nd spacing, then by placing an additional sensor at d distance from the sensors of displaced $\mathbb{X}_3$, two lags equal to 1 and $N-1$ are generated respectively. This implies that for $M \geq 4$ and $N \geq 5$, the weight functions are given by $w(1) = 1$, $w(2) = w(3) = 0$, which shows the improved sparsity of DiTCAAS compared to TCA, where TCA at best provides $w(1) = w(2) = w(3) = 1$. Now some specific cases are discussed for different values of N.

For $N = 3$, the additional sensor will generate lags equal to 1 and 2 through interaction with surrounding sensors of displaced $\mathbb{X}_3$, resulting in $w(2) = 1$. For the case of even M and $N = 3$, it is clear that $\frac{M}{2}-1$ pairs of sensors in displaced $\mathbb{X}_2$ will be separated by a spacing of 3 in adddition to $M-2$ pairs of sensors in displaced $\mathbb{X}_3$. Then, $w(3) = \frac{M}{2} - 1 + M - 2 = \frac{3M-6}{2}$. For the case of odd M and $N = 3$, the only difference is that $\frac{M-1}{2} - 1 = \frac{M-3}{2}$ pairs of sensors in displaced $\mathbb{X}_2$ are separated by 3, which will give an overall $w(3) = \frac{3M-7}{2}$. For the case when $N = 4$, the additional sensor through interaction with surrounding sensors of displaced $\mathbb{X}_3$ will generate lags equal to 1 and 3 resulting in $w(3) = 1$, which completes the proof. □

Array Parameters	SNA (7, 8, 2)	SNA (7, 8, 3)	MRA	CADiS (9, 7, 3)	TCA (5, 9)	DiTCAAS (5, 8)
Aperture	63	63	73	77	81	136
Con. Lags	127	127	147	54	99	20
Uni. Lags	127	127	147	131	131	153
$w(1)$	1	1	1	0	1	1
$w(2)$	6	3	4	0	1	0
$w(3)$	1	2	1	6	1	0

Table 6.1: Sparse array characteristics for 15 sensors.

6.5 Simulation Results with CS-Based DOA Estimation

In this section the performance of DiTCAAS is investigated in comparison with other sparse arrays in the presence of mutual coupling. For DOA estimation, CS-based method is employed, details of which can be found in [62]. For performance analysis, 15-sensor sparse arrays including the second and third order super nested array $N_1 = 7$, $N_2 = 8$, TCA $M = 5$, $N = 9$, sparse CADiS $M = 9$, $N = 7$, $p = 3$, MRA as $\{0, 1, 6, 14, 22, 30, 38, 46$ $54, 62, 64, 66, 69, 71, 73\}d$ [57] and DiTCAAS $M = 5$, $N = 8$ with additional sensor at $(3M-2)N+kN+1$ where $k = 3$ and represented as $\{0, 5, 10, 15, 20, 25, 30, 35, 72, 80, 112,$ $120, 128, 129, 136\}d$ are considered. The characteristics of these sparse arrays including aperture, conseuctive lags, unique lags and weight functions $w(1)$, $w(2)$ and $w(3)$ are shown in Table 6.1.

Although DiTCAAS generates the lowest number of consecutive lags at 20 compared to other sparse arrays, it generates the highest number of unique lags at 153, even more than the MRA and is well suited for application in CS-based DOA estimation. Analyzing the weight functions, the second order super nested array has a very high $w(2) = 6$ compared to the third order super nested array, which has $w(2) = 3$. Sparse CADiS with only non zero $w(3) = 6$ has the sparsest structure of all the sparse arrays, with unique

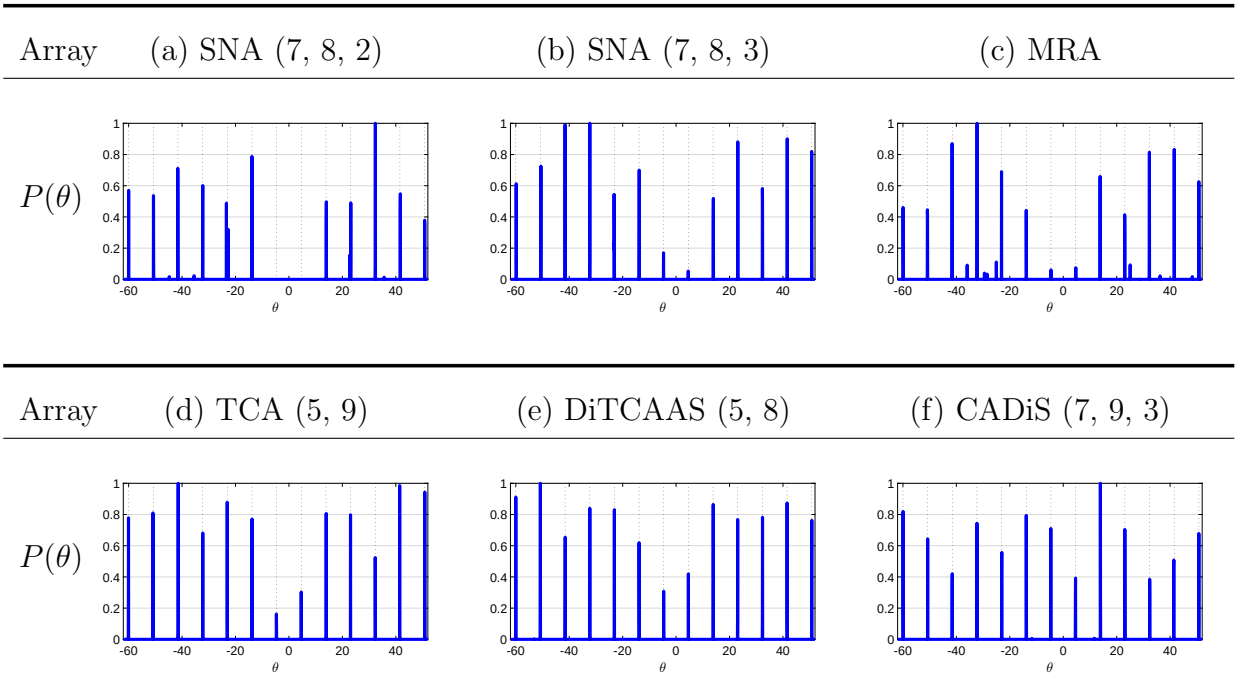

Figure 6.4: Comparison among 15 sensors 2^{nd} order SNA, 3^{rd} order SNA, MRA, TCA, DiTCAAS and sparse CADiS in the presence of mutual coupling with $|c_1|$=0.4.

lags equal to TCA with 131 unique lags while DiTCAAS with only non zero $w(1) = 1$ is second in sparsity only to sparse CADiS.

For the simulation, mutual coupling model is incorporated from the work in [88]. First the DOA spectrum for 13 sources is presented with considered parameters as 1000 snapshots, 10 dB SNR and mutual coupling coefficient $|c_1|$= 0.4 in Figure 6.4, where it can be clearly seen that the second order super nested array fails to resolve the sources and is severely affected by mutual coupling. Although MRA is significantly sparser than the second order super nested array, it still suffers from a degraded spectrum with lots of spurious peaks. The third order super nested array is able to resolve all the sources but with a degraded spectrum for two sources. On the other hand, TCA, sparse CADiS and DiTCAAS detect all the 13 peaks with a clean spectrum.

In the next step, the DOA estimation error performance of these sparse arrays is analyzed with the help of RMSE curves in a variety of scenarios in the presence of mutual coupling. First, the RMSE performance is investigated for varying intensity of mutual coupling coefficient $|c_1|$. The parameters chosen for this simulation are 13 sources with 10

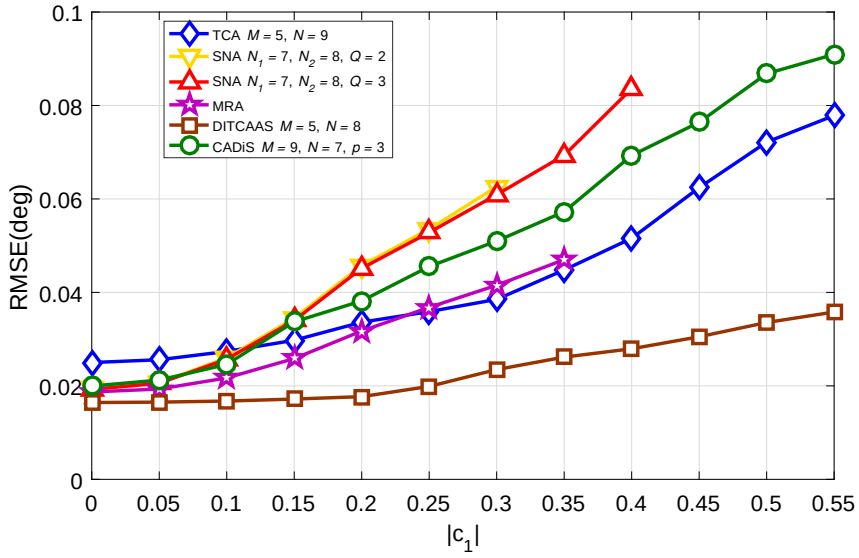

Figure 6.5: RMSE versus mutual coupling coefficient

dB SNR each impinging on an array and processed with 1000 snapshots at each sensor. The mutual coupling coefficient $|c_1|$ is varied from 0 to 0.55 and the result is presented in Figure 6.5, where each point on the curve is an average of 200 independent simulation runs. It can be seen that the TCA initially has a higher error among other sparse arrays in low mutual coupling conditions, but as the mutual coupling intensity increases, super nested arrays suffer from increased error in their estimates due to relatively less number of lags and higher weights $w(2)$ compared to other sparse arrays. As the second order super nested array has the highest $w(2)$, its operation range and resistance to mutual coupling significantly reduces and starts missing sources beyond $|c_1|= 0.3$. MRA has a lower error compared to super nested array and sparse CADiS, but due to a higher $w(2)$, its operation range is also limited to $|c_1|= 0.35$. With increasing mutual coupling, TCA achieves lower error than sparse CADiS and MRA due to a higher $w(2)$ for MRA and higher $w(3)$ for sparse CADiS, introducing error in the estimates. In comparison to all these sparse arrays, DiTCAAS has the lowest error with a significant difference compared to all other sparse arrays due to its desirable sparsity and higher number of unique lags. Even at $|c_1|= 0.55$, DiTCAAS incurs half the error of TCA, which showcases the potential of DiTCAAS.

For the second case, RMSE is investigated for varying SNR from 0 to 20 dB with a

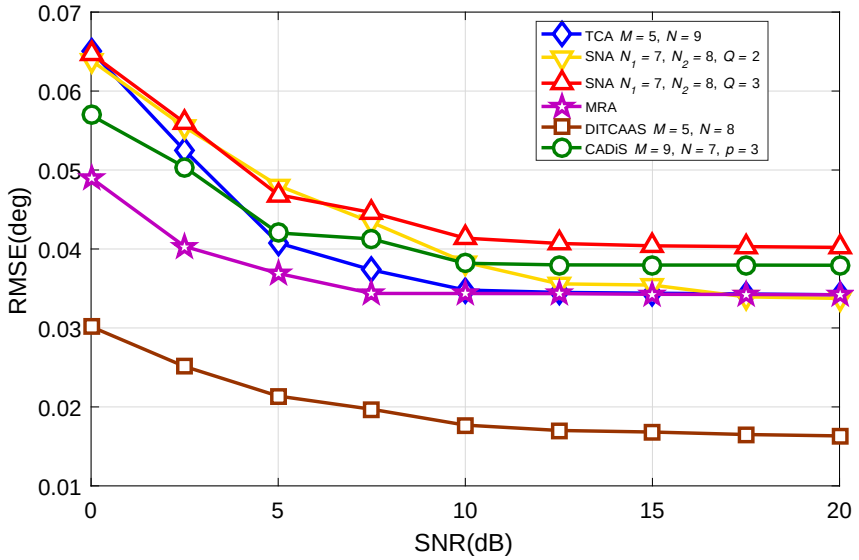

Figure 6.6: RMSE versus SNR

step of 2.5 dB, for each of the 13 sources. The number of snapshots and mutual coupling coefficient are fixed at 1000 and $|c_1|= 0.25$, respectively and the result is shown in Figure 6.6. It can be seen again that DiTCAAS has the lowest error among all the sparse arrays and shows robustness in low SNR conditions. MRA has the second lowest RMSE among other sparse arrays in low SNR conditions and TCA matches its error performance in moderate SNR conditions.

Assuming equal SNR for all the sources is unrealistic as different sources originate from different directions and encounter different channel conditions to reach their destination. As a result all the sources arriving at the destination have different SNR and a more realistic and practical way to model them is to assume a dynamic range of SNR for different sources. Keeping this in mind, a 10 dB dynamic range is chosen for the 13 sources with 1000 snapshots and the RMSE performance is investigated with varying intensity of mutual coupling. Due to dynamic range assumption, the operation range of the sparse arrays considered for Figure 6.5 will be reduced and the operation range of $|c_1|$ is considered from 0 to 0.45. The result is shown in Figure 6.7, where it can be seen that the operation range of all the sparse arrays is reduced to a relatively lower value of $|c_1|$ compared to the results of Figure 6.5. TCA in the 10 dB dynamic range assumption suffers from an increased error compared to other sparse arrays and is only overtaken by

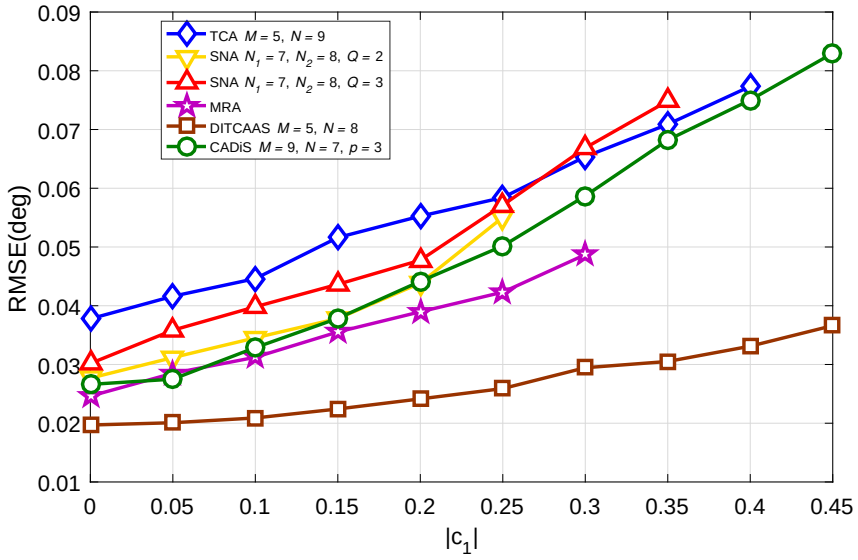

Figure 6.7: RMSE versus mutual coupling coefficient with 10 dB dynamic range

the third order super nested array beyond $|c_1|= 0.3$. Again the proposed DiTCAAS has the lowest error among all the sparse arrays in the considered range and has less than half the error compared to sparse CADiS despite its sparsest structure.

Finally, the RMSE performance of these sparse arrays is considered in a tough environment, where the processing power at the destination is limited and only few snapshots are available for the analysis and parameter estimation. A moderate level of mutual coupling is assumed along with a dynamic range for the SNR to simulate a very practical communication scenario. The considered simulation parameters include 10 dB dynamic range of SNR, mutual coupling coefficient $|c_1|= 0.2$ and number of snapshots varied from 500 to just 25 which is relatively closer to the 15 sensors assumed for the simulation. Such a model will investigate the robustness of the considered sparse arrays. The result is presented in Figure 6.8. It can be seen that the second order super nested array only operates within a narrow range of snapshots from 500 to 300, beyond which it starts missing the sources. MRA and third order super nested array are able to sustain themselves till 50 and 75 snapshots, respectively. All other sparse arrays like TCA, sparse CADiS and DiTCAAS are able to function in the full considered range of snapshots as low as 25. DiTCAAS again proves that it is the most robust array of all the sparse arrays and has the lowest error of them all. DiTCAAS beats MRA which has the second lowest RMSE,

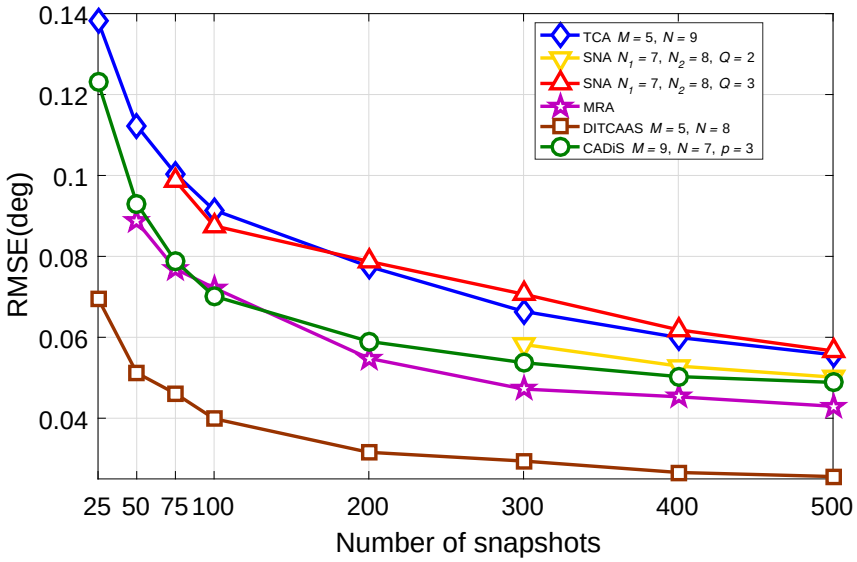

Figure 6.8: RMSE versus number of snapshots with 10 dB dynamic range and $|c_1|= 0.2$

by a big margin especially in extremely low number of snapshots environment.

Overall, DiTCAAS has proved itself to be a very robust array for CS-based DOA estimation. Due to its good sparsity and very high number of unique lags resulting from its co-array, it not only tolerates heavy mutual coupling, but also achieves the lowest error among all the main types of sparse arrays by a big margin. If a relatively larger aperture is allowed for an array in a signal processing scenario, then DiTCAAS is the best sparse array for CS-based DOA estimation.

6.6 Summary

In this chapter, a new sparse array called DiTCAAS has been proposed based on the TCA. The construction of DiTCAAS from TCA is a two-step process, where the subarrays $\mathbb{X}_2$ and $\mathbb{X}_3$ of TCA are displaced by a factor of $(2M-2)N$ in the first step. This displacement of the subarrays leads to an increase in unique lags, but the minimum spacing between the sensors becomes an integer multiple of half wavelength. To avoid spatial aliasing, an additional sensor is added at half wavelength from one of the sensors of the displaced $\mathbb{X}_3$ in the second step. Two locations are proposed for the placement of this additional sensor, which generates significantly higher number of unique lags for DiTCAAS, even more than

the lags provided by MRA. Due to a very sparse structure with the only non-zero weight being $w(1) = 1$ and higher number of unique lags, DiTCAAS has shown the lowest RMSE and highest robustness against heavy mutual coupling compared to super nested arrays, MRA, TCA and sparse CADiS. Overall, DiTCAAS is an ideal sparse array for CS-based DOA estimation.

Chapter 7

Conclusions and Future Work

7.1 Conclusions

In this thesis, several contributions are presented for array signal processing based on traditional and sparse arrays. Beamforming and DOA estimation are integral parts of array signal processing and this thesis was aimed at solving some key probems related to them. Wideband beamforming holds numerous applications in the bandwidth hungry data traffic of present day world. Several techniques exist to design fixed wideband beamformers based on traditional arrays and least squares based eigenfilter method is one of the key methods (Chapter 2). The standard eigenfilter method was revisited in this thesis and it was shown that the design formulation of the cost function suffers from a serious flaw due to which the achieved design generates unacceptable passband/look direction response. This problem was studied from the perspective of both FIR filter design as well as the fixed wideband beamformer design. The problem was clearly highlighted with the help of several design examples and an additional constraint was added to stabilize the achieved design so that consistent design performance according to the desired response can be achieved. Simulation results show the validity and significance of the proposed method (Chapter 3).

Traditional arrays based on ULAs have limited applications in array signal processing due to the large number of sensors required for a particular signal processing scenario and this problem has been addressed by the application of sparse arrays which reduce the

cost of the signal processing projects. Sparse arrays have been exploited from the perspective of their difference co-array structures which provide significantly higher number of lags compared to ULAs for the same number of sensors. These lags are the consecutive and unique lags utilized in the application of DOA estimation with the help of difference co-array based DOA estimators like SS-MUSIC and CS-based methods. Several types of sparse arrays exist including MRA, MHA, nested array, prototype coprime array, conventional coprime array, CACIS, CADiS and super nested array. Coprime arrays generally have better sparsity than nested arrays, which brings their application in countering mutual coupling but MRA and nested arrays provide hole-free co-arrays with more lags for DOA estimation (Chapter 4).

A new sparse array TCA based on a conventional coprime array has been proposed which holds all the properties of a conventional coprime array but with $\lceil \frac{M}{2} \rceil$ redundant sensors. For the same number of sensors, TCAs possess greater number of unique lags than the hole-free structure of the nested array and nested CADiS, and comparable number of unique lags to the sparsest CADiS. The number of consecutive lags of the TCAs are around 75 percent to those of nested arrays which showcases their application in both subspace and CS-based DOA estimation methods. Moreover, they can be easily constructed for an arbitrary number of sensors. TCAs have a significantly sparser array structure with robustness against severe mutual coupling especially when using CS based DOA estimation. With increasing array size, TCAs also offer better error performance in parameter estimates compared to super nested arrays and MRA for both CS and SS-MUSIC based methods in the presence of mutual coupling, as shown by the simulation results. TCAs maintain desirable levels of sparsity related to their weight functions irrespective of the array size unlike other sparse arrays (Chapter 5).

Although TCA holds numerous desirable features, the number of unique lags offered by TCA are close to the sparsest CADiS and nested array and significantly lower than MRA , which limits the estimation error performance offered by TCA through CS-based methods. In this direction, the structure of TCA was studied to explore the possibility of an array which can provide significantly higher number of unique lags with improved sparsity for a given number of sensors. The result of this investigation is a new sparse array DiTCAAS

based on a TCA. The construction of DiTCAAS from TCA takes place in a two-step process where the subarrays $\mathbb{X}_2$ and $\mathbb{X}_3$ of TCA are displaced by a factor of $(2M-2)N$ in the first step. This displacement of the subarrays generates an increase in the unique lags but the minimum spacing between the sensors becomes an integer multiple of half wavelength. To avoid spatial aliasing, an additional sensor is added at half wavelength from one of the sensors of the displaced $\mathbb{X}_3$ in the second step. Two strategic locations are proposed for the placement of this additional sensor, which generates significantly higher number of unique lags for DiTCAAS, even more than the number of lags provided by MRA. Due to its sparse structure with the only non-zero weight being $w(1) = 1$ and higher number of unique lags, DiTCAAS has shown the lowest RMSE and highest robustness against heavy mutual coupling than super nested arrays, MRA, TCA and sparse CADiS. DiTCAAS has proved its potential in a very practical scenario with limited snapshots, varying channel conditions and mutual coupling by achieving the lowest estimation error (Chapter 6).

The two key contributions of this thesis are TCA and DiTCAAS which hold distinct potential in the application of DOA estimation with mutual coupling. TCA can be utilized for both subspace based methods like SS-MUSIC and CS-based methods. On the other hand, DiTCAAS is specifically designed for the application of CS-based methods and performs significantly better than TCA from the perspective of estimation error. In the event of a signal processing scenario, where space for deployment of sensors is limited, TCA with relatively smaller aperture as compared to DiTCAAS is the ideal candidate while DiTCAAS is the perfect candidate where space constraints are not a major issue.

7.2 Future Work

For the future work, some possible directions are as follows.

In this thesis, the characteristics of TCA and DiTCAAS have been studied from the perspective of DOA estimation. Utilizing their difference co-array for application in beamforming would be of a special interest along with a comparative study of their performance with other sparse arrays.

TCA has shown its application for both SS-MUSIC and CS-based DOA estimation methods due to a decent combination of consecutive and unique lags. The sparsity factor of TCA with $w(1) = w(2) = w(3) = 1$ is attractive to counter mutual coupling. One future direction can be aimed at maintaining the sparsity of TCA and investigating an increase of consecutive lags through the addition of another sensor.

As most of the work in this thesis was aimed at designing 1-D sparse arrays, the structure of TCA and DiTCAAS can be explored for a 2-D sparse array design, which is aimed at increased number of lags with reduced mutual coupling in comparison with recently proposed 2-D sparse arrays such as the hourglass arrays [113].

Recently, higher order statistics of data have been utilized for DOA estimation. In this direction, sparse arrays with efficient fourth order difference co-arrays have been developed [106], [114]. A possible direction is to utilize a combination of coprime arrays to search for an enhanced fourth-order difference co-array.

Bibliography

[1] W. Liu and S. Weiss, *Wideband Beamforming: Concepts and Techniques.* Chichester, UK: John Wiley & Sons, 2010.

[2] H. L. Van Trees, *Optimum Array Processing, Part IV of Detection, Estimation, and Modulation Theory.* New York: Wiley, 2002.

[3] B. Allen and M. Ghavami, *Adaptive Array Systems, Fundamentals and Applications.* Chichester, England: John Wiley & Sons, 2005.

[4] R. A. Monzingo and T. W. Miller, *Introduction to Adaptive Arrays.* New York: Wiley and Sons, 1980.

[5] M. S. Brandstein and D. Ward, Eds., *Microphone Arrays: Signal Processing Techniques and Applications.* Berlin: Springer, 2001.

[6] S. Haykin, *Array Signal Processing.* Englewood Cliffs: Prentice Hall, 1985.

[7] D. H. Johnson and D. E. Dudgeon, *Array Signal Processing: Concepts and Techniques*, ser. Signal Processing Series. Englewood Cliffs, NJ: Prentice Hall, 1993.

[8] J. E. Hudson, *Adaptive Array Principles*, ser. IEE Electromagnetic Waves. London: The Institution of Electrical Engineers, 1981.

[9] S. Boyd and L. Vandenberghe, *Convex Optimization.* Cambridge: Cambridge University Press, 2004.

[10] A. Björck, *Numerical Methods for Least Squares Problems.* Philadelphia, PA: Society for Industrial and Applied Mathematics (SIAM), 1996.

[11] A. Tkacenko, P. P. Vaidyanathan, and T. Q. Nguyen, "On the eigenfilter design method and its applications: a tutorial," *IEEE Transactions on Circuits and Systems — II: Analog and Digital Signal Processing*, vol. 50, pp. 497–517, September 2003.

[12] M. S. Bartlett, "Smoothing periodograms from time-series with continuous spectra," vol. 161, pp. 686–687, 1948.

[13] J. Capon, "High-resolution frequency-wavenumber spectrum analysis," *Proceedings of the IEEE*, vol. 57, no. 8, pp. 1408–1418, August 1969.

[14] V. F. Pisarenko, "The retrieval of harmonics from a covariance function," *Geophys. J. R. astr. Soc.*, vol. 33, pp. 347–366, 1973.

[15] R. Kumaresan and D. Tufts, "Estimating the angles of arrival of multiple plane waves," *IEEE Trans. Aerosp. Electron. Syst.*, vol. AES-19, no. 1, pp. 134–139, January 1983.

[16] G. Bienvenu and L. Kopp, "Optimality of high resolution array processing using the eigensystem approach," *IEEE Transactions on Acoustics, Speech, and Signal Processing*, vol. 31, no. 5, pp. 1235–1248, October 1983.

[17] R. Schmidt, "Multiple emitter location and signal parameter estimation," *IEEE Transactions on Antennas and Propagation*, vol. 34, pp. 276–280, March 1986.

[18] R. Roy and T. Kailath, "ESPRIT estimation of signal parameters via rotational invariance techniques," *IEEE Transactions on Acoustics, Speech, and Signal Processing*, vol. 37, no. 7, pp. 984–995, July 1989.

[19] P. Stoica and A. Nehorai, "MUSIC, maximum likelihood, and Cramer-Rao bound," *IEEE Transactions on Acoustics, Speech, and Signal Processing*, vol. 37, no. 5, pp. 720–741, May 1989.

[20] ——, "Performance study of conditional and unconditional direction-of-arrival estimation," *IEEE Transactions on Acoustics, Speech, and Signal Processing*, vol. 38, no. 10, pp. 1783–1795, October 1990.

[21] P. Stoica and K. C. Sharman, "Maximum likelihood methods for direction-of- arrival estimation," *IEEE Transactions on Acoustics, Speech, and Signal Processing*, vol. 38, no. 7, pp. 1132–1143, July 1990.

[22] P. Stoica, P. Babu, and J. Li, "SPICE: A sparse covariance-based estimation method for array processing," *IEEE Transactions on Signal Processing*, vol. 59, no. 2, pp. 629–638, Feb. 1990.

[23] E. J. Candes and M. B. Wakin, "An introduction to compressive sampling," *IEEE Signal Process. Mag.*, vol. 25, no. 2, pp. 21 – 30, March 2008.

[24] D. L. Donoho, "Compressed sensing," *IEEE Trans. Inf. Theory*, vol. 52, no. 4, pp. 1289–1306, April 2006.

[25] E. J. Candès, "The restricted isometry property and its implications for compressed sensing," *Comptes Rendus Mathematique*, vol. 346, no. 9, pp. 589 – 592, 2008. [Online]. Available: http://www.sciencedirect.com/science/article/pii/S1631073X08000964

[26] P. Pal and P. P. Vaidyanathan, "Nested arrays: A novel approach to array processing with enhanced degrees of freedom," *IEEE Transactions on Signal Processing*, vol. 58, no. 8, pp. 4167–4181, Aug. 2010.

[27] P. P. Vaidyanathan and P. Pal, "Sparse sensing with co-prime samplers and arrays," *IEEE Transactions on Signal Processing*, vol. 59, no. 2, pp. 573–586, Feb. 2011.

[28] D. D. Ariananda and G. Leus, "Compressive wideband power spectrum estimation," *IEEE Transactions on Signal Processing*, vol. 60, no. 9, pp. 4775–4789, Sep. 2012.

[29] Y. Chen, Y. Chi, and A. J. Goldsmith, "Exact and stable covariance estimation from quadratic sampling via convex programming," *IEEE Trans. Inf. Theory*, vol. 61, no. 7, pp. 4034–4059, July 2015.

[30] [Online]. Available: https://public.nrao.edu/telescopes/vla/

[31] [Online]. Available: http://www.almaobservatory.org/en/home/

[32] [Online]. Available: https://www.skatelescope.org/

[33] C. A. Balanis, *Antenna Theory: Analysis and Design*. New York, NY, USA: Wiley, 2016.

[34] M. I. Skolnik, *Introduction to Radar Systems*. New York, NY, USA: McGraw Hill, 2001.

[35] R. N. Bracewell, *Radio astronomy techniques*. Germany: Springer, 1962.

[36] P. Li and P. Stoica, *MIMO radar signal processing*. Hoboken, NJ: J. Wiley & Sons, 2009.

[37] P. Suetens, *Fundamentals of medical imaging*. Cambridge New York: Cambridge University Press, 2009.

[38] S. Pillai, Y. Bar-Ness, and F. Haber, "A new approach to array geometry for improved spatial spectrum estimation," *Proc. IEEE*, vol. 73, no. 10, pp. 1522–1524, Oct. 1985.

[39] S. Pillai and F. Haber, "Statistical analysis of a high resolution spatial spectrum estimator utilizing an augmented covariance matrix," *IEEE Transactions on Acoustics, Speech, and Signal Processing*, vol. ASSP-35, no. 11, pp. 1517–1523, Nov. 1987.

[40] Y. Abramovich, D. Gray, A. Gorokhov, and N. Spencer, "Positive-definite Toeplitz completion in DOA estimation for non uniform linear antenna arrays Part I: Fully augmentable arrays," *IEEE Transactions on Signal Processing*, vol. 46, no. 9, pp. 2458–2471, Sep. 1998.

[41] Y. Abramovich, D. Gray, and A. Gorokhov, "Positive-definite Toeplitz completion in DOA estimation for non uniform linear antenna arrays Part II: Partially augmentable arrays," *IEEE Transactions on Signal Processing*, vol. 47, no. 6, pp. 1502–1521, June 1999.

[42] C. L. Liu and P. P. Vaidyanathan, "Remarks on the spatial smoothing step in coarray MUSIC," *IEEE Signal Processing Letters*, vol. 22, no. 9, pp. 1438–1442, September 2015.

[43] P. Pal and P. P. Vaidyanathan, "Coprime sampling and the MUSIC algorithm," in *Proc. IEEE Digital Signal Processing Workshop and IEEE Signal Processing Education Workshop*, Sedona, US, January 2011, pp. 289–294.

[44] C. L. Liu, P. P. Vaidyanathan, and P. Pal, "Coprime coarray interpolation for DOA estimation via nuclear norm minimization," in *Proc. IEEE Int. Symp. Circuits and Syst.*, Montreal, Canada, May 2016, pp. 2639–2642.

[45] H. Qiao and P. Pal, "Unified analysis of co-array interpolation for direction-of-arrival estimation," in *Proc. IEEE Int. Conf. Acoust., Speech, and Sig. Proc.*, New Orleans, LA, USA, March 2017, pp. 3056–3060.

[46] T. E. Tuncer, T. K. Yasar, and B. Friedlander, "Direction of arrival estimation for non uniform linear arrays by using array interpolation," *Radio Science*, vol. 42, no. 4, Aug. 2007.

[47] W. K. Ma, T. H. Hsieh, and C. Y. Chi, "DOA estimation of quasi-stationary signals via Khatri-Rao subspace," in *Proc. IEEE Int. Conf. Acoust., Speech, and Sig. Proc.*, Taipei, Taiwan,, April 2009, pp. 2165–2168.

[48] ——, "DOA estimation of quasi-stationary signals with less sensors than sources and unknown spatial noise covariance: A Khatri-Rao subspace approach," *IEEE Transactions on Signal Processing*, vol. 58, no. 4, pp. 2168–2180, April 2010.

[49] Y. D. Zhang, M. G. Amin, and B. Himed, "Sparsity-based DOA estimation using co-prime arrays," in *Proc. IEEE ICASSP*, Vancouver, Canada, May 2013, pp. 3967 –3971.

[50] A. Moffet, "Minimum-redundancy linear arrays," *IEEE Transactions on Antennas and Propagation*, vol. 16, no. 2, pp. 172–175, March 1968.

[51] T. J. Shan, M. Wax, and T. Kailath, "On spatial smoothing for direction-of-arrival estimation of coherent signals," *IEEE Transactions on Acoustics, Speech, and Signal Processing*, vol. 33, no. 4, pp. 806–811, August 1985.

[52] B. Friedlander and A. J. Weiss, "Direction finding using spatial smoothing with interpolated arrays," *IEEE Trans. Aerosp., Electron. Syst.*, vol. 28, pp. 574–587, April 1992.

[53] S. Pillai and B. H. Kwon, "Forward/backward spatial smoothing techniques for coherent signal identification," *IEEE Transactions on Acoustics, Speech, and Signal Processing*, vol. 37, pp. 8–15, January 1989.

[54] S. Qin, Y. D. Zhang, and M. G. Amin, "Generalized coprime array configurations for direction-of-arrival estimation," *IEEE Transactions on Signal Processing*, vol. 63, no. 6, pp. 1377–1390, March 2015.

[55] P. Pal and P. P. Vaidyanathan, "On application of LASSO for sparse support recovery with imperfect correlation awareness," in *Proc. Asilomar Conference on Signals, Systems and Computers*, Pacific Grove, US, November 2012, pp. 958–962.

[56] Y. M. Zhang, M. G. Amin, and B. Himed, "Sparsity-based DOA estimation using co-prime arrays," in *Proc. IEEE International Conference on Acoustics, Speech, and Signal Processing*, Vancouver, Canada, May 2013, pp. 3967–3971.

[57] M. Ishiguro, "Minimum redundancy linear arrays for a large number of antennas," *Radio Science*, vol. 15, no. 6, pp. 1163–1170, 1980.

[58] G. Bloom and W. Golomb, "Application of numbered undirected graphs," *Proc. IEEE*, vol. 65, no. 4, pp. 562–570, April 1977.

[59] C. Liu and P. P. Vaidyanathan, "Super nested arrays: Linear sparse arrays with reduced mutual coupling Part I: Fundamentals," *IEEE Transactions on Signal Processing*, vol. 64, no. 15, pp. 3997–4012, August 2016.

[60] ——, "Super nested arrays linear sparse arrays with reduced mutual coupling Part II: Higher order extensions," *IEEE Transactions on Signal Processing*, vol. 64, no. 16, pp. 4203–4217, August 2016.

[61] A. Raza and W. Liu, "Critical analysis of the eigenfilter method for the design of FIR filters and wideband beamformers," in *Proc. 22nd International Conference on Automation and Computing (ICAC)*, Colchester, UK, September 2016, pp. 504–509.

[62] A. Raza, W. Liu, and Q. Shen, "Thinned coprime arrays for DOA estimation," in *Proc. of the European Signal Processing Conference*, Kos, Greece, September 2017, pp. 395–399.

[63] W. Liu, "Adaptive wideband beamforming with sensor delay-lines," *Signal Processing*, vol. 89, pp. 876–882, May 2009.

[64] H. Duan, B. P. Ng, C. M. See, and J. Fang, "Applications of the SRV constraint in broadband pattern synthesis," *Signal Processing*, vol. 88, pp. 1035–1045, April 2008.

[65] Y. Zhao, W. Liu, and R. J. Langley, "Efficient design of frequency invariant beamformers with sensor delay-lines," in *Proc. IEEE Workshop on Sensor Array and Multichannel Signal Processing*, Darmstadt, Germany, July 2008, pp. 335–339.

[66] C. A. Olen and R. T. Compton, "A numerical pattern synthesis algorithm for arrays," *IEEE Transactions on Antennas and Propagation*, vol. 38, no. 10, pp. 1666–1676, October 1990.

[67] Y. P. Zhou and M. A. Ingram, "Pattern synthesis for arbitrary arrays using an adaptive array method," *IEEE Transactions on Antennas and Propagation*, vol. 47, no. 5, pp. 862–869, May 1999.

[68] C. L. Lawson and R. J. Hanson, *Solving Least Squares Problems*, ser. Automatic Computation. Englewood Cliffs, NJ: Prentice Hall, 1974.

[69] P. P. Vaidyanathan and T. Q. Nguyen, "Eigenfilters: A new approach to least-squares FIR filter design and applications including nyquist filters," *IEEE Transactions on Circuits & Systems*, vol. 34, no. 1, pp. 11–23, January 1987.

[70] T. Q. Nguyen, "Design of arbitrary FIR digital filters using the eigenfilter method," *IEEE Transactions on Signal Processing*, vol. 41, no. 3, pp. 1128–1139, March 1993.

[71] S. C. Pei and C. C. Tseng, "A new eigenfilter based on total least squares error criterion," *IEEE Transactions on Circuits & Systems I: Regular Papers*, vol. 48, pp. 699–709, 2001.

[72] C. Zhang and T. Chen, "Towards optimal least square filters using the eigenfilter approach," *Proc. IEEE International Conference on Acoustics, Speech, and Signal Processing*, vol. 4, pp. 4171–4174, May 2002.

[73] S. Doclo and M. Moonen, "Comparison of least-squares and eigenfilter techniques for broadband beamforming," *in Proc. 3rd IEEE Benelux Signal Processing Symposium*, pp. 73–76, March 2002.

[74] Y. Zhao, W. Liu, and R. J. Langley, "Subband design of fixed wideband beamformers based on the least squares approach," *Signal Processing*, vol. 91, pp. 1060–1065, April 2011.

[75] S. C. Pei and J. J. Shyu, "Design of FIR Hilbert transformers and differentiators by eigenfilter," *IEEE Transactions on Circuits & Systems*, vol. 35, no. 11, pp. 1457–1461, November 1988.

[76] ——, "Eigenfilter design of higher-order digital differentiators," *IEEE Transactions on Acoustics, Speech, and Signal Processing*, vol. 37, no. 4, pp. 505–511, April 1989.

[77] ——, "Eigen-approach for designing FIR filters and all-pass phase equalizers with prescribed magnitude and phase response," *IEEE Transactions on Circuits and Systems — II: Analog and Digital Signal Processing*, vol. 39, no. 3, pp. 137–146, March 1992.

[78] ——, "Complex eigenfilter design of arbitrary complex coefficient FIR digital filters," *IEEE Transactions on Circuits and Systems II: Analog and Digital Signal Processing*, vol. 40, no. 1, pp. 32–40, January 1993.

[79] A. Nashashibi and C. Charalambous, "2-D FIR eigenfilters," *Proc. IEEE International Symposium on Circuits and Systems*, vol. 2, pp. 1037–1040, June 1988.

[80] S. C. Pei and J. J. Shyu, "2-D FIR eigenfilters: A least-squares approach," *IEEE Transactions on Circuits & Systems*, vol. 37, no. 1, pp. 24–34, January 1990.

[81] ——, "Design of two-dimensional FIR eigenfilters for sampling-structure conversion," *IEEE Transactions on Circuits and Systems for Video Technology*, vol. 3, no. 2, pp. 158–162, April 1993.

[82] T. I. Laakso, T. Q. Nguyen, and R. D. Koilpillai, "Designing allpass filters using the eigenfilter method," *Proc. IEEE International Conference on Acoustics, Speech, and Signal Processing*, vol. 3, pp. 77–80, April 1993.

[83] J. J. Shyu and S. C. Pei, "Design of IIR multi-band filters using IIR all-pass eigenfilters," *Proc. IEEE . 35th Midwest Symp. Circuits and Systems*, vol. 1, pp. 601–604, August 1992.

[84] C. Y. F. Ho, B. W. K. Ling, H. H. H. Dam, and K. L. Teo, "Minimax passband group delay nonlinear phase peak constrained FIR filter design without imposing desired phase response," *International Journal of Innovative Computing, Information and Control*, vol. 8, no. 5(B), pp. 3863–3874, 2012.

[85] F. Harrou and M. N. Nounou, "Monitoring linear antenna arrays using an exponentially weighted moving average-based fault detection scheme," *Systems Science & Control Engineering*, vol. 2, no. 1, pp. 433–443, 2014.

[86] A. Raza and W. Liu, "Revisit of the eigenfilter method for the design of FIR filters and wideband beamformers," *Systems Science & Control Engineering*, vol. 6, no. 1, pp. 482–491, 2018. [Online]. Available: https://doi.org/10.1080/21642583.2018.1539928

[87] S. Pillai, *Array Signal Processing*. New York, NY, USA: Springer, 1989.

[88] C. L. Liu and P. P. Vaidyanathan, "Super nested arrays with less mutual coupling than nested arrays," in *Proc. IEEE International Conference on Acoustics, Speech, and Signal Processing*, 2016, pp. 2976–2980.

[89] J. Dai, D. Zhao, and X. Ji, "A sparse representation method for DOA estimation with unknown mutual coupling," *IEEE Antennas Wireless Propag. Lett.*, vol. 11, pp. 1210–1213, 2012.

[90] B. Friedlander and A. J. Weiss, "Direction finding in the presence of mutual coupling," *IEEE Transactions on Antennas and Propagation*, vol. 39, no. 3, pp. 273–284, 1991.

[91] H. T. Hui, "Decoupling methods for the mutual coupling effect in antenna arrays: A review," *Recent Patents on Engineering*, vol. 1, pp. 187–193, 2007.

[92] ——, "Improved compensation for the mutual coupling effect in a dipole array for direction finding," *IEEE Trans. Antennas Propag.*, vol. 51, no. 9, pp. 2498–2503, September 2003.

[93] M. Lin and L. Yang, "Blind calibration and DOA estimation with uniform circular arrays in the presence of mutual coupling," *IEEE Antennas Wireless Propag. Lett.*, vol. 5, no. 1, pp. 315–318, Dec. 2006.

[94] K. M. Pasala and E. M. Friel, "Mutual coupling effects and their reduction in wideband direction of arrival estimation," *IEEE Transactions on Aerospace and Electronic Systems*, vol. 30, no. 4, pp. 1116–1122, 1994.

[95] F. Sellone and A. Serra, "A novel online mutual coupling compensation algorithm for uniform and linear arrays," *IEEE Transactions on Signal Processing*, vol. 55, no. 2, pp. 560–573, Feb. 2007.

[96] T. Svantesson, "Modeling and estimation of mutual coupling in a uniform linear array of dipoles," in *Proc. IEEE International Conference on Acoustics, Speech, and Signal Processing*, vol. 5, 1999, pp. 2961–2964.

[97] ——, "Mutual coupling compensation using subspace fitting," in *Proc. IEEE Sensor Array Multichannel Signal Process. Workshop*, 2000, pp. 494–498.

[98] Z. Ye, J. Dai, X. Xu, and X. Wu, "DOA estimation for uniform linear array with mutual coupling," *IEEE Trans. Aerosp. Electron. Syst.*, vol. 45, pp. 280–288, Jan. 2009.

[99] E. Vertatschitsch and S. Haykin, "Nonredundant arrays," *Proc. IEEE*, vol. 74, no. 1, pp. 217–217, Feb 1986.

[100] I. Gupta and A. Ksienski, "Effect of mutual coupling on the performance of adaptive arrays," *IEEE Transactions on Antennas and Propagation*, vol. AP-31, no. 5, pp. 785–791, Sep 1983.

[101] Y. Zhang, S. Qin, and M. Amin, "DOA estimation exploiting coprime arrays with sparse sensor spacing," *Proc. IEEE International Conference on Acoustics, Speech, and Signal Processing*, pp. 2267–2271, 2014.

[102] Q. Shen, W. Liu, W. Cui, and S. Wu, "Underdetermined DOA estimation under the compressive sensing framework: A review," *IEEE Access*, vol. 4, pp. 8865–8878, 2016.

[103] F. S. Rawnaque and J. R. Buck, "Comparing the effect of aperture extension on the peak sidelobe level of sparse arrays," *The Journal of the Acoustical Society of America*, vol. 142(5), pp. EL467–EL472, 2017.

[104] K. Han and A. Nehorai, "Wideband gaussian source processing using a linear nested array," *IEEE Signal Processing Letters*, vol. 20, pp. 1110–1113, Nov 2013.

[105] ——, "Improved source number detection and direction estimation with nested arrays and ULAs using jackknifing," *IEEE Transactions on Signal Processing*, vol. 61, pp. 6118–6128, Nov 2013.

[106] Q. Shen, W. Liu, W. Cui, and S. L. Wu, "Extension of Co-Prime Arrays Based on the Fourth-Order Difference Co-Array Concept," *IEEE Signal Processing Letters*, vol. 23, no. 5, pp. 615–619, May 2016.

[107] E. BouDaher, F. Ahmad, M. G. Amin, and A. Hoorfar, "DOA estimation with coprime arrays in the presence of mutual coupling," in *Proc. Eur. Signal Process. Conf.*, 2015, pp. 2830–2834.

[108] J. Liu, Y. Zhang, S. Ren, and S. Cao, "Augmented nested arrays with enhanced DOF and reduced mutual coupling," *IEEE Transactions on Signal Processing*, vol. 65, pp. 5549–5563, 2017.

[109] K. Adhikari and J. R. Buck, "Spatial spectral estimation with product processing of a pair of colinear arrays," *IEEE Transactions on Signal Processing*, vol. 65, pp. 2389–2401, May 2017.

[110] Q. Shen, W. Liu, W. Cui, S. L. Wu, Y. D. Zhang, and M. Amin, "Low-complexity direction-of-arrival estimation based on wideband coprime arrays," *IEEE Transactions on Acoustics, Speech, and Language Processing*, vol. 23, pp. 1445–1456, Sep 2015.

[111] M. J. Hinich, "Processing spatially aliased arrays," *The Journal of the Acoustical Society of America*, vol. 64(3), pp. 792–794, 1978.

[112] A. Raza, W. Liu, and Q. Shen, "Displaced thinned coprime arrays with an additional sensor for DOA estimation," in *Proc. of the 18th IEEE International Symposium on Signal Processing and Information Technology (ISSPIT)*, Louisville, KY, USA, December 2018.

[113] C. L. Liu and P. P. Vaidyanathan, "Hourglass arrays and other novel 2-D sparse arrays with reduced mutual coupling," *IEEE Transactions on Signal Processing*, vol. 65, no. 13, pp. 3369–3383, Jul. 2017.

[114] J. Cai, W. Liu, R. Zong, and Q. Shen, "An expanding and shift scheme for constructing fourth-order difference coarrays," *IEEE Signal Processing Letters*, vol. 24, no. 4, pp. 480–484, 2017.